

TUNED VIBRATION ABSORBER DESIGN FOR A SUPPORTED HOLLOW
CYLINDRICAL STRUCTURE

A THESIS SUBMITTED TO
THE GRADUATE SCHOOL OF NATURAL AND APPLIED SCIENCES
OF
MIDDLE EAST TECHNICAL UNIVERSITY

BY

TUĞRUL AKSOY

IN PARTIAL FULFILLMENT OF THE REQUIREMENTS
FOR
THE DEGREE OF MASTER OF SCIENCE
IN
MECHANICAL ENGINEERING

SEPTEMBER 2015

Approval of the thesis:

**TUNED VIBRATION ABSORBER DESIGN FOR A SUPPORTED HOLLOW
CYLINDRICAL STRUCTURE**

submitted by **TUĞRUL AKSOY** in partial fulfillment of the requirements for the degree of **Master of Science in Mechanical Engineering Department, Middle East Technical University** by,

Prof. Dr. Gülbin Dural Ünver
Dean, Graduate School of **Natural and Applied Sciences**

Prof. Dr. Tuna Balkan
Head of Department, **Mechanical Engineering**

Asst. Prof.Dr. Gökhan O. Özgen
Supervisor, **Mechanical Engineering Dept., METU**

Examining Committee Members:

Prof. Dr. Mehmet Çalışkan
Mechanical Engineering Dept., METU

Asst. Prof. Dr. Gökhan O. Özgen
Mechanical Engineering Dept., METU

Assoc. Prof. Dr. Yiğit Yazıcıoğlu
Mechanical Engineering Dept., METU

Asst. Prof. Dr. Kutluk Bilge Arıkan
Mechatronic Engineering Dept., Atılım University

Assoc. Prof. Dr. Ender Ciğeroğlu
Mechanical Engineering Dept., METU

Date: 08.09.2015

I hereby declare that all information in this document has been obtained and presented in accordance with academic rules and ethical conduct. I also declare that, as required by these rules and conduct, I have fully cited and referenced all material and results that are not original to this work.

Name, Last name: Tuğrul AKSOY
Signature:

ABSTRACT

TUNED VIBRATION ABSORBER DESIGN FOR A SUPPORTED HOLLOW CYLINDRICAL STRUCTURE

Aksoy, Tuğrul

M. S. Department of Mechanical Engineering

Supervisor: Assist. Prof. Gökhan O. Özgen

September 2015, 93 pages

Supported hollow structural elements have a usage area in various types of structures or machines. They exhibit an oscillatory behavior under various excitations since their modal frequencies are quite low. This behavior results in vibrations which reach huge amplitudes especially at the tip of the structures. This situation may be harmful for the structural integrity of the structures and may reduce the service life. Moreover, these vibrations can distort the performance of the machines' which involve the supported hollow structure.

In this thesis study, a tuned vibration absorber (also called as tuned mass damper) design is proposed to suppress the vibrations of a supported hollow cylindrical structure under impulsive loading. Within the scope of this study, a tuned vibration absorber (TVA) designed and applied on a sample supported hollow cylinder structure. Then, the mitigation in vibration amplitudes as a result of this application is investigated.

In order to see the effectiveness of the TVA application, a physical structure involving a supported hollow cylindrical structure is designed and manufactured. TVA is designed by considering the modal parameters of this physical structure and applied on it. Experiments are carried out in order to verify the effectiveness of the TVA application on the dynamics of the system. After then, dynamic test are carried

out on the system and the mitigation in vibration levels is investigated as the result of the TVA application.

Keywords: Supported hollow cylinder vibrations, tuned vibration absorbers, tuned mass dampers

ÖZ

DESTEKLENMİŞ İÇİ BOŞ SİLİNDİRİK BİR YAPI İÇİN AYARLI TİTREŞİM EMİCİ TASARIMI

Aksoy, Tuğrul

Yüksek lisans, Makine Mühendisliği Bölümü

Tez Yöneticisi: Yrd. Doç Dr. Gökhan O. Özgen

Eylül 2015, 93 sayfa

Desteklenmiş içi boş yapısal elemanlar, çeşitli yapılarda ve makinalarda kullanım alanı bulmaktadırlar. Bu yapısal elemanlar, doğal frekanslarının oldukça düşük olması nedeniyle çeşitli tahrikler altında salınımlı davranış göstermektedirler. Bu davranış, özellikle yapıların uç kısımlarında yüksek genliklere ulaşan titreşimlere yol açabilmektedir. Bu durum, söz konusu yapıların yapısal bütünlüğü açısından zararlı olabilmekte ve servis ömürlerini azaltabilmektedir. Ayrıca bu titreşimler, desteklenmiş içi boş yapısal elemanları içeren makinaların performansını da bozabilmektedir.

Bu tez çalışmasında, desteklenmiş içi boş bir silindirik yapının titreşim seviyelerini azaltmak için bir ayarlı titreşim emici (ayarlı kütle sönümleyici olarak da adlandırılır) tasarımı önerilmiştir. Çalışma kapsamında bir ayarlı titreşim emici (TVA) tasarlanmış ve örnek bir desteklenmiş içi boş silindirik yapının üzerine uygulanmıştır. Sonrasında, bu uygulama sonucunda titreşim büyüklüklerinde meydana gelen azalma incelenmiştir.

TVA uygulamasının etkinliğini görebilmek amacıyla, desteklenmiş içi boş silindirik bir yapı içeren deneysel bir prototip tasarlanmış ve üretilmiştir. TVA tasarımı da bu deneysel prototipin modal parametreleri dikkate alınarak gerçekleştirilmiş ve prototipin üzerine uygulanmıştır. Sonrasında, sistem üzerinde dinamik testler

gerçekleştirilmiş ve TVA uygulaması sonucunda titreşim seviyelerinde meydana gelen azalma incelenmiştir.

Anahtar kelimeler: Desteklenmiş içi boş silindir titreşimleri, ayarlı titreşim emiciler, ayarlı kütle sönümleyicileri

ACKNOWLEDGMENTS

The author wants to thank his supervisor Asst. Prof. Dr. Gökhan ÖZGEN and his manager Mr. Bülent ACAR for their precious advices, critics and suggestions throughout the thesis study.

The author also wishes to thank his colleagues Caner GENÇOĞLU, Bilgehan ERDOĞAN and Haşim ÖZEL because of their substantial efforts and assistances during the experimental studies.

The author would also like to thank Tahsin ŞAHİN due to his worthwhile assistance while the production of experimental prototype.

Finally author sends his greatest thanks to his family due to their support and encouragement over many years.

TABLE OF CONTENTS

ABSTRACT	v
ÖZ.....	vii
ACKNOWLEDGMENTS.....	ix
TABLE OF CONTENTS	x
LIST OF TABLES	xii
LIST OF FIGURES.....	xiii
NOMENCLATURE.....	xvii
CHAPTERS	
1. INTRODUCTION	1
2. LITERATURE SURVEY	3
2.1. BASIC THEORY OF TUNED VIBRATION ABSORBERS	3
2.1.1. The Undamped Tuned Vibration Absorbers	4
2.1.2. The Damped Tuned Vibration Absorbers	8
2.2. TUNED VIBRATION ABSORBER DESIGN STUDIES FOR RESONANT VIBRATION PROBLEMS	11
2.3. TVA DESIGN STUDIES FOR SLENDER STRUCTURES	15
2.4. VARIOUS TYPES OF TVA APPLICATIONS	20
3. DESCRIPTION OF THE VIBRATION CONTROL PROBLEM.....	25
3.1. DESCRIPTION OF THE PHYSICAL STRUCTURE	25

3.2.	DEFINITION OF THE VIBRATION PROBLEM.....	32
3.3.	VALIDATION OF THE FINITE ELEMENT MODEL OF THE STRUCTURE.....	33
4.	DESIGN OF TVA	49
4.1.	DETERMINATION OF THE TVA PARAMETERS	49
4.2.	REALIZATION OF THE TVA DESIGN.....	64
4.3.	EXPERIMENTAL VERIFICATION OF THE TVA PARAMETERS	69
5.	CHARACTERIZATION OF THE VIBRATION CONTROL PERFORMANCE OF TVA	73
5.1.	COMPARISON FOR THE WITHOUT MASS CASE	74
5.2.	COMPARISON FOR THE MASS ADDED CASE	77
5.3.	TOTAL ANALYSIS-TEST COMPARISON	80
6.	CONCLUSION AND FUTURE WORK	85
	REFERENCES.....	87
	APPENDICES	91
	Appendix A: Technical Specifications of the Accelerometers.....	91
	Appendix B: Technical Specifications of the Impact Hammer.....	92
	Appendix C: Technical Specifications of the Modal Shaker	93

LIST OF TABLES

TABLES

Table 2-1: Modal test and MATLAB results for the plain gun barrel [7].....	16
Table 2-2: Modal impact testing results with vibration absorber [7].....	17
Table 3-1: Modal analysis results obtained from FEA	32
Table 3-2: Results for the first three modes of the physical structure.....	41
Table 3-3: Comparison of the natural frequency and mode shape results	44
Table 4-1: Selected TVA Parameters.....	55
Table 4-2: Maximum harmonic response amplitudes for different angular orientations of the TVA.....	60
Table 4-3: The final TVA parameter combination.....	64
Table 4-4: Damping ratios with respect to various magnet positions	72
Table 5-1: Comparison of the optimum and realized TVA parameters	80
Table 5-2: Comparison of the maximum harmonic displacements and total reductions	83

LIST OF FIGURES

FIGURES

Figure 2-1: Addition of small k-m vibration absorber to the main K-M system [1] ...	5
Figure 2-2: Change of the two resonance frequencies with respect to the mass ratio .	7
Figure 2-3: Vibration amplitudes of the main system with respect to various disturbing frequencies	7
Figure 2-4: Responses of the main mass with respect to various damping values	10
Figure 3-1: CAD model of the sample physical structure.....	26
Figure 3-2: Optimized dimensions of the back and front foot plates.....	27
Figure 3-3: General view of the fabricated structure	27
Figure 3-4: Clamp-tube connection detail	28
Figure 3-5: General mesh structure of the physical structure	29
Figure 3-6: Tie constraints between the parts of physical structure.....	30
Figure 3-7: Fixed boundary condition regions.....	30
Figure 3-8: 1 st mode (tip-off) of the prototype (FEA result).....	31
Figure 3-9: 2 nd mode (side-off) of the prototype (FEA result).....	31
Figure 3-10: 3 rd mode of the prototype (FEA result)	32
Figure 3-11: Accelerometer locations on the physical structure.....	34
Figure 3-12: Impact hammer used in the modal tests	35
Figure 3-13: Excitation location.....	35
Figure 3-14: Sample force-time data obtained during modal tests	36
Figure 3-15: LMS hardware used in the modal tests	36
Figure 3-16: PCB accelerometers	37
Figure 3-17: Sample acceleration-time data obtained during modal tests	37
Figure 3-18: 1 st mode (tip-off) of the prototype (test result).....	38
Figure 3-19: 2 nd mode (side-off) of the prototype (test result).....	38
Figure 3-20: 3 rd mode of the prototype (test result)	39
Figure 3-21: Driving point input and response directions	40
Figure 3-22: Coherence data obtained from the driving point.....	40
Figure 3-23: FRF data obtained from the driving point.....	41
Figure 3-24: Test-analysis comparison for the 1 st (tip-off) mode	42

Figure 3-25: Test-analysis comparison for the 2 nd (side-off) mode	42
Figure 3-26: Test-analysis comparison for the 3 rd mode.....	43
Figure 3-27: MAC number matrix for the comparison of experimental and FEA models	44
Figure 3-28: Location of the FRF measurement accelerometer.....	45
Figure 3-29: FRF comparison in x-axes.....	46
Figure 3-30: FRF comparison in y-axes.....	46
Figure 3-31: FRF comparison in z-axes	47
Figure 4-1: Forcing location on the prototype model	51
Figure 4-2: Harmonic displacement response at the tip of prototype (0-20 Hz).....	52
Figure 4-3: Harmonic displacement response at the tip of prototype (0-100 Hz).....	52
Figure 4-4: TVA modelling on the FEA model	53
Figure 4-5: Constraint between two points of the spring/dashpot feature	54
Figure 4-6: Harmonic displacement reading point.....	56
Figure 4-7: Harmonic responses for different TVA masses ($\omega_n=9.3$ Hz; $\zeta=0.3$).....	57
Figure 4-8: Harmonic responses for different damping ratios ($m=400$ grams; $\omega_n=9.3$ Hz).....	57
Figure 4-9: Harmonic responses for different tuning frequencies ($m=400$ grams; $\zeta=0.3$).....	58
Figure 4-10: Maximum harmonic response amplitudes with respect to different TVA masses.....	58
Figure 4-11: Maximum harmonic response amplitudes with respect to different tuning frequencies	59
Figure 4-12: Maximum harmonic response amplitudes with respect to different damping ratios	59
Figure 4-13: Angular orientation of the TVA on the FEA model.....	60
Figure 4-14: Maximum harmonic response amplitudes for different angular orientations of the TVA.....	61
Figure 4-15: Harmonic responses for different angular orientations of the TVA.....	61
Figure 4-16: Additional mass part and its location on the FEA model.....	62
Figure 4-17: Harmonic responses for the unmodified cases	63
Figure 4-18: Harmonic responses for the modified with optimized TVA cases.....	63

Figure 4-19: Harmonic responses obtained with the final TVA parameter combination..... 64

Figure 4-20: CAD model of the TVA assembly 65

Figure 4-21: Fabricated TVA assembly and components..... 66

Figure 4-22: Slotted configuration of the magnet plates..... 67

Figure 4-23: Measurement of the TVA mass..... 68

Figure 4-24: Modal shaker and accelerometer locations on the TVA assembly 70

Figure 4-25: FRF results obtained for different magnet-copper plate distances..... 71

Figure 4-26: Sample FRF comparison for the damping ratio identification..... 72

Figure 5-1: TVA location on the physical structure..... 73

Figure 5-2: Fastening of the TVA assembly 74

Figure 5-3: Without mass case - Comparison of the test FRF results (x-direction) .. 75

Figure 5-4: Without mass case - Comparison of the test FRF results (y-direction) . 75

Figure 5-5: Without mass case - Comparison of the test FRF results (z-direction)... 76

Figure 5-6: Analysis-test FRF comparison for the modified case (x-axes) 76

Figure 5-7: Analysis-test FRF comparison for the modified case (y-axes) 77

Figure 5-8: Analysis-test FRF comparison for the modified case (z-axes) 77

Figure 5-9: Attachment of the additional mass on the physical structure..... 78

Figure 5-10: Mass added case – Comparison of the test FRF results (x-direction)... 78

Figure 5-11: Mass added case - Comparison of the test FRF results (y-direction).... 79

Figure 5-12: Mass added case - Comparison of the test FRF results (z-direction).... 79

Figure 5-13: Total harmonic displacement comparison for the optimized TVA (Analysis)..... 81

Figure 5-14: Total harmonic displacement comparison for the realized TVA (Analysis)..... 81

Figure 5-15: Total harmonic displacement comparison (Experimental) 82

Figure 5-16: Comparison of the harmonic displacements for unmodified case 83

Figure 5-17: Comparison of the harmonic displacements for modified case 83

NOMENCLATURE

TVA: tuned vibration absorber

DVA: dynamic vibration absorber

TMD: tuned mass damper

SDOF: single degree of freedom

MDOF: multiple degrees of freedom

g: gravity acceleration

Hz: hertz

dB: decibel

mm: milimeters

M: mass of the main system

m : mass of the vibration absorber

K: stiffness of the main system

k: stiffness of the vibration absorber

x_1 : response of the main system

x_2 : response of the tuned vibration absorber

a_1 : response amplitude of the main system

a_2 : response amplitude of the vibration absorber

P_0 : excitation amplitude

ω : excitation frequency

ω_n : natural frequency

x_{st} : static deflection

μ : mass ratio

ω_a : natural frequency of the vibration absorber

Ω_n : natural frequency of the main system

c : damping coefficient of the vibration absorber

j : square root of minus one

f : natural frequency ratio

g : forced frequency ratio

c_c : critical damping coefficient

f_{opt} : optimum natural frequency of the vibration absorber

ζ : damping ratio

MAC: modal assurance criteria

FFT: fast fourier Transform

FRF: frequency response function

PSD: power spectral density

FEA: finite element analysis

CHAPTER 1

INTRODUCTION

Tuned vibration absorbers (TVA) can be effectively used to suppress resonant and forced vibration response in mechanical structures. However, each tuned vibration absorber application will have to be handled as a standalone design project since there is quite a bit of variation in the types of vibration problems. Besides, tuned vibration absorbers have to be integrated to the structure of interest which does not necessarily have standardized mechanical interfaces.

In this thesis study, design of a tuned vibration absorber to suppress the resonant vibration response of a supported hollow cylinder structure is investigated. The structure is a representative structure constructed to simulate a scenario where the beam like structures tip response is dominated resonant vibrations with main contribution coming from its lowest transverse vibration modes. The structure is modeled in 3 dimensions and lowest structural modes are transverse bending modes which are also very closely spaced. An SDOF tuned vibration absorber is designed to suppress the vibration response around these two lowest modal frequencies. The two modes are in fact transverse modes that are almost orthogonal and the single tuned vibration absorber is to be integrated to be interacting with both modes which are one of the several design challenges of the particular application. Other challenges include the determination of the basic tuned vibration absorber parameters (mass, stiffness and damping ratio) and orientation of the TVA system on the structure.

In the beginning of study, a literature survey is presented in the second chapter. This literature survey is divided into four parts. In the first part, fundamentals of the tuned vibration absorber theory are explained which is based on single degree of freedom tuned vibration absorber application on a single degree of freedom system. Second chapter is also divided into two sections. In the first section, the basic theory of undamped tuned vibration absorber is explained and the damped vibration absorber theory is presented in the second section. Second part of this chapter is allocated to the guidelines for suppressing resonant vibration problems in mechanical structures.

In the third part, tuned vibration absorber design works for the transverse vibrations of slender structures are presented. Various types of tuned vibration absorber applications are explained in the final part of this chapter.

Third chapter is allocated for the description of the vibration control problem and this chapter is divided into three parts. In the first part, physical structure is described and analysis results are performed on the finite element model of this structure. The vibration control problem is explained with details in the second part. In the third part of this chapter, experimental verification of the finite element model of the physical structure is explained.

In the fourth chapter, design of the tuned vibration absorber is clarified. This chapter is also divided into three parts. In the first part, optimization study for the identification of the tuned vibration absorber parameters is explained with details. In the second part of the fifth chapter, the conceptual design solution for the realization of the tuned vibration absorber parameters is presented. Characterization tests performed to verify the tuned vibration absorber parameters are explained in the third part.

In the fifth chapter, the tuned vibration absorber design is verified via experiments carried out on a physical structure. Experiments and main results are explained elaborately.

In the final chapter, main results of the study are evaluated and the conclusion is presented. In addition, the predictions and suggestions about the future of this study are established.

CHAPTER 2

LITERATURE SURVEY

Tuned vibration absorbers are frequently used systems for controlling and reducing the vibration amplitudes of structures and machines. They can be designed for absorption of vibrational energy at a single frequency. They can also be designed to be effective in a frequency bandwidth.

A comprehensive literature research is performed in this thesis for the various types of TVA designs and applications. Report of the literature survey conducted for this thesis work is separated into four parts. In the first part of the literature survey report, fundamentals of the tuned vibration absorber theory are presented. Secondly, sources that give information about tuned vibration absorber design guidelines for the resonant vibration problems are presented. In the third part, various tuned vibration absorber design studies conducted for reducing the transverse vibrations of slender structures are examined. Various types of tuned vibration absorber design alternatives are presented with details in the final section of this chapter.

2.1. BASIC THEORY OF TUNED VIBRATION ABSORBERS

Machines and mechanical components are usually subjected to a steady alternating force which acts at constant frequency. This forcing (excitation) may result in excessive vibrations if the frequency of excitation is equal or close to a resonance frequency of structure. These vibrations may cause to the machines' or structures' damage or sudden failure. In order to eliminate this problem, the stiffness or mass properties of the systems' can be altered. However, this is impractical for most cases. Therefore, the usage of tuned (dynamic) vibration absorbers is proposed to prevent the severe vibrations of the systems. The dynamic vibration absorber application is invented by Frahm in 1909 [1].

Tuned vibration absorbers basically consist of stiffness (K) and mass (M) elements. Depending on the requirement, damping element is introduced to the vibration

absorber. Especially, if the vibration absorption is required in a bandwidth, the damping element should be used within the vibration absorber and the damping amount is adjusted according to the bandwidth which vibration reduction is desired.

Fundamentals of the tuned vibration absorber theory are examined in two parts of this section of literature survey. In the first part, undamped vibration absorber theory is explained. The damped tuned vibration absorber theory is presented in the second part.

2.1.1. The Undamped Tuned Vibration Absorbers

The simplest form of tuned vibration absorber is shown in Figure 2-1 and it consists of a stiffness element which has a spring constant and a mass. Natural frequency of the absorber is selected as equal to the excitation frequency ω . It will be proven that the vibration of main system is reduced since the absorber functions in a way that the spring force acts at opposite direction of excitation. In order to prove this statement, the equations of motion are written as follows [1]:

$$\begin{aligned} M\ddot{x}_1 + (K + k)x_1 - kx_2 &= P_0 \sin(\omega t) \\ m\ddot{x}_2 + k(x_2 - x_1) &= 0 \end{aligned} \quad (\text{Eqn. 2.1})$$

where

M : mass of the main system

K : stiffness of the main system

m : mass of the tuned vibration absorber

k : stiffness of the tuned vibration absorber

x_1 : Response of the main system

x_2 : Response of the tuned vibration absorber

P_0 : Excitation amplitude

ω : Excitation frequency

t : Time

The forced vibration of the system is in the following form:

$$\begin{aligned} x_1 &= a_1 \sin \omega t \\ x_2 &= a_2 \sin \omega t \end{aligned} \quad (\text{Eqn. 2.2})$$

Where a_1 is the amplitude of the response of main system and a_2 is the amplitude of the response of tuned vibration absorber.

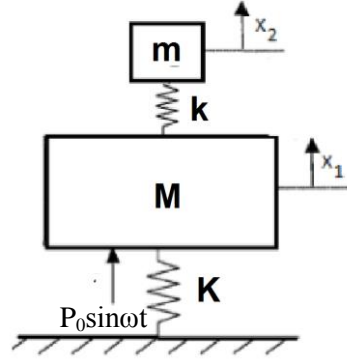


Figure 2-1: Addition of small k-m vibration absorber to the main K-M system

[1]

Combining (Eqn. 2.1) and (Eqn. 2.2) and eliminating $\sin\omega t$ terms results in following equations [1]:

$$a_1(-M\omega^2 + K + k) - ka_2 = P_0$$

$$-ka_1 + a_2(-m\omega^2 + k) = 0 \quad (\text{Eqn. 2.3})$$

By performing some simplifications, (Eqn. 2.3) is simplified as in (Eqn. 2.4) [1]

$$\frac{a_1}{x_{st}} = \frac{1 - \frac{\omega^2}{\omega_a^2}}{\left(1 - \frac{\omega^2}{\omega_a^2}\right)\left(1 + \frac{k}{K} - \frac{\omega^2}{\Omega_n^2}\right) - \frac{k}{K}}$$

$$\frac{a_2}{x_{st}} = \frac{1}{\left(1 - \frac{\omega^2}{\omega_a^2}\right)\left(1 + \frac{k}{K} - \frac{\omega^2}{\Omega_n^2}\right) - \frac{k}{K}} \quad (\text{Eqn. 2.4})$$

where

$x_{st} = P_0/K$: static deflection of main system

$\omega_a^2 = k/m$: square of the natural frequency of the absorber

$\Omega_n^2 = K/M$: square of the natural frequency of the main system

$\mu = m/M$: mass ratio

From (Eqn. 2.4) it can be clearly seen that the amplitude of a_1 becomes zero if the absorber natural frequency (ω_a) is equal to the excitation frequency (ω). It can also be found that the amplitude of absorber response (a_2) is equal to P_0/k which implies the fact that the absorber spring (k) applies a force equal and opposite to the excitation forcing (P_0).

If the natural frequency of the absorber is chosen as equal to the natural frequency of the main system

i.e. ($\omega_a = \Omega_n$ or $\frac{k}{m} = \frac{K}{M}$ or $\frac{k}{K} = \frac{m}{M}$), the (Eqn. 2.4) becomes [1]:

$$\frac{a_1}{x_{st}} = \frac{1 - \frac{\omega^2}{\omega_a^2}}{\left(1 - \frac{\omega^2}{\omega_a^2}\right)\left(1 + \mu - \frac{\omega^2}{\omega_a^2}\right) - \mu}$$

$$\frac{a_2}{x_{st}} = \frac{1}{\left(1 - \frac{\omega^2}{\omega_a^2}\right)\left(1 + \mu - \frac{\omega^2}{\omega_a^2}\right) - \mu} \quad (\text{Eqn. 2.5a, b})$$

It can be seen that the both of (Eqn 2.5a) and (Eqn. 2.5b) have the same denominator. This denominator is in quadratic form and of course has two roots. These roots represent the newly formed two resonance frequencies of the main system and can be calculated the ω from the following equation [1]:

$$\left(\frac{\omega}{\omega_a}\right)^2 = \left(1 + \frac{\mu}{2}\right) \mp \sqrt{\mu + \frac{\mu^2}{4}} \quad (\text{Eqn. 2.6})$$

The relation between the mass ratio and the two resonance frequencies of the system is represented in Figure 2-2. According to this graph, it can be seen that the resonance frequencies shifts from the original natural frequency as the mass ratio increases. It means that as the absorber mass increases the separation between the two resonances also increases.

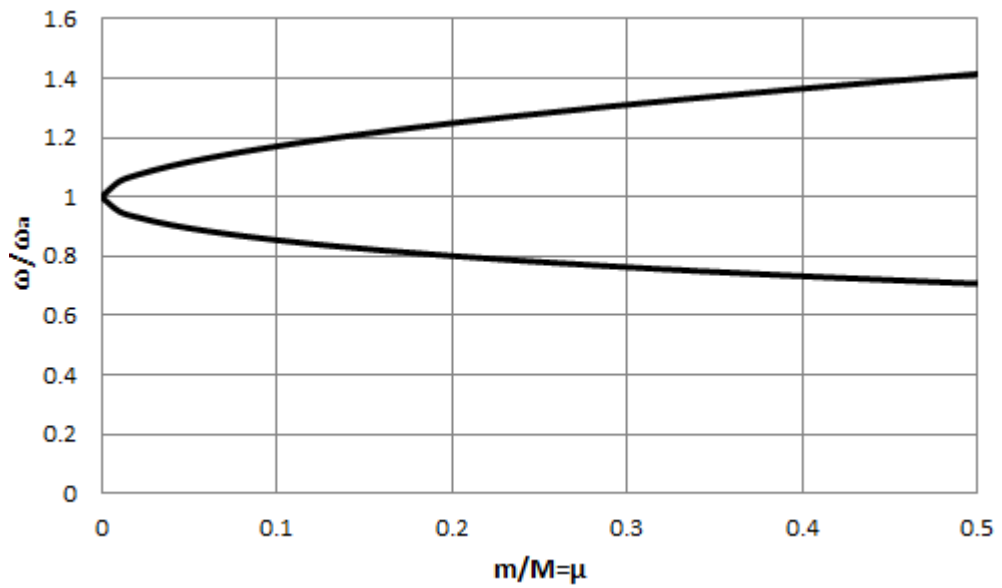


Figure 2-2: Change of the two resonance frequencies with respect to the mass ratio

In Figure 2-3, the change in absolute vibration amplitude of main system is shown for with and without absorber cases. The newly formed two resonances as a result of absorber addition to the system can be clearly seen from the figure. These two peaks should be controlled if the vibration absorption is sought for a wide frequency band instead of a single target frequency.

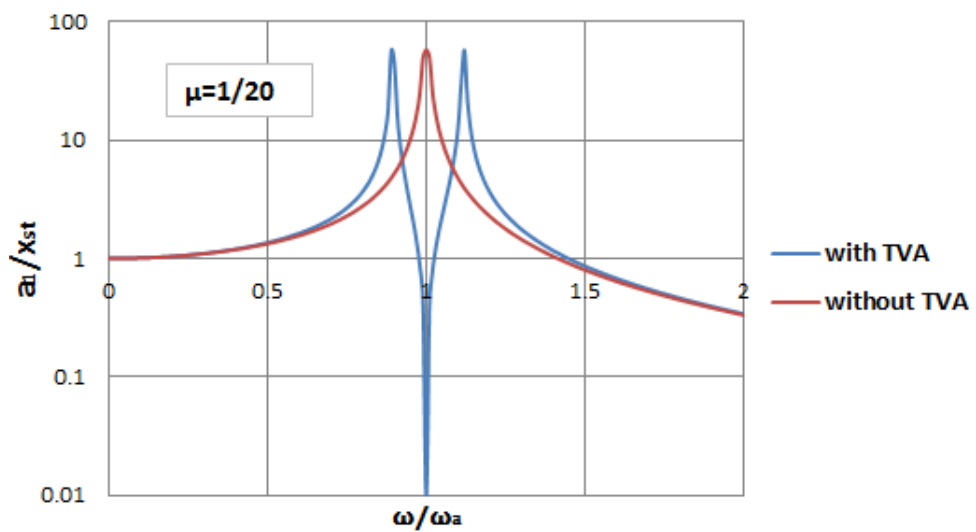


Figure 2-3: Vibration amplitudes of the main system with respect to various disturbing frequencies

2.1.2. The Damped Tuned Vibration Absorbers

If a dashpot is adapted to the system in Figure 2-1 by placing between the main mass M and absorber mass m , the equations of motion become [1]:

$$\begin{aligned} M\ddot{x}_1 + Kx_1 + k(x_1 - x_2) + c(\dot{x}_1 - \dot{x}_2) &= P_0 \sin \omega t \\ m\ddot{x}_2 + k(x_2 - x_1) + c(\dot{x}_2 - \dot{x}_1) &= 0 \end{aligned} \quad (\text{Eqn. 2.7})$$

where c is the damping coefficient of the tuned vibration absorber. The responses would be in harmonic form with a phase difference and can be written as in Eqn. 2.8. The equations of motion can be rewritten as in Eqn. 2.9 by assuming these responses:

$$\begin{aligned} x_1 &= a_1 e^{j\omega t} \\ x_2 &= a_2 e^{j\omega t} \end{aligned} \quad (\text{Eqn. 2.8})$$

$$\begin{aligned} -M\omega^2 \ddot{a}_1 + Kx_1 + k(a_1 - a_2) + j\omega c(\dot{a}_1 - \dot{a}_2) &= P_0 \\ -m\omega^2 \ddot{a}_2 + k(a_2 - a_1) + j\omega c(\dot{a}_2 - \dot{a}_1) &= 0 \end{aligned} \quad (\text{Eqn. 2.9})$$

The response of the main mass M , which we are interested in, can be derived from Eqn. 2.9 as follows [1]:

$$a_1 = P_0 \sqrt{\frac{(k - m\omega^2)^2 + \omega^2 c^2}{[(-M\omega^2 + K)(-m\omega^2 + k) - m\omega^2 k]^2 + \omega^2 c^2 (-M\omega^2 + K - m\omega^2)^2}} \quad (\text{Eqn. 2.10})$$

It is logical to write the Eqn. 2.10 in dimensionless form in order to express the response more easily. By making some simplifications, Eqn. 2.10 is written as follows [1]:

$$\frac{a_1}{x_{st}} = \sqrt{\frac{(2\frac{c}{c_c})^2 + (g^2 - f^2)^2}{(2\frac{c}{c_c}g)^2 (g^2 - 1 + \mu g^2)^2 + [\mu f^2 g^2 - (g^2 - 1)(g^2 - f^2)]^2}} \quad (\text{Eqn. 2.11})$$

where

$\mu=m/M$	(the mass ratio)
$\Omega_n^2=K/M$	(natural frequency of the main system)
$\omega_a^2=k/m$	(natural frequency of the absorber)
$g=\omega/\Omega_n$	(forced frequency ratio)
$f=\omega_a/\Omega_n$	(natural frequency ratio)
$x_{st}=P_0/K$	(static deflection)
$c_c=2m\Omega_n$	(critical damping)

Figure 2-4 represents the dimensionless amplitudes of the main mass response as a function of the forced frequency ratio (g). In this plot, the mass ratio (μ) is taken as $1/20$, the natural frequency ratio (f) is taken as 1 . From this figure, it can be seen that the response becomes as in Figure 2-3 when the damping ratio is zero and an SDOF system response is obtained when the damping ratio becomes infinity. If the other two values of damping (0.10 and 0.32) are examined, it is observed that the maximum response increases with increasing damping. Moreover, the target frequency which the response is desired to be minimized deviates from the resonance frequency with damping addition. Therefore, it can be said that there should be an optimum damping value between zero and infinity which is effective in a broad frequency range.

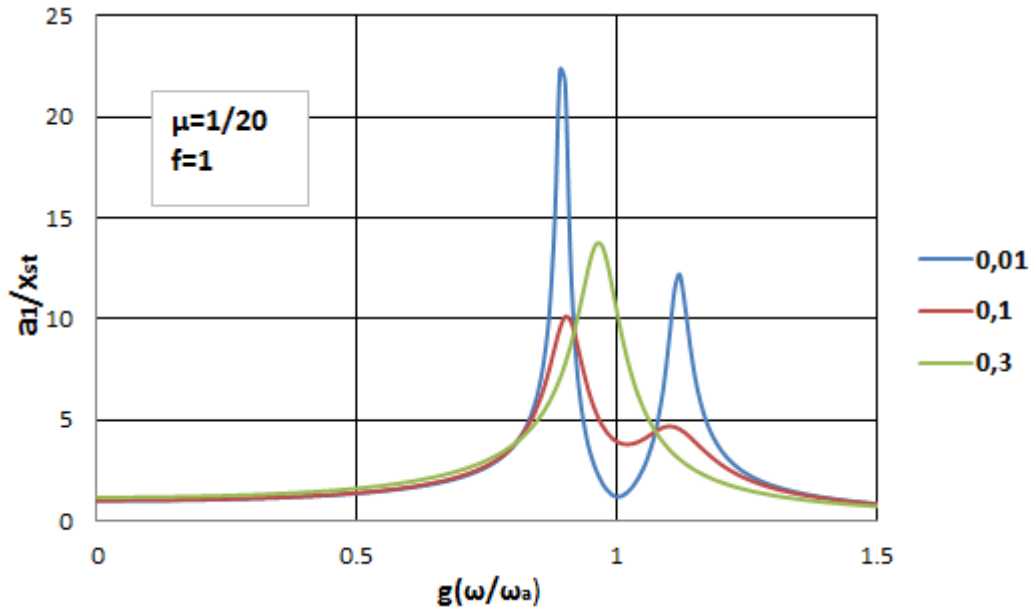


Figure 2-4: Responses of the main mass with respect to various damping values

From Figure 2-4, it is also observed that all of the curves pass through the same two points P and Q, regardless their damping values. Hence, the most effective response curve should also pass through these points and make a horizontal tangent with the higher one. Moreover, these points can be equalized by manipulating the target natural frequency ratio (f), thus there is also an optimum value for f . Performing some mathematical computations, this optimum value of the tuning can be found as a function of mass ratio as follows [1]:

$$f_{opt} = \frac{1}{1+\mu} \quad (\text{Eqn. 2.12})$$

Likewise, the optimum damping ratio is calculated in terms of the mass ratio μ as the result of long calculations as follows [1]:

$$\frac{c}{c_c} = \sqrt{\frac{3\mu}{8(1+\mu^3)}} \quad (\text{Eqn. 2.13})$$

Eqn. 2.12 and Eqn. 2.13 which are given above are found by Den Hartog who is the inventor of tuned vibration absorber theory and known as Den Hartog's equations. This theory is valid for an SDOF vibratory system. However, design of tuned vibration absorbers for the vibrations of multi degree of freedom systems more

complicated studies and researches may be necessary. In Section 2.4, some examples of these types of studies are presented.

2.2. TUNED VIBRATION ABSORBER DESIGN STUDIES FOR RESONANT VIBRATION PROBLEMS

Resonant vibration problems are caused by the nature of the structure rather than the external excitation. In this type of problems, vibration reduction is usually desired in the natural frequencies or around the natural frequencies of the structure. In this section of the literature survey, some examples of tuned vibration absorber design studies that give information about the control of resonant vibration problems are given.

In their studies, Özgüven and Çandır developed a method in order to find the optimum parameters of two SDOF dynamic vibration absorbers to suppress the first and second modes of a beam [2]. The main structure is taken as a cantilever beam with structural damping and two viscously damped vibration absorbers are proposed to minimize the vibration amplitudes of this beam which is excited by constant and frequency-squared harmonic forcing. The assumed-modes method is used to find the response of the beam.

At the beginning, the first absorber is tuned to the first resonance of the beam while the second absorber is tuned to the second resonance of the beam, theoretically. Then the parameters of the second absorber are kept as constant and parameters of the first absorber are optimized so that the minimum response is obtained for the first resonance. After that, the second absorber parameters are optimized to minimize the second resonance while the first absorber parameters are kept fixed. This procedure is repeated successively until the stable values are reached for both of the two absorbers. The free end of the beam is determined as the location where the response is to be minimized, thus the absorbers are to be attached. The results proved that the first absorber parameters are affected by the existence of the second absorber whereas the second absorber parameters are not affected from the existence of first absorber so much. It is also observed that the effect of an absorber to the mode which it is not tuned to becomes significant with decreasing mass ratio of that absorber.

In their studies, Zuo and Nayfeh employed the descent-subgradient algorithm in order to obtain the maximum minimal damping in a certain frequency range for a structure with a MDOF tuned mass damper or multiple SDOF tuned mass dampers [3]. Tuned mass damper parameters are calculated by using the minimax optimization approach based on the descent-subgradient method for a 2DOF system. Moreover, H_2 and H_∞ optimization methods, which require disturbance inputs on the system and outputs from the system, are employed to solve the same problem and the performances of these three methods are compared.

The minimax optimization method is also used by aiming to damp the first three flexural modes of a free-free beam [3]. Parameters of 3 DOF viscously damped TMD, 3 DOF hysteretically damped TMD and 3 SDOF viscously damped TMDs that are applied on 39-DOF discretized free-free beam are optimized by minimax method. Moreover, the three tuned mass damper parameters are calculated separately for the first three modes by using the classical Den Hartog method. The performances of these four methods are compared by considering the modal damping ratios achieved. It is observed that the 3DOF TMD with viscous damping provided the best damping performance.

An experiment is performed with a 2-DOF TMD designed by minimax optimization in order to damp the first two flexural modes of a free-free steel beam which the movement in the longitudinal direction is constrained. Optimized 2-DOF TMD is realized by flexures whose stiffness and damping values are adjustable. Tension of the blades is altered by adjusting screw to obtain the desired stiffness. Damping is provided by the fluid between cup and plunger and the damping coefficient is adjusted by moving the cup in vertical direction. The experiment is done by an impact hammer and force to acceleration transfer function is derived from the response at the tip of the beam. As a result of the experiment, the predicted damping for the first modes of the beam is approximated sufficiently.

In their study, Snowdon et al. [4] proposed the use of cruciform dynamic vibration absorber for vibrating structures and systems. The cruciform dynamic absorber consists of two beams having masses at their free ends and connected from their centers at right angles. It would be attached to the vibrating system from the junction

point of two beams. One of the branches is tuned to the first natural frequency of the vibratory structure while the second branch can be tuned to the second or third natural frequency or to the operating frequency of a machine exciting the vibratory structure. As a result, the cruciform vibration absorber can be used for the cases where the combined action of two absorbers is needed. Viscoelastic layer damping treatment can be applied to the beams of the absorber, thus the usage of viscous fluid damper is not necessary. This makes the absorber compatible for any orientation on the vibratory structure.

The cruciform dynamic absorber is theoretically applied to a simple mounting system, a centrally driven clamped-clamped beam and a clamped circular plate driven from its midpoint. For the simple mounting system, firstly both branches of the absorber are tuned to first resonance of the system and damped identically by considering three absorber mass ratios. Then one of the branches is remained as undamped and tuned to fourth, tenth and twenty-fifth multiples of the first resonance for three different mass ratios. Transmissibility graphs of these two cases shown that the resonance of the system is suppressed sufficiently, however new peaks arose in a narrow frequency band for the second case. For the clamped-clamped beam excited from its center, the absorber is proposed to be attached to the center of the clamped-clamped beam. One of the branches of the absorber is tuned to the first resonance while the other branch is tuned to second and tuned resonance respectively. It is seen that the transmissibility values at tuned frequencies is decreased efficiently. Moreover, the second branch is tuned to twice of the second resonance as the last case of clamped-clamped beam analysis. As the result, the first beam resonance again suppressed sufficiently and the newly formed peak due to the second tuning frequency is not significant. For the clamped circular plate driven by a sinusoidal excitation, the absorber is planned to attach to the excitation point since the vibrations are expected to be the highest here. The two branches of the absorber are damped and tuned to first and second, first and third, second and third resonances of the circular plate respectively. Finally, one of the branches is damped and tuned to the first resonance of the circular plate while the other branch is remained as undamped and tuned to 1.5 times the second resonance.

Vakakis and Paipetis [5] examined the effect of a viscously damped dynamic vibration absorber (VDDA) on a multi-degree of freedom vibratory system. They used the method of A_q polynomials, which is developed by them, in order to investigate the dynamic behavior of a multi-degree of freedom linear system which the upper half is connected to a viscously damped dynamic vibration absorber.

The method of fixed points, which assumes that certain frequencies exist for which the response of the system is independent of damping if the vibratory system has only one damping element between two of its positions, is employed for the optimization of VDDA and used within the expression derived for the force transmitted to the ground when a harmonic excitation is applied on the upper mass of the MDOF system. By means of this optimization procedure, the minimization of transmissibility is aimed. For that purpose, the parameters of absorber's natural frequency ratio to the main system ($\alpha=\omega_a/\omega_0$) and absorber damping ratio ($\zeta=c_a/2(K_a m_a)^{1/2}$) is used.

Firstly α parameter is optimized in the range of 0.1-1.5 for mass ratio of $\mu=0.5$ and in the paths followed by three fixed points. The optimum value of α is obtained as equal to 0.463 for which the transmissibility ratios of three fixed points reach the possible minimum values combination. Moreover it is derived that the optimum value of α can be approximated by the relation of $\alpha_{opt}=(6+5\mu+\mu^2)/(10+15\mu+7\mu^2+\mu^3)$ for a two degrees of freedom system with one VDDA. Secondly, the damping ratio of absorber (ζ) is determined for the mass ratio of $\mu=0.5$ and absorber frequency ratio of $\alpha=0.463$. Optimization procedure of damping ratio results in two damping values. First optimum damping ratio is $\zeta=0.326$ and it targets the maximum values of first two fixed points. The second appropriate damping ratio is found as $\zeta=0.5246$ and this ratio makes the maximums of the responses at low and high frequencies equal.

For the application of this analysis, an anti-vibration mounting is designed in order to isolate the ground from the vibrations of the rotating machinery that are caused by its potential unbalance. Due to symmetry reasons the dynamic absorber is split to two parts with parameters of $m_a/2$, $K_a/2$ and $c_a/2$. Damping is provided by a silicone-filled cylinder with a piston moving inside. The mass of absorber (m_a) is connected to this piston. The upper mass of the main system (m) is the mass of the machine and its

base, the lower mass is also equal to m . Lower and upper masses are connected with springs with constant K and also the whole system is supported on the springs with constant K via steel rods.

Pombo and Laura [6] investigated the usage of two dynamic vibration absorbers for a laboratory model where the forcing excitation is in the form of $F(t) = \sum_{i=1}^2 F_i \cos \omega_i t$. Here, the forcing frequencies ω_1 and ω_2 are almost equal to the lowest natural frequencies of the system.

A gear mechanism driven by an electric motor produces sinusoidal forces with frequencies of $f_1=5.45$ Hz and $f_2=8.85$ Hz. Two steel disks enable the variation of two lowest natural frequencies of the system. This system yield in two modes; first is the translational mode along y -axis with natural frequency of 5.45 Hz and the second is the rotational mode around the vertical axis with a natural frequency of 8.85 Hz. As a result of experiments, four new natural frequencies arise because of the DVAs. In addition, two peak amplitudes of 1.2 mm and 0.53 mm decrease to 0.31 mm and 0.02 mm due to the presence of two dynamic vibration absorbers.

2.3. TVA DESIGN STUDIES FOR SLENDER STRUCTURES

Since their natural frequencies are quite low, slender structures exhibit vibratory behavior under any type of excitation. Their oscillatory behavior is usually caused by the transverse modes. In this part of the literature survey, TVA design studies performed to overcome the transverse vibrations of the slender structures are examined.

First study of this section is about the TVA application on a gun barrel which suffers from the oscillatory behavior due to firing event. Kathe et al. [7] investigated the effect of mounting a vibration absorber to a gun barrel's muzzle brake. In this study, a model is created via MATLAB[®] software for the plain gun barrel, then it is verified with the aid of modal impact testing that is performed on the real gun barrel. MATLAB model and modal impact test results are summarized in Table 2-1:

Table 2-1: Modal test and MATLAB results for the plain gun barrel [7]

Mode	Magnitude (Test)	Natural Frequency (Test)	Coherence (Test)	Natural Frequency (MATLAB model)
	dB(g/lbf)	(Hz)		(Hz)
1	-10.87	60.25	0.9990	59.03
2	-24.71	167.25	0.9543	168.34
3	-10.008	304.5	0.9306	322.62
4	-24.71	448.25	0.9314	518.79

After the plain barrel is modeled and tested, a vibration absorber is modeled and tested in order to see its effect on the frequency response of the barrel. The vibration absorber basically consists of a 1,831 kg mass which is suspended from spring rods that are attached to a collar. This collar is press-fitted onto the muzzle brake. The spring rods are 6,35 mm in diameter and 147,32 mm in length.

Four-rod and eight-rod vibration absorber combinations are modeled and run via MATLAB. Meanwhile, modal impact testing is applied for eight rod, four rod and two rod versions. Modal test and MATLAB model results for the gun barrel with these vibration absorber configurations are presented in Table 2-2 (Full: eight-rod; half: four-rod; quarter: two-rod). According to these results, it is observed that the first two modes are shifted to higher frequency while the other modes do not change at all. Besides, the two-rod version yields the maximum reduction in the response magnitude (3 dB reduction).

Table 2-2: Modal impact testing results with vibration absorber [7]

Full Vibration Absorber				
Mode	Magnitude (Test)	Natural Frequency (Test)	Coherence (Test)	Natural Frequency (MATLAB model)
	dB(g/lbf)	(Hz)		(Hz)
1	-28.642	38.5	0.9937	35.19
2	-10.614	71.25	0.9991	72.64
3	-29.886	168.5	0.9887	169.95
4	-9.323	307.0	0.9139	319.01
5	-9.513	456.25	0.8915	499.48
Half Vibration Absorber				
Mode	Magnitude (Test)	Natural Frequency (Test)	Coherence (Test)	Natural Frequency (MATLAB model)
	dB(g/lbf)	(Hz)		(Hz)
1	-27.683	31.25	0.9998	29.28
2	-10.793	64.5	1.0000	65.04
3	-27.711	169.75	0.9993	169.27
4	-6.541	304.0	0.8724	322.43
5	-6.054	460.75	0.8821	516.28
Quarter Vibration Absorber				
Mode	Magnitude (Test)	Natural Frequency (Test)	Coherence (Test)	
	dB(g/lbf)	(Hz)		
1	-29.94	25.5	0.9996	
2	-13.033	62.5	0.9995	
3	-24.251	169.5	0.9777	
4	-8.395	304.75	0.8640	
5	-6.412	458.5	0.8528	

The US Patent 6167794 comprises two types of vibration absorber for gun barrels [8]. First vibration absorber type simply consists of a mass-spring device and it is attached to a location on the gun barrel where the vibration activity is the most important. Here, the TVA is attached to the tip of the gun barrel since the vibration amplitudes are the highest. Ground ended compression springs are used for this vibration absorber which are at pre-compressed state. In the second type of TVA discussed in US Patent 6167794 thermal shrouds of the gun barrel are used as the inertia elements. Stiffness elements of the vibration absorber are the springs that connect the free end of the thermal shroud to the gun barrel. The vibration absorber includes a dynamically tunable spring collar which is fixed to the end of the shroud and it enables the relative motion between the muzzle ends of the thermal shroud and gun barrel. The springs are pre-compressed to provide the concentricity of thermal shroud and gun barrel centerlines and maintain the contact between barrel muzzle and spring collar.

In Büyükcivelek's thesis study, gun barrel vibrations which are caused by the ground excitation are taken into consideration [9]. In order to reduce the vibration levels of the longer gun barrel to the short gun barrel, tuned vibration absorber design is proposed. In the design process, verified finite element model of the gun barrel and PSD data of the ground excitation are used as inputs and tip displacement of the gun barrel is chosen as output. From the PSD data, it is found that the first resonance of barrel dominates the response of gun barrel, thus the tuning frequency of the TVA is chosen around the first mode of the barrel. Firstly, harmonic analyses are run on the FE model of the gun barrel in order to examine the TVA mass effect. Then, spectrum analyses are run by applying the input PSD data in order to optimize the mass and damping parameters of TVA. After the identification of TVA parameters, conceptual TVA design solutions are researched that would satisfy these parameters. A spring-mass-damper type of TVA is selected as the best alternative solution. In this solution, two helical springs are used as the stiffness elements and a dashpot is employed as the damping element of TVA.

Bonsel, Fey and Nijmeijer [10] applied a linear dynamic vibration absorber (i.e. tuned vibration absorber) to a piecewise linear beam system to suppress its first resonance. This system consists of a steel beam which is supported by leaf springs and a second beam at the middle of the beam. A pin is attached to this second beam and it contacts with the main beam when it has a negative deflection. As a result it behaves as one-sided spring. There exists rotating machinery at the middle of the beam which produces an excitation at 60 Hz. The tuned vibration absorber which consists of two cantilever beams and two masses of 0.5 kg at its ends is applied on the beam system. By moving the masses along the beam the stiffness of TVA can be tuned precisely. The eigenfrequency of TVA is tuned to 19 Hz which is the first harmonic resonance of the beam system. Firstly, undamped TVA is applied to the piecewise beam system and anti-resonance is observed at this resonance frequency whereas new resonances arise around this anti-resonance. After that, certain amount of damping is added to the TVA system and it is seen that the newly formed resonances are also suppressed.

Gu, Chang and Xiang proposed the use of tuned mass dampers in their studies, in order to increase the flutter wind speed of a long-span bridge [11]. They derived the equations of motion of the bridge with TMDs and employed the Routh-Hurwitz stability criterion to examine the aerodynamic instability of the bridge. For the experimental study, a sectional model of Tiger Gate Bridge, which is a steel box deck suspension bridge in China, is tested in a wind tunnel and the numerical results are verified by this way. The effects of structural damping of the bridge, the frequency and mass inertial moment inertia ratios of the tuned mass dampers to the bridge are examined to see how they are effective on the flutter control of bridge.

Two identical tuned mass dampers are located at the two sides of the cross section at the center of the bridge. In this way, the TMDs can yield counter moment to suppress torsional vibrations. The TMD frequencies are tuned as very close to the flutter frequency so that the critical flutter wind speed increase. TMDs consist of two springs, two mass blocks and a pendulum-container system as the damping device. The upper plates of TMDs are rigidly connected to the bridge.

Ten sets of TMD parameters (ratio of mass moment of inertia, frequency ratio and damping ratio) are investigated. Moreover, three different structural damping ratios (%0.7, %2.13 and %4.05) for the bridge are examined. It is seen that the TMDs having the mass moment of inertia ratio between %5.6 and %10 can increase the flutter speed significantly. It is also concluded that the tuned mass dampers are more effective on flutter speed when the structural damping of the bridge is low. Finally, it is found that the frequency ratio of TMDs to the bridge and the damping ratio of TMDs affect the flutter speed control, however, the frequency ratio is more effective than the damping ratio.

2.4. VARIOUS TYPES OF TVA APPLICATIONS

There are several types of tuned vibration absorber applications which have different constructions, use various damping types, stiffness elements etc. In this section of the literature survey of various types of TVA applications found from the field research are presented.

In their studies, Hill, Snyder and Cazzolato designed a dogbone vibration absorber in order to suppress several modes of vibration rather than single target frequency [12]. In other words, the vibration absorber is developed to facilitate the vibration absorption at multiple resonance frequencies. This type of vibration absorber is also called as “dual mass absorber”. It consists of two rods supporting two masses at the ends. One of these rods is smooth and the other rod is threaded. The threaded rod is rotated with a motor to move the masses, thus the TVA resonances are altered by this movement.

The first six mode shapes of TVA are obtained via finite element analysis and it is observed that the mode pairs 1-2, 3-4 and 5-6 have similar motion characteristics. However, the masses move in phase in the modes 1,3,5 and out of phase in the modes 2,4,6. The close proximity of these mode pairs are also seen from the modal frequencies. This relation between the pairing modes is important for expanding the bandwidth of the absorber.

In his study, Dr. Lamb [13] sought to design a tuned vibration absorber in order to suppress the vibrations of the control room of a CaCl_2 plant which the working staff

suffers. For this purpose, firstly the power spectrum of the vibration data is obtained considering the sources of peak amplitudes. According to this power spectrum, the main reason of discomfort is the motion occurring at around 3.5 Hz (sway mode) and it should be reduced by %70. According to the frequency response for the motion of control room, it is seen that the sway motion is magnified by factor of 85 relative to foundation motion.

A cantilever type tuned vibration absorber is found as appropriate for this structure. Three locations are selected on the columns of frame for the TVA application. In order to achieve a desired mitigation in a narrow band of 1 Hz, the optimum tuned vibration absorber mass found as 1500 lbm. This value is computed by considering the optimum damping ratio. Various combinations of TMD flexure bar lengths and constrained-layer viscoelastic damping materials are investigated in order to find the best combination. SBR Rubber layers and a flexure bar of 950 mm are found as the best combination which provides %12 damping ratio.

Vibration levels in the control room are measured and compared with the vibration levels before TMD application. It is seen that the vibration amplitudes are reduced below 0,005 g limit which results in a significant improvement of staff's comfort.

Mirsanei et al. [14] developed an adaptive tuned dynamic vibration absorber (DVA) based on a slider crank mechanism. This DVA design is applied to reduce the vibration amplitudes of a vibratory resonant beam. The base structure is selected as a simply supported beam including a motor with rotary disc. The beam is fixed with a fixed joint from one end and a roller joint from another end. The motor is connected to a speed control unit in order to change the speed of rotation so that the vibration force can be varied. The masses attached to the links of mechanism are moved by means of a servo motor until the system is tuned.

As a result of the experiments, it is seen that the adaptive tuned DVA could decrease the rate of vibration in every forces acting by changing the speed of motor and rotary disc. However with DVA which is not adaptive and tuned to one excitation frequency, the primary system becomes two DOF. Therefore, if the machine operates

at other frequencies or if the forcing on the machine has several frequencies the vibration amplitudes may become large.

Maly and Napolitano [15] proposed the design of a magnetic tuned-mass damper to suppress the airfoil vibrations (i.e. buffet) of an aircraft which are caused by vortex flow during the high angle-of-attack maneuvers. Buffeting of twin vertical tails of the aircraft excites the bending and torsional modes. Therefore the TMD's are decided to place at the top of the vertical tails. Analysis shown that 10-pound TMD is required; however, because of the space limitations due to the TMD motion, the TMD is divided into ten parts each weighing one pound. For damping mechanism, rare-earth magnet configuration is selected since the viscoelastic materials would not stand to the dynamic environment of the aircraft and highly affected from the temperature variations.

Fundamental natural frequencies of the structure are predicted via finite element analysis as 15 Hz for the bending mode and 43 Hz for the torsion mode. It is seen that the buffet pressure PSD peaks in the frequency range of 10-50 Hz. Therefore the 15-Hz bending mode is targeted for the design of TMD.

A prototype TMD is designed which consist of mechanical springs, a mass and magnets moving relative to a conductor, thus provide damping. Firstly the transmissibility of TMD is measured in order to measure the natural frequency and damping of the TMD. Then a cantilever beam is employed as a base structure which the bending mode frequency approxiately equal to the bending frequency of the aircraft vertical tail and frequency responses are found for with and without TMD cases. A 48"×4"×1" aluminum beam which has a bending frequency of 13,5 Hz at cantilevered condition is used and the TMD is bolted to the beam. Random excitaton is applied to the beam from the attachment point of TMD. It is seen that the original 13,5 Hz mode is separated into two modes at 10,9 Hz and 15,7 Hz. Moreover the amplitude of the response is reduced by 20 times.

Sayyad and Gadhave [16] investigated the effect of a magnetic vibration absorber on a cantilever beam which is subjected to harmonic excitation whose frequencies are varying. The vibration suppression is tried to achieve by changing the position of

magnetic vibration absorber along the beam. Magnetic vibration absorber is made from three magnets with two poles facing each other set in front of each other. The intermediate magnet acts as mass element and the repelling forces acting on it acts as the restoring force.

Stiffness and natural frequency of the absorber change according to the distance between magnets. The main system which the absorber will be applied is a cantilever beam whose the first natural frequency is 42,6 Hz. Therefore, magnetic absorber is tuned to change the natural frequency from $0,8 f_n$ (34,08 Hz) to $1,2 f_n$ (51,12 Hz), so the distance between magnets is chosen as 70 mm.

The experimental studies are performed with a cantilever beam which is clamped to a rigid support and the absorber is clamped to the free side of the beam. The cantilever beam is excited by means of an exciter and the excitation frequency is gradually increased. For each frequency the vibration amplitude of the main system is measured. Then the position of the absorber along the beam is changed and the excitation frequency is increased again. This procedure is repeated for a number of positions of absorber along the beam. As a result of these experiments, it is observed that the amplitude of vibrations is reduced from 2390 microns to 260 microns with the magnetic vibration absorber addition.

Harris F.A. investigated the use of one 2-DOF vibration absorber and two SDOF vibration absorbers for the control of structural vibration of a mock payload cylinder [17]. For this study, a scaled cylindrical model of a payload fairing is used. Target frequencies are chosen as 62 Hz and 139 Hz by considering the frequency response data obtained experimentally. A large separation between two target frequencies is sought due to the high damping of the foam used in DVAs as stiffness and damping elements.

Firstly two 1DOF DVA design parameters are specified in order to achieve the closest resonance frequencies. Then stacked 2DOF DVA parameters are developed so as to achieve the equal impedance with two SDOF design by considering the limitations specified above. DVAs consist of foam blocks which are used as the spring-damper elements and steel plates which are used as the mass elements.

Besides, small nuts are added to the top plate for tuning the DVAs to resonant frequencies to within 2-3 Hz of the targeted frequencies.

After designing the DVAs as explained above, they are attached to interior of the cylinder radially. Totally 4 kg of DVAs are added to the cylinder which is 1/20 of the total mass of cylinder. A shaker is used to excite the system and totally 30 accelerometer are used to measure the structural vibrations. As a result of the experiments, the average of the squared transfer functions of all 30 accelerometer measurements in velocity per input force to the cylinder are obtained. According to these results, it is observed that the peaks around the target frequencies 62 Hz and 139 Hz are reduced by 19 dB and 9 dB respectively.

CHAPTER 3

DESCRIPTION OF THE VIBRATION CONTROL PROBLEM

In this chapter, the representative physical structure under consideration which involves a supported hollow cylindrical component is described and the dynamics of this structure is explored.

In Section 3.1, the physical design and the finite element model constructed for this structure are explained with details. Vibration problem of this structure and its main causes are presented in Section 3.2. In the last section, experimental verification of the finite element model is presented.

3.1. DESCRIPTION OF THE PHYSICAL STRUCTURE

A sample physical structure which includes a supported hollow cylindrical component is designed as shown in Figure 3-1. In this model, supported hollow cylindrical structure is called as the ‘tube’ part. Tube part stands on two legs and an interface part is attached to tip of the tube in order to excite the structure from there. Legs are connected to the foot plate parts which are fixed to the ground.

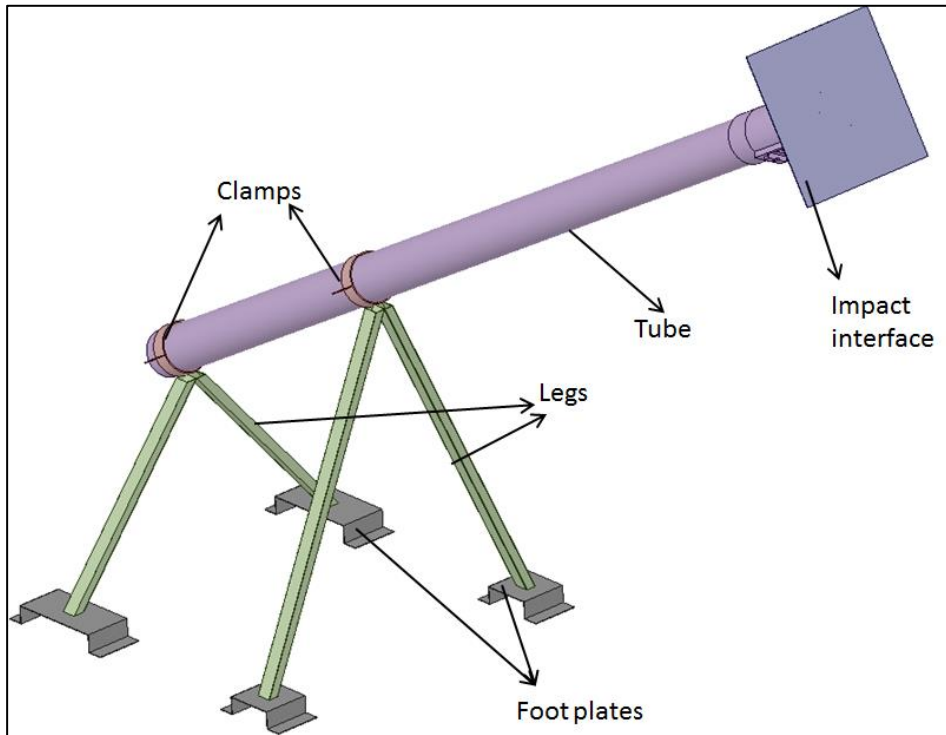


Figure 3-1: CAD model of the sample physical structure

Foot plates are made of thin metal sheets in order to make the structure flexible so that it can be easily excited. Firstly, the back and front foot plates are estimated to have the same dimensions. However, it is seen that the natural frequencies of the two transverse modes are very close to each other. Therefore, the length of back foot plate is increased so that a certain amount of difference between the two transverse modes can be obtained and they can be suppressed together. Final optimized dimensions of the back and foot plates are presented in Figure 3-2. As seen in this figure, lengths of the back and front foot plates are different while the other dimensions are the same. Thickness of the foot plates is adjusted to 1 mm and the material of foot plates are selected as St-37 steel.

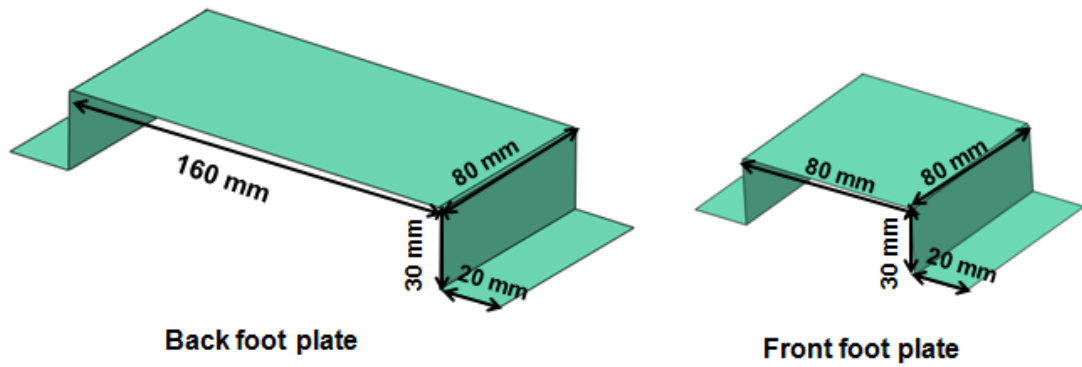


Figure 3-2: Optimized dimensions of the back and front foot plates

A prototype of the physical structure is fabricated as demonstrated in Figure 3-3. Foot plates are shown in red boxes in this figure and they are fixed to the ground with four M8x20 bolts. In the assembly, leg parts are welded to the foot plate and clamp parts. Impact interface part is glued to the tube. Clamps are tightened on the tube with two screws located on two sides of the clamps. Thin rubber layers are placed between the clamps and tube in order to spread the tightening force. Details of the connection between clamps and the tube are shown in Figure 3-4.

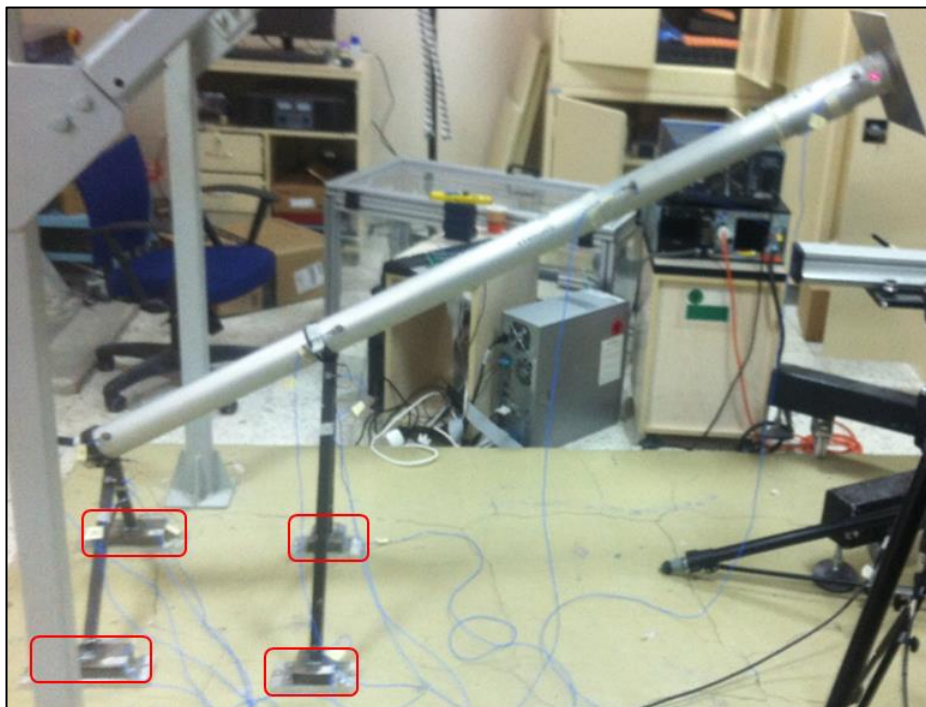


Figure 3-3: General view of the fabricated structure

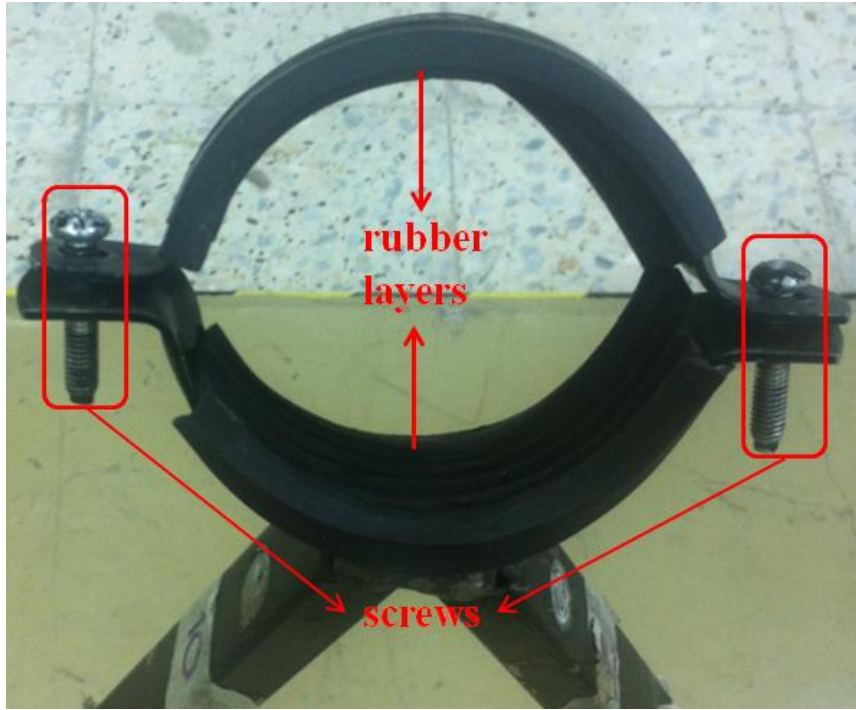


Figure 3-4: Clamp-tube connection detail

Modal analyses are performed using the finite element model of the physical structure prepared in ABAQUS[®] software. These modal analyses are done with the Lanczos eigensolver option of the ABAQUS. Lanczos method is the default eigenvalue extraction method of the ABAQUS since it has the most general capabilities [18]. The eigenvalue extraction problem for an undamped finite element model can be stated as follows:

$$(-\omega^2 \mathbf{M}^{MN} + \mathbf{K}^{MN})\boldsymbol{\varphi}^N = \mathbf{0} \quad (\text{Eqn. 3.1})$$

where \mathbf{M}^{MN} denotes the mass matrix, \mathbf{K}^{MN} denotes the stiffness matrix and $\boldsymbol{\varphi}^N$ is the eigenvector. M and N denotes the degrees of freedom [18].

Finite element model of the physical structure consists of 47073 nodes, 38227 elements and a total of 230133 degrees of freedom. All parts are modelled using shell elements since their thicknesses are small with respect to other dimensions. The S4 (four-node doubly curved general-purpose shell) elements in the ABAQUS element library are used while the mesh structure is built. General mesh structure can be seen in Figure 3-5.



Figure 3-5: General mesh structure of the physical structure

All mechanical connections between the different parts of the structure are modelled with the ‘TIE CONSTRAINT’ option of the ABAQUS. With this option, the parts are connected from all degrees of freedoms. These connections are shown in Figure 3-6. For simplicity, screws on the clamps and bolts on the foot plates are not involved in the finite element model. The model is fixed from the foot plates by using the ‘ENCASTRE’ boundary condition option of ABAQUS as shown in Figure 3-7.

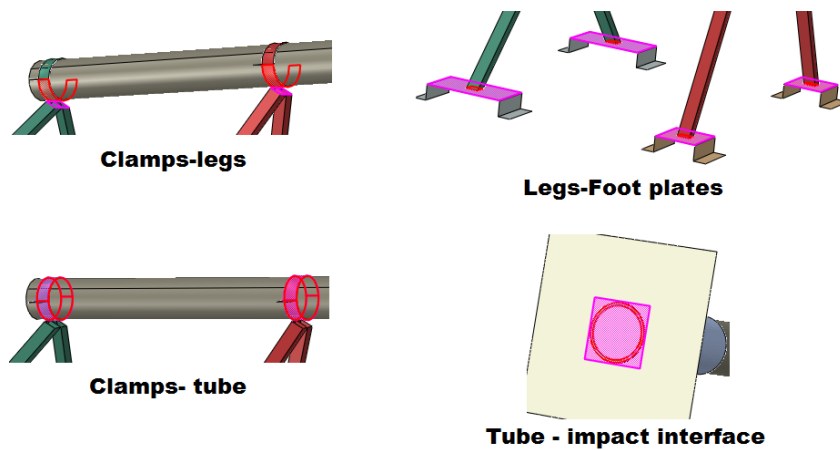


Figure 3-6: Tie constraints between the parts of physical structure

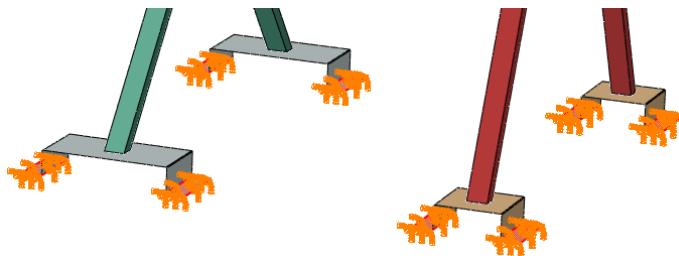


Figure 3-7: Fixed boundary condition regions

Mode shapes of the structure which are calculated using the FEA model are given in the Figure 3-8, Figure 3-9 and Figure 3-10. In these figures mode shapes are presented with deformed and undeformed cases. Modal frequencies corresponding to each of the modes are also presented in Table 3-1.

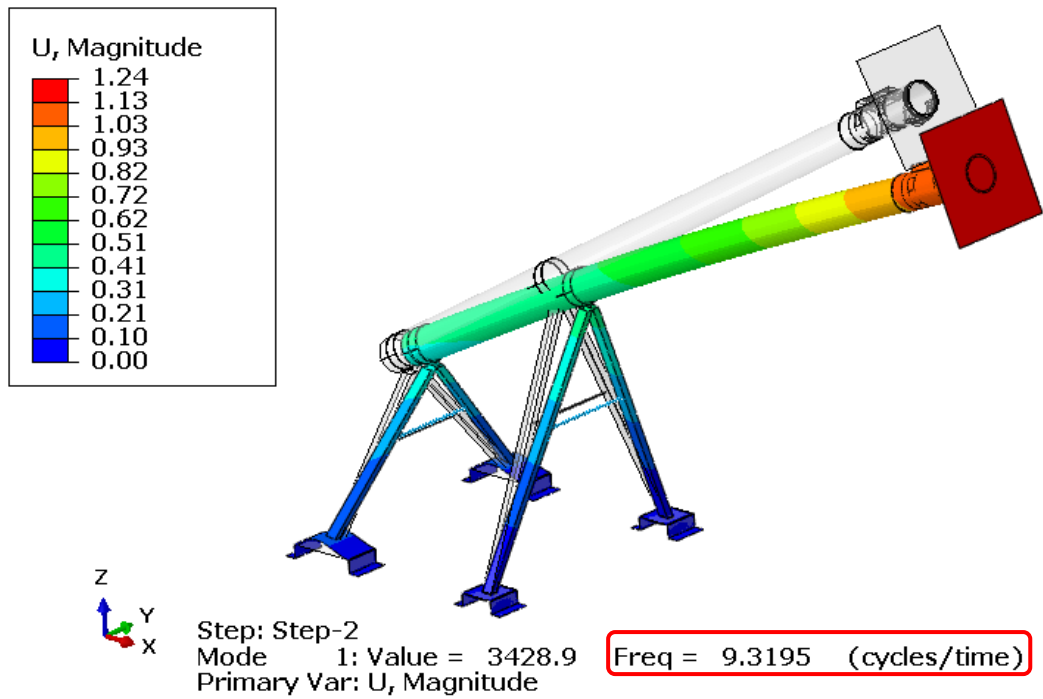


Figure 3-8: 1st mode (tip-off) of the prototype (FEA result)

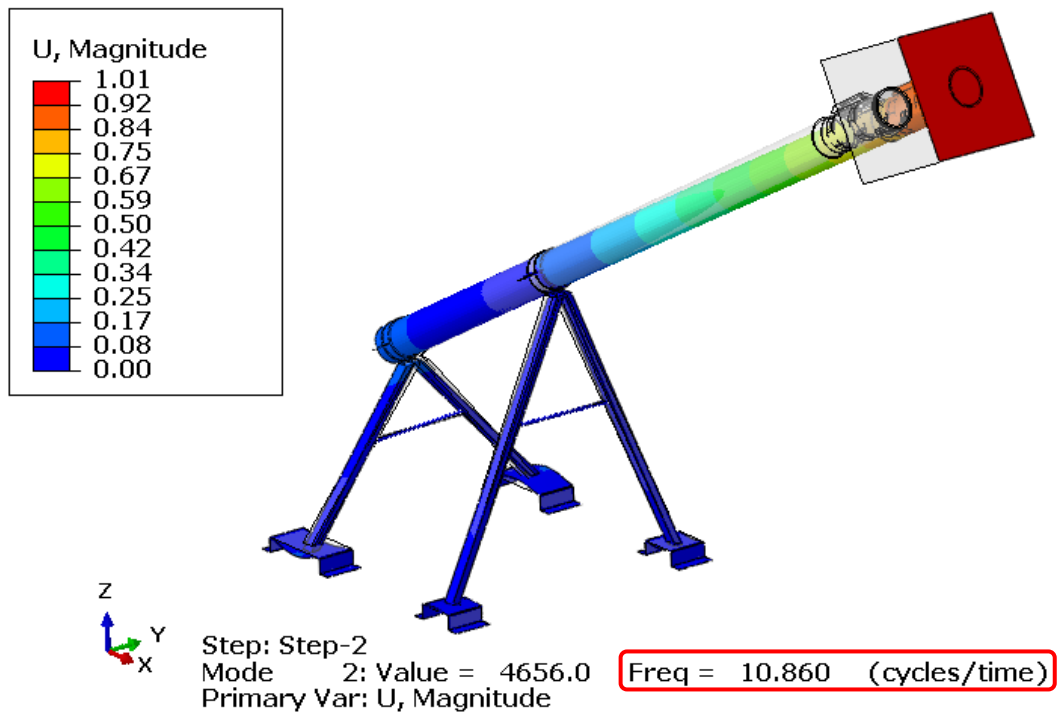


Figure 3-9: 2nd mode (side-off) of the prototype (FEA result)

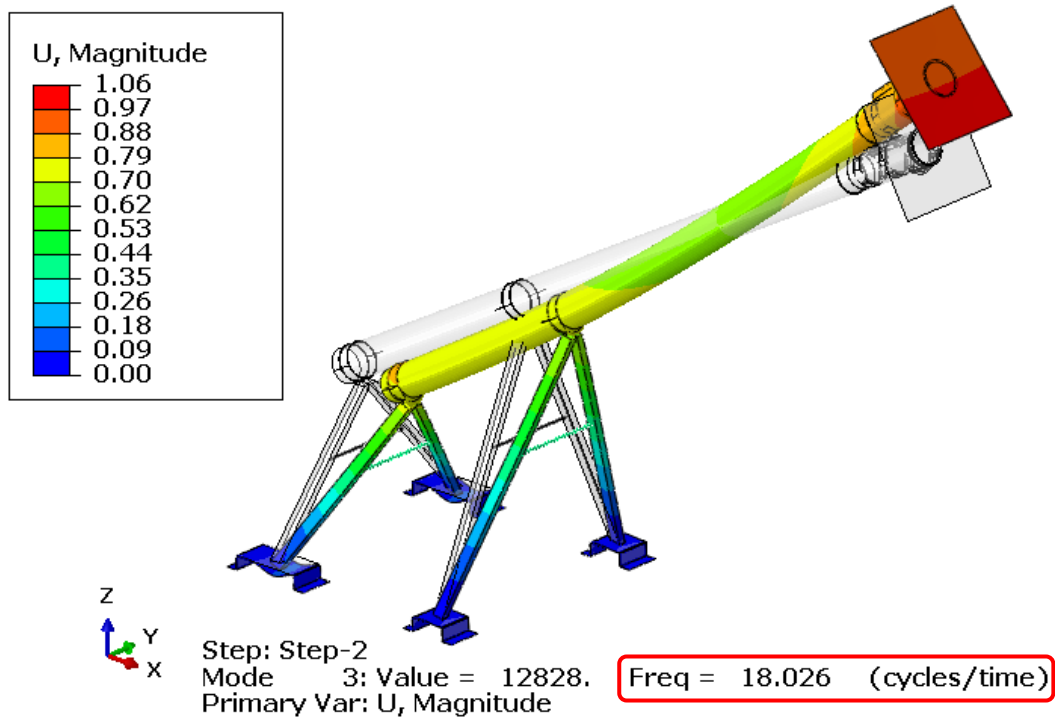


Figure 3-10: 3rd mode of the prototype (FEA result)

Table 3-1: Modal analysis results obtained from FEA

	Modal frequency (Hz)
Mode 1 (tip-off)	9,320
Mode 2 (side off)	10,860
Mode 3	18,026

3.2. DEFINITION OF THE VIBRATION PROBLEM

The vibration response of the physical structure which are targeted to be reduced, are expected to be caused by an impulsive loading applied in normal direction through the impact interface. Due to the impulsive loading, the system is excited over a wide range of frequencies up to a certain frequency level. For that reason, vibratory response of the cylindrical component of the structure is expected to be dominated by the response around the natural frequencies of system; and the vibration problem under consideration is essentially a resonant vibration problem. As a result, two dominant transverse modes of the physical structure are targeted for vibration suppression using a tuned vibration absorber.

For this structure, main contribution to vibrational deformation pattern of the two transverse vibration modes is the flexibility of the supporting foot plates rather than the bending of the tube. Therefore, rigid body-like motion of the tube is more dominant on these two transverse modes rather than the structural (bending) motion. From the modal analysis results, it is observed that these two transverse modes are almost perpendicular to each other (See Figure 3-8 and Figure 3-9). Moreover, modal displacements are at their maximum at the tip of the structure for both modes. Therefore, tuned vibration absorber design is performed by aiming to minimize the tip response of the structure for each the two transverse modes. Target vibration reduction metric is chosen as the magnitude of harmonic displacement value at the tip of the structure. This value will be computed from the resultant of harmonic displacement results obtained in three degrees of freedoms.

3.3. VALIDATION OF THE FINITE ELEMENT MODEL OF THE STRUCTURE

In order to validate the finite element model of the physical structure, experimental frequency response measurements are carried out on the physical prototype and modal parameters are identified experimentally to be compared with analysis results. These tests are performed in laboratory environment. Accelerometers used during modal tests are numbered and located on the physical structure as shown in Figure 3-11. As it can be seen from this figure, a total of 13 accelerometers are used during modal tests.

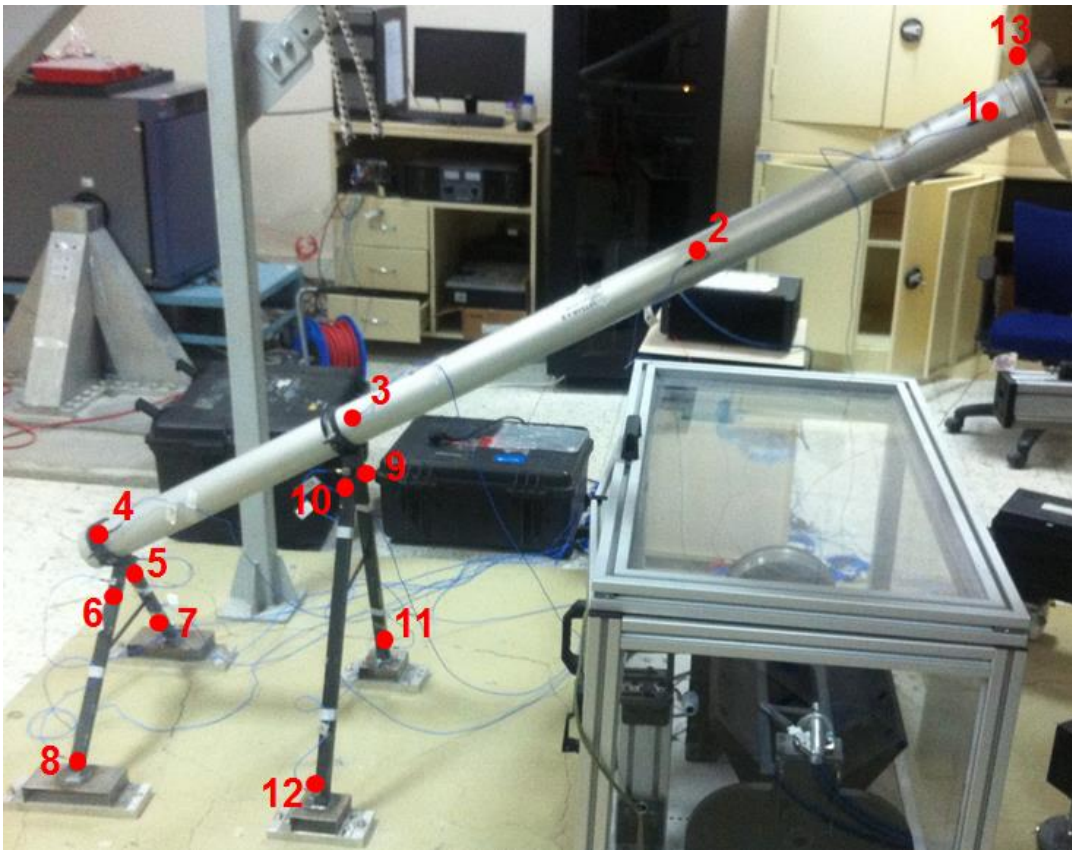


Figure 3-11: Accelerometer locations on the physical structure

Modal tests are performed by means of an impact hammer using a suitable tip which is capable of applying an excitation force up to 500 Hz (See Figure 3-12). Technical specifications of this impact hammer are presented in Appendix B: Technical Specifications of the Impact Hammer [20]. Hammer strikes are applied from the tip of the physical structure as shown in Figure 3-13. Sample force-time data obtained during the modal tests is shown in Figure 3-14.



Figure 3-12: Impact hammer used in the modal tests



Figure 3-13: Excitation location

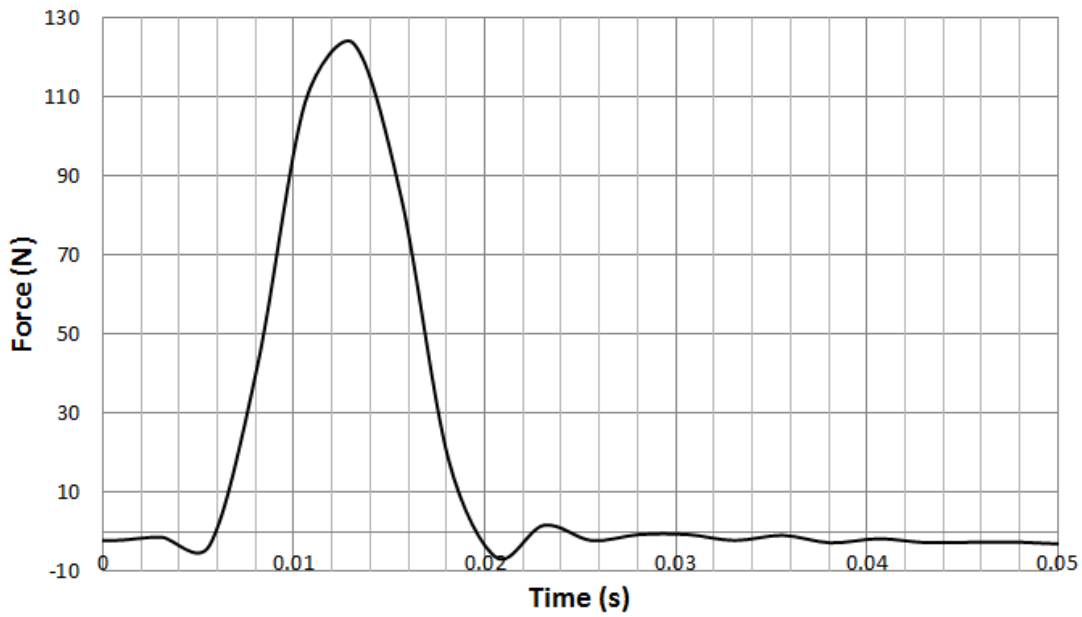


Figure 3-14: Sample force-time data obtained during modal tests

LMS hardware is used during the tests and ‘IMPACT TESTING’ module of the LMS Test LAB software is employed. The LMS equipment used during the test is shown in Figure 3-15.



Figure 3-15: LMS hardware used in the modal tests

Triaxial ICP[®] type accelerometers produced by the PCB Piezotronics company are used. Technical specifications of these accelerometers are presented in Appendix A: Technical Specifications of the Accelerometers [21]. An example of these accelerometers can be seen in Figure 3-16. A sample acceleration-time data obtained from the accelerometer located at driving point is demonstrated in Figure 3-17.



Figure 3-16: PCB accelerometers

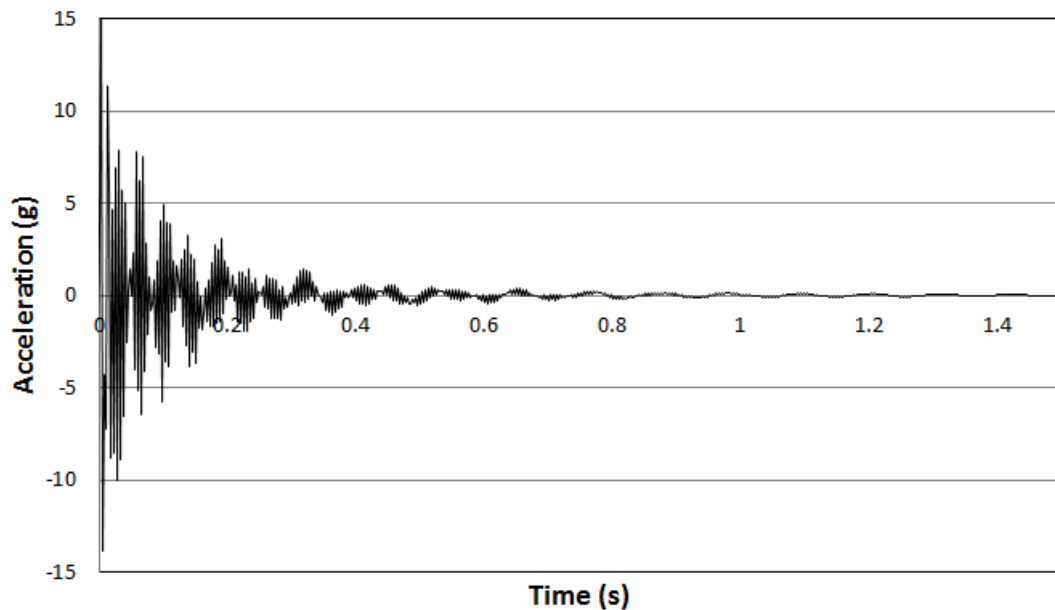


Figure 3-17: Sample acceleration-time data obtained during modal tests

Modal tests are performed with 400 Hz sampling frequency and 0.097656 Hz frequency resolution. As a result of the modal tests, the mode shapes shown in Figure 3-18, Figure 3-19 and Figure 3-20 are identified. Modal frequencies are presented in red boxes of the figures.

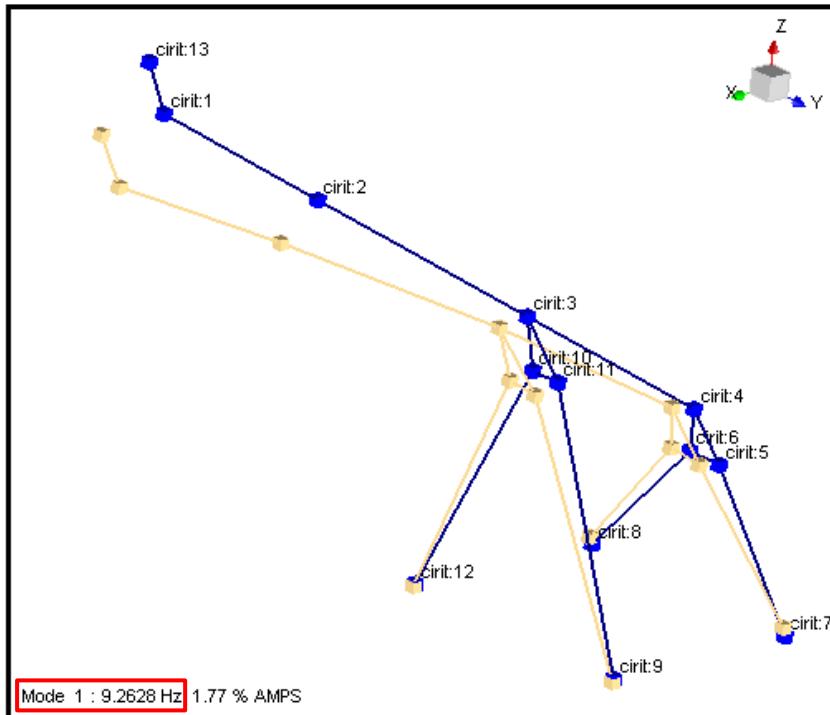


Figure 3-18: 1st mode (tip-off) of the prototype (test result)

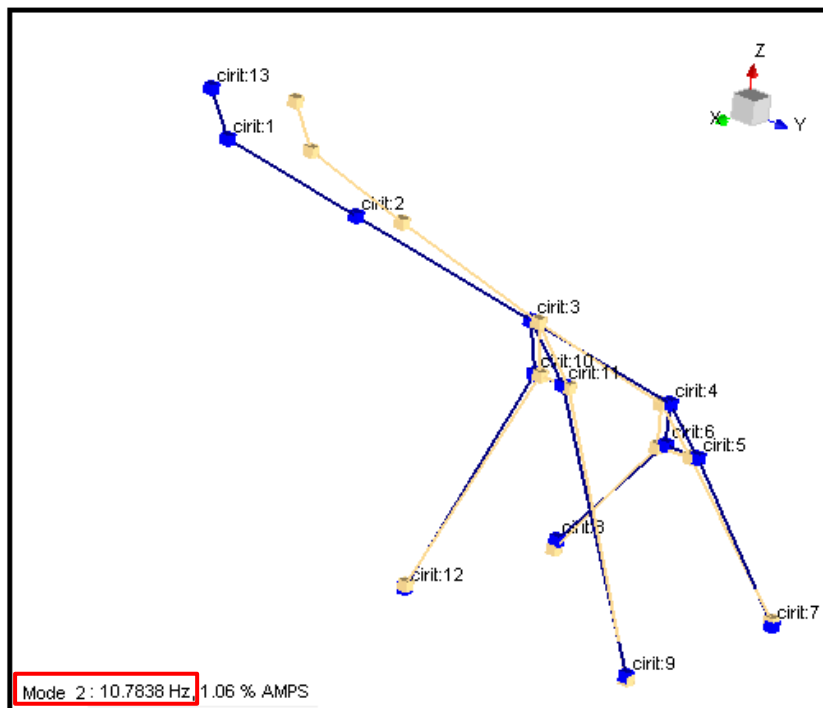


Figure 3-19: 2nd mode (side-off) of the prototype (test result)

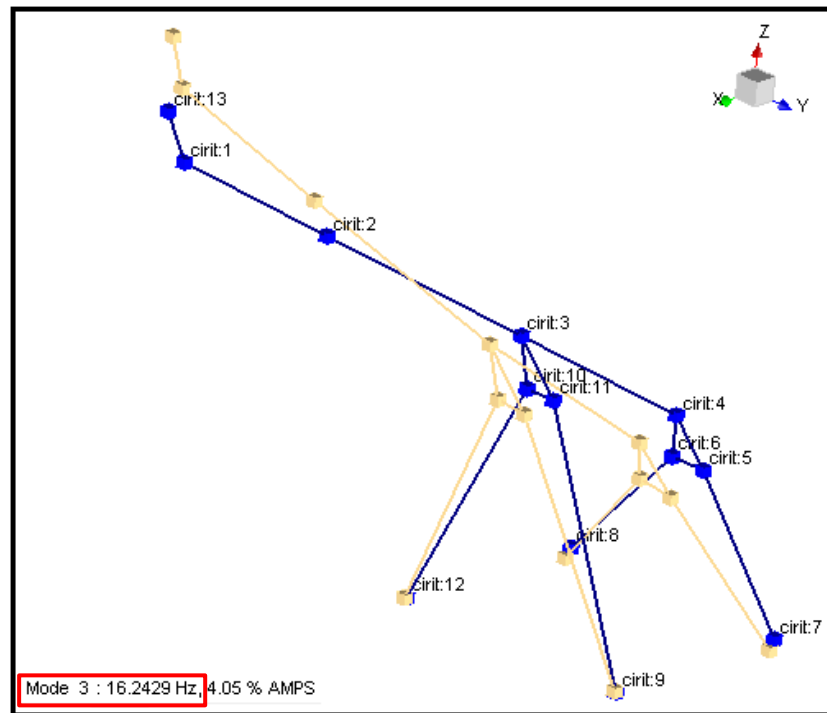


Figure 3-20: 3rd mode of the prototype (test result)

Sample coherence function and the corresponding frequency response function obtained from the driving point accelerometer (See Figure 3-21) are shown in Figure 3-22 and Figure 3-23, respectively. According to Figure 3-22, it can be concluded that the spectral data is reliable since the coherence values are very close to unity.

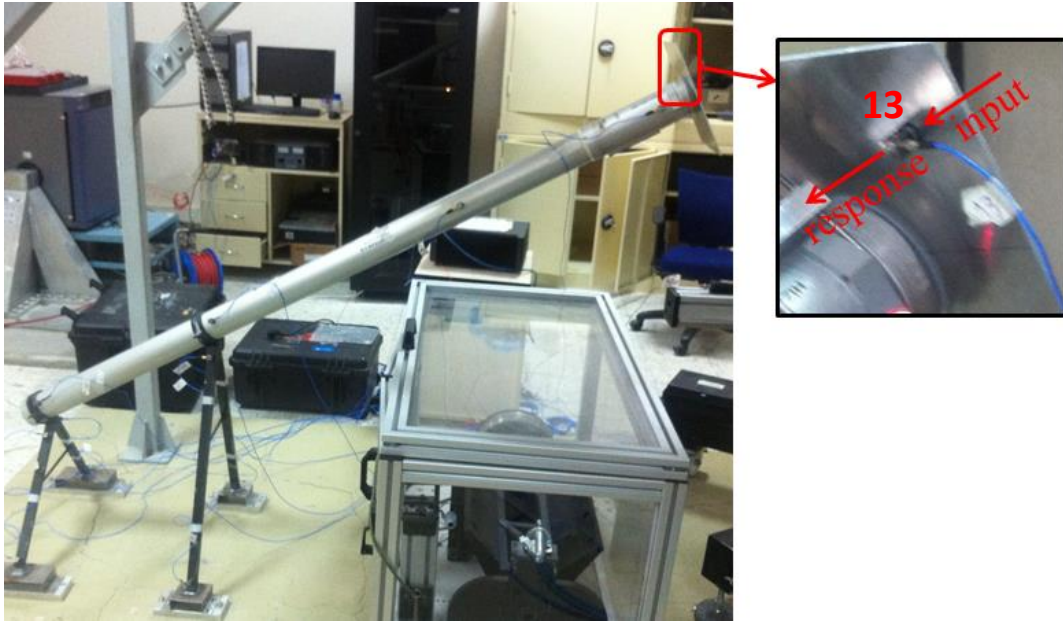


Figure 3-21: Driving point input and response directions

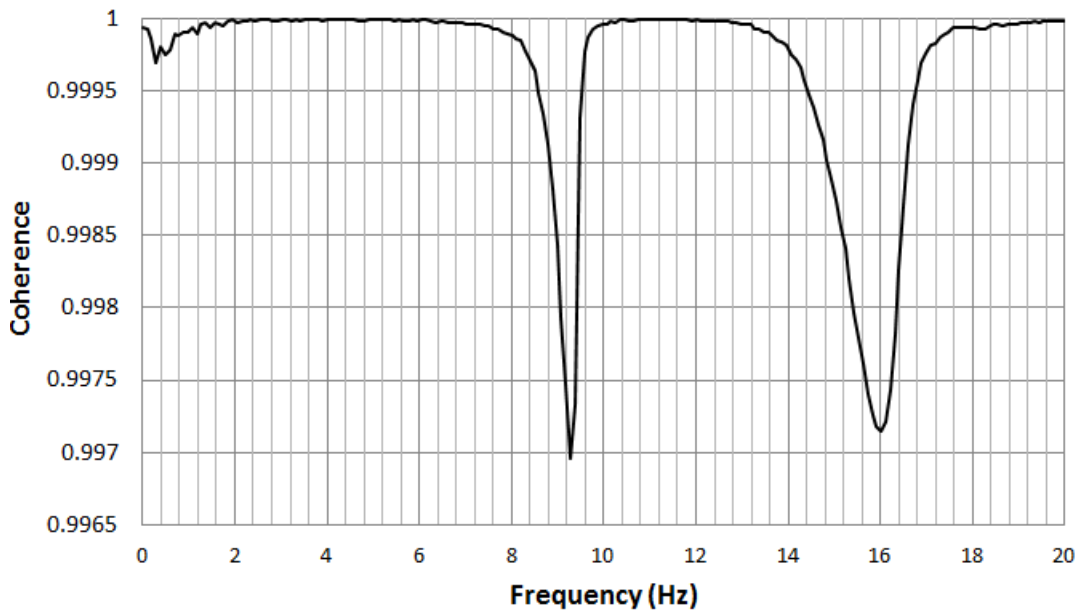


Figure 3-22: Coherence data obtained from the driving point

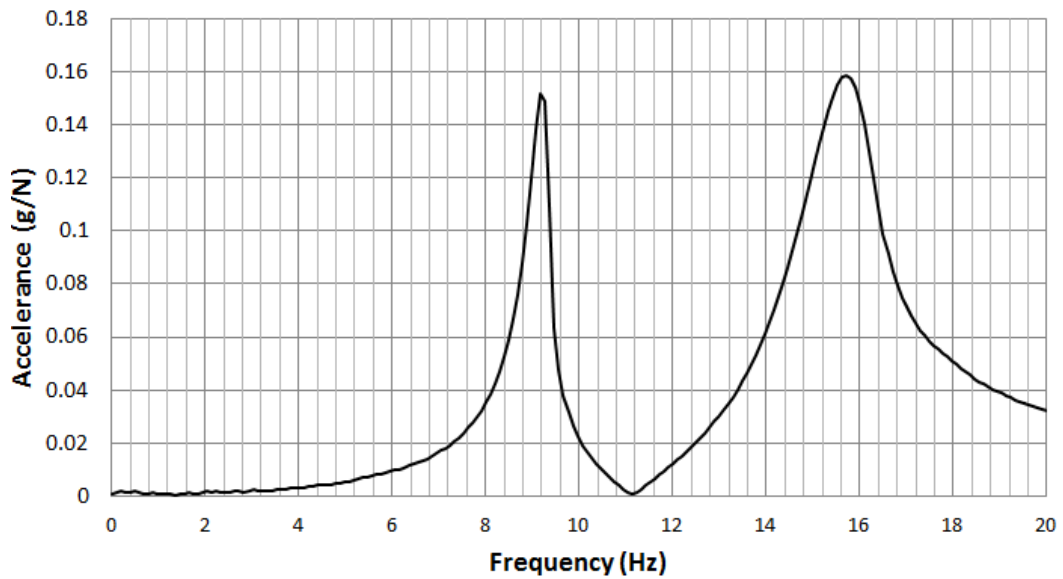


Figure 3-23: FRF data obtained from the driving point

In Table 3-2, modal test results are presented for the first three modes which have been clearly identified at the end of the tests. By examining the participation factors given in Table 3-2, it can also be said that the first two modes are the dominant modes for the dynamics of physical structure.

Table 3-2: Results for the first three modes of the physical structure

Mode number	Modal frequency (Hz)	Damping ratio (%)	Coherence (%)	Modal participation factors (%)
1	9.26	1,77	99.23	40.64
2	10.78	1,06	99.90	38.24
3	16.24	4,05	96.16	8.89

In order to verify the finite element model of the physical structure, modal test and analysis results are correlated via LMS Virtual.LAB 13[©] software. In Figure 3-24, Figure 3-25 and Figure 3-26, first three mode shapes obtained from test and analysis models are compared visually. From these figures, it can be observed that the first three mode shape results are compatible.

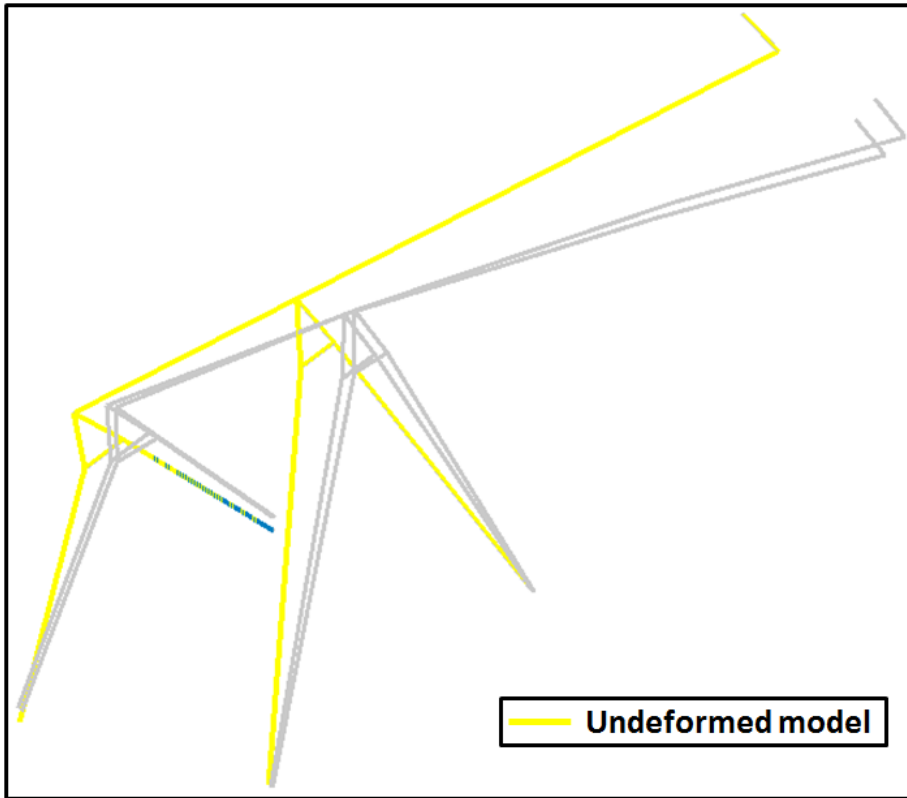


Figure 3-24: Test-analysis comparison for the 1st (tip-off) mode

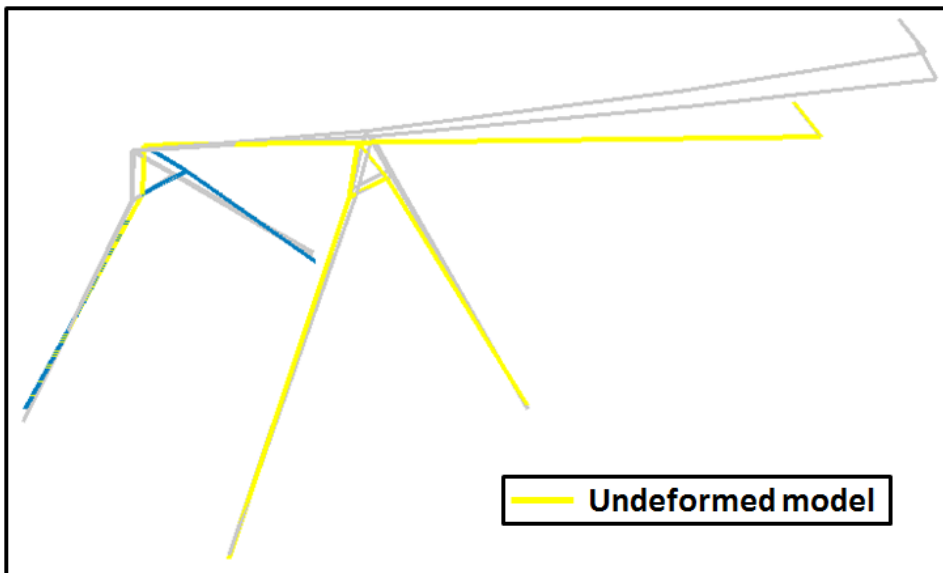


Figure 3-25: Test-analysis comparison for the 2nd (side-off) mode

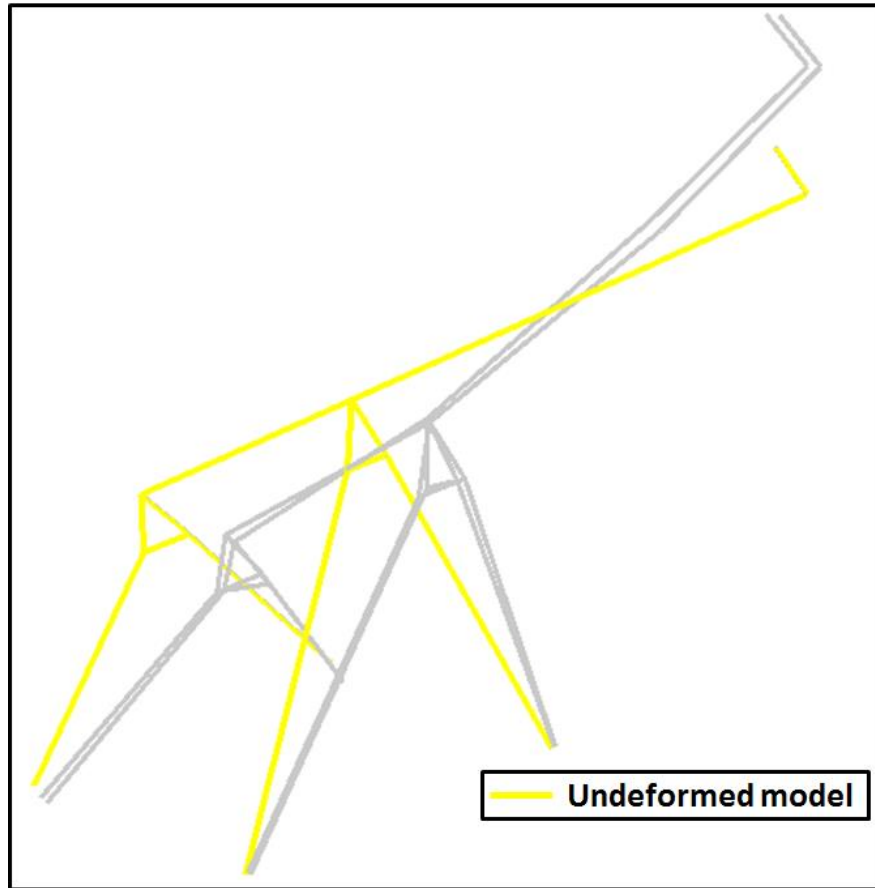


Figure 3-26: Test-analysis comparison for the 3rd mode

In order to compare the mode shapes obtained from the modal test and finite element analysis quantitatively, Modal Assurance Criteria (MAC) study is performed over the LMS Virtual.LAB 13[©] software. MAC number is a measure for the consistency of eigenvectors obtained from different methods. If the MAC number is equal to unity, it indicates that the mode shapes are absolutely consistent. If the MAC number is equal to zero, modal vectors are completely inconsistent. In practice, a MAC number value near to unity is considered as an indication of consistency. MAC number can be calculated from the following formula [22]:

$$MAC = \frac{|\{\psi_{t,i}\}^T \{\psi_{a,j}\}|^2}{(\{\psi_{t,i}\}^T \{\psi_{t,i}\})(\{\psi_{a,j}\}^T \{\psi_{a,j}\})} \quad (\text{Eqn. 3.2})$$

In this formula, $\psi_{t,i}$ denotes the i^{th} mode shape obtained from the experimentally whereas $\psi_{t,j}$ denotes the j^{th} mode shape obtained from the FEA study. As a result of

the MAC study, MAC number matrix is obtained as shown in Figure 3-27. From this figure, it can again be seen that the first two modes obtained from the experimental and FEA studies are consistent.

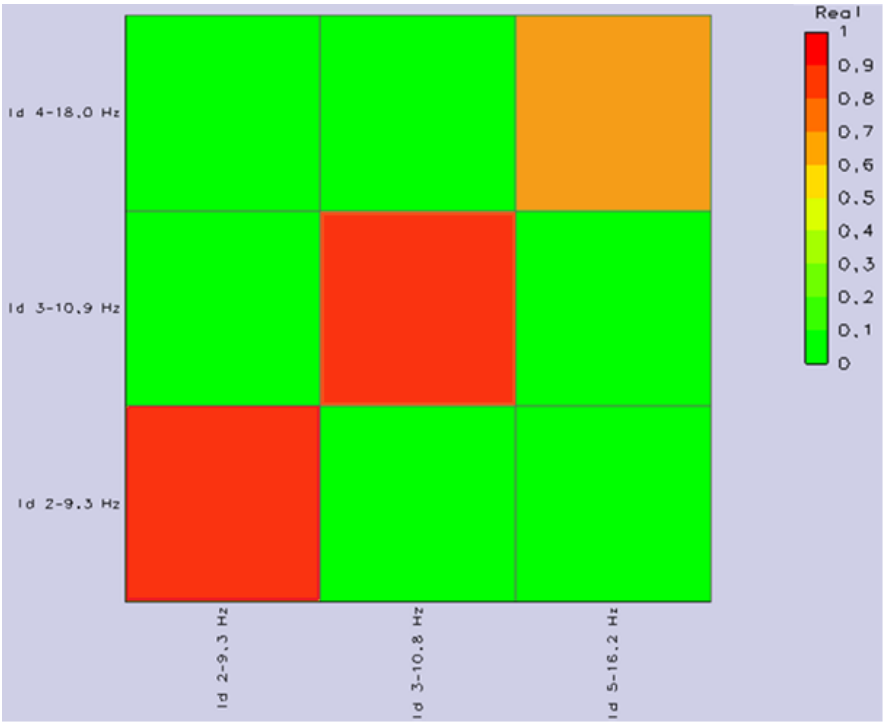


Figure 3-27: MAC number matrix for the comparison of experimental and FEA models

In Table 3-3, natural frequency results are presented and compared for the first three mode results of the modal test and finite element analysis. It is observed that the first two modal frequencies are almost the same. However, the 3rd modal frequencies are slightly different, but this mode’s effect on the system’s motion is very little.

Table 3-3: Comparison of the natural frequency and mode shape results

	Modal Test (Hz)	FE Analysis (Hz)	Difference (Hz)	MAC value
1st mode (tip-off)	9.263	9.320	0.057	0.931
2nd mode (side-off)	10.784	10.860	0.076	0.914
3rd mode	16.243	18.026	1.763	0.647

In addition to the modal frequency and mode shape comparisons, FRF results obtained using finite element analysis and experimental works are also compared. For comparison purposes, acceleration FRF's are in three axes from the accelerometer shown in Figure 3-28 are used.

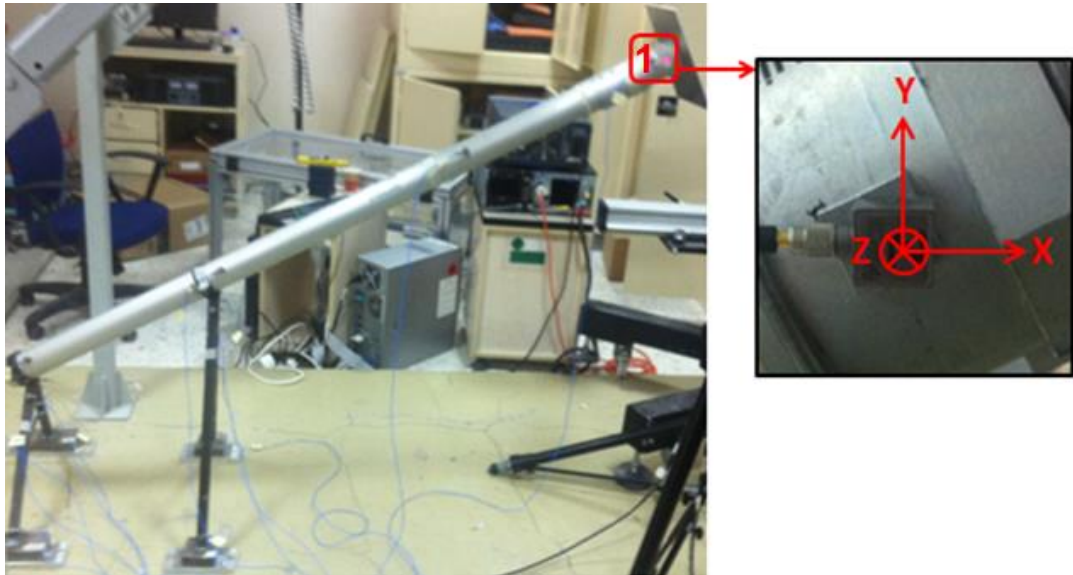


Figure 3-28: Location of the FRF measurement accelerometer

Accelerance FRF results obtained from the experiments and finite element analysis are plotted together in Figure 3-29, Figure 3-30 and Figure 3-31. From these figures, it can be observed that the peaks at the first two modes are comparable whereas the third mode peaks slightly deviate from each other. This is probably caused by the fact that the rubber layers between the clamps and tube are not precisely modelled since their material properties are not exactly known. In addition, leakage problem may arise due to the time data used during the modal data extraction (See Figure 3-17). This may also be a reason for the imprecise determination of the damping values from the experimental data.

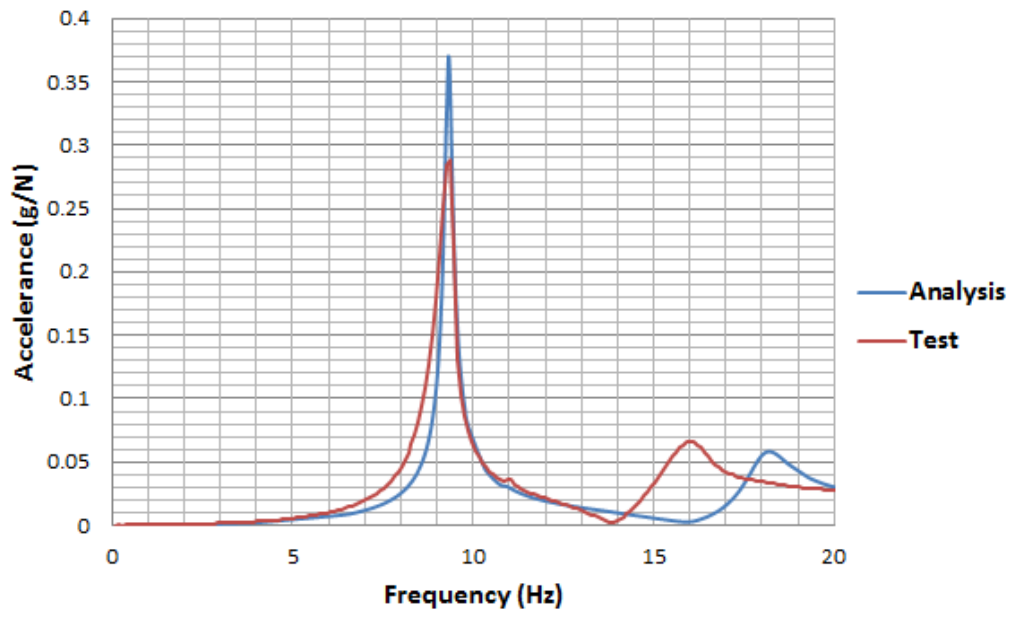


Figure 3-29: FRF comparison in x-axes

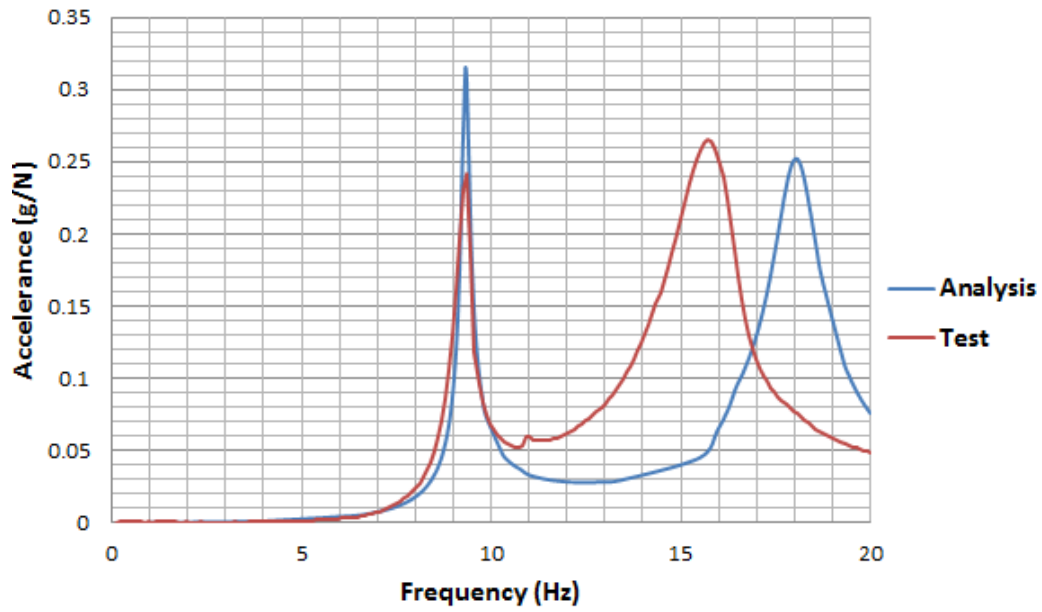


Figure 3-30: FRF comparison in y-axes

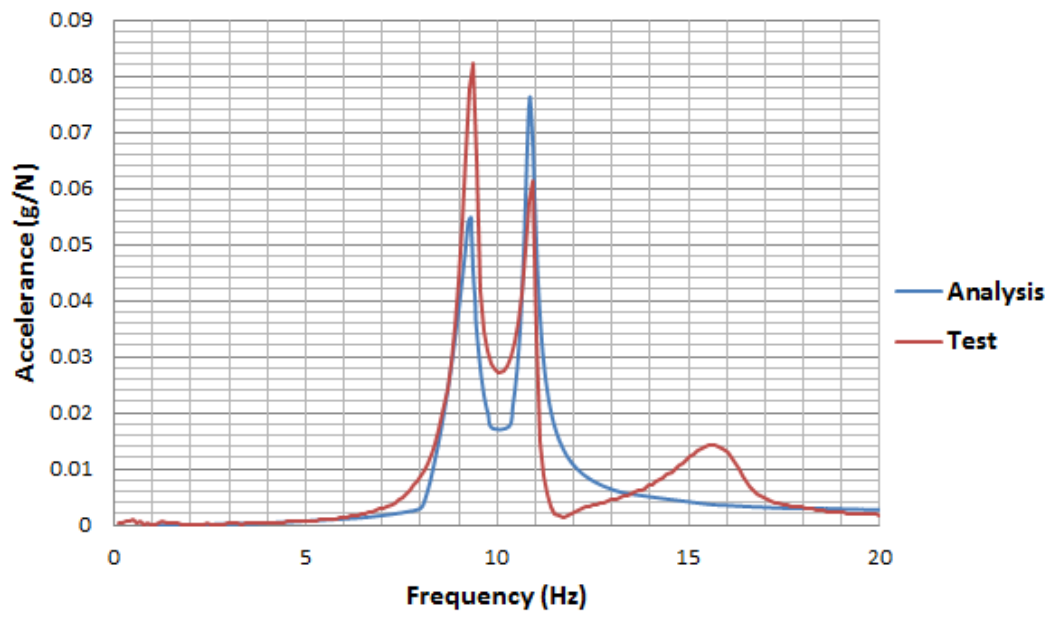


Figure 3-31: FRF comparison in z-axes

CHAPTER 4

DESIGN OF TVA

Tuned vibration absorber design process can be divided into three steps:

- I. Identification of the TVA parameters
- II. Realization of the TVA design
- III. Experimental characterization of the TVA parameters

In the first step, mass, stiffness and damping of the TVA are identified. FEA method is employed in order to compute these TVA parameters as in the case of physical structure design instead of using the analytical expressions. That's why the physical structure is a complex system, thus the equations given for the TVA design in Chapter 2.1 may be insufficient since they are valid for an SDOF system. Therefore the TVA parameters are optimized with finite element analysis method on ABAQUS software.

Next, the TVA parameters specified in Section 4.1 are sought to be materialized in Section 4.2. Several design solutions are investigated and the most appropriate design for the physical structure is selected in such a way that the specified TVA parameters can be satisfied. In Section 4.3, realized and fabricated TVA system is characterized experimentally in order to see whether it satisfies the optimized TVA parameters.

4.1. DETERMINATION OF THE TVA PARAMETERS

Determination of the TVA parameters involves the identification of the mass, stiffness and damping coefficient values of the TVA. If the mass of TVA is defined, the stiffness determination can be replaced by the tuning frequency determination. Likewise, determination of the damping coefficient can be replaced by the determination of damping ratio if the mass and stiffness (or tuning frequency) values of the TVA are defined. If the TVA is supposed to be designed as multi degree of

freedom or multiple TVA design is desired, these parameters are identified as multiple.

For a TVA design, vibration reduction can be targeted for either the resonance frequencies of main system or the excitation frequency. If the forcing acting on the system is in random excitation type, PSD graph of the excitation is extracted and the dominant frequency on this PSD graph can be chosen as target frequency. In this study, excitation is impulsive which resembles to a half-sine pulse. Therefore, there is no dominant excitation frequency and this type of forcing excites a spectrum up to a certain frequency level [23]. Hence, the response of the system is shaped by the nature of the system. As a result, the dominant resonance frequencies of the physical structure are targeted for vibration suppression.

TVA design process is conducted via finite element analysis method as mentioned before. For that purpose, harmonic analyses are run on the physical structure FEA model. Harmonic analyses are performed with the subspace based steady-state dynamics analysis option of the ABAQUS software which is a mode-based analysis procedure. In other words, modal analysis is required prior to this analysis. In this procedure, harmonic response is calculated based on the system's eigenfrequencies and modes [18]. Subspace based steady-state dynamics procedure allows the usage of dashpot type damping while the other steady-state dynamics procedure does not. For that reason, this type of procedure is selected so that the damping of TVA could be modelled. Beside this, the damping of main system is modelled with Rayleigh damping. Coefficients of Rayleigh damping are determined by depending on the damping results obtained from the modal tests. Rayleigh damping includes the mass proportional and stiffness proportional terms. The damping ratio is expressed in terms of frequency as [18]:

$$\zeta = \frac{\alpha}{2\omega} + \frac{\beta\omega}{2} \quad (\text{Eqn. 4.1})$$

Since the impulsive excitation on the prototype is effective on a certain frequency range as mentioned before, this situation is reflected via harmonic analysis by sweeping a certain frequency range. In the harmonic analyses, forcing is applied from the impact interface part as shown in the Figure 4-1. This forcing is applied as a

point load at unit magnitude and in the direction perpendicular to the impact interface. From the Figure 4-1, it can be seen that the forcing location has an offset between the axes of the tube. By this way of forcing, the case causing to the maximum vibration amplitudes could be simulated.

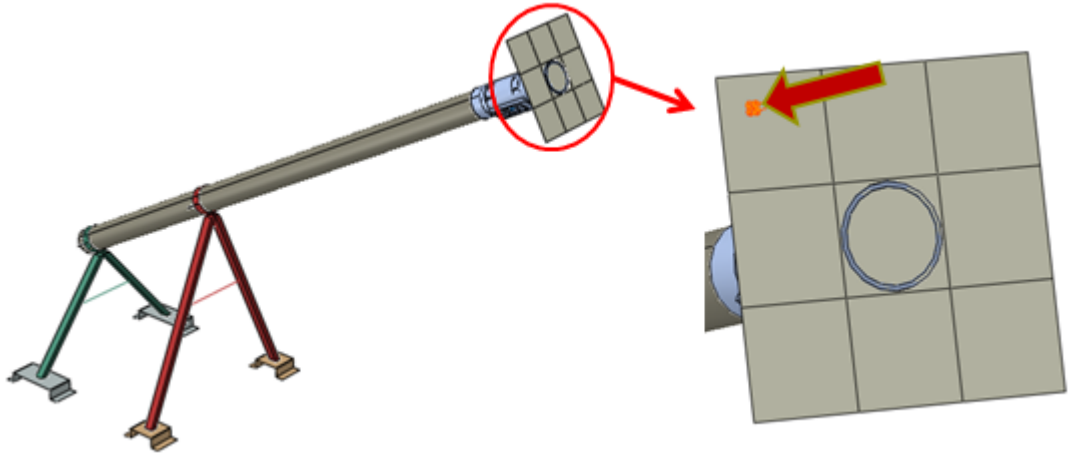


Figure 4-1: Forcing location on the prototype model

For the harmonic analyses, frequency range is selected between 1-20 Hz. The forcing shown in the Figure 4-1 is applied in unit magnitude and the total harmonic displacement response is read from the location shown in Figure 4-6. Total harmonic displacement value is calculated as a resultant of the harmonic displacements in three degrees of freedoms. After that, the frequency range is adjusted as between 1-100 Hz and the harmonic response is obtained as shown in Figure 4-3. It is seen that the peaks in the harmonic responses are distinct in 1-20 Hz frequency range. Therefore, this frequency range is found as sufficient in harmonic analyses in order to save the computation time and effort.

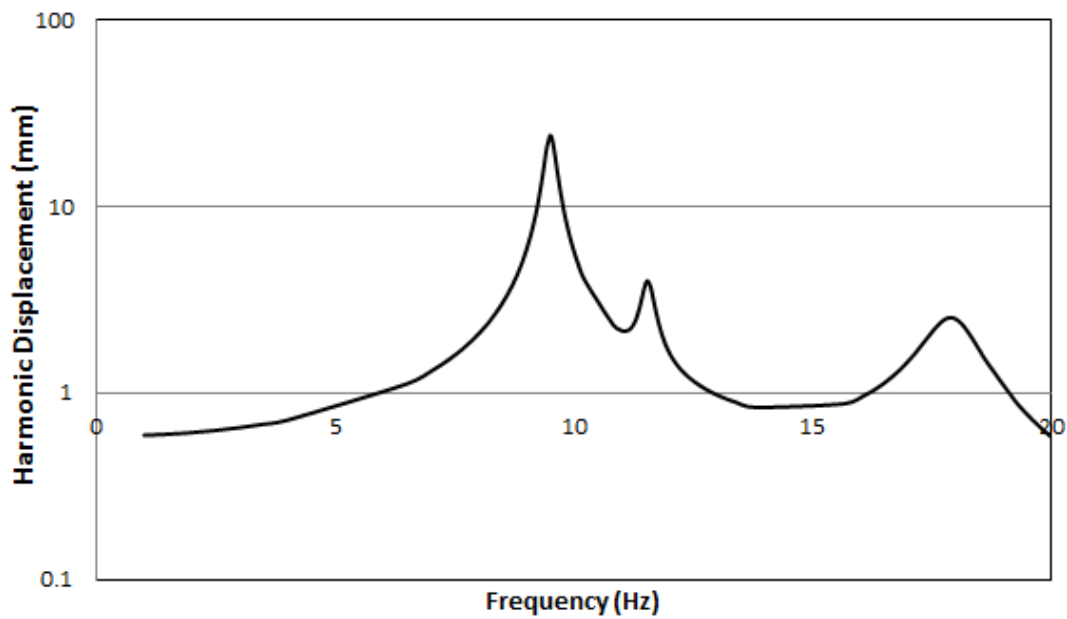


Figure 4-2: Harmonic displacement response at the tip of prototype (0-20 Hz)

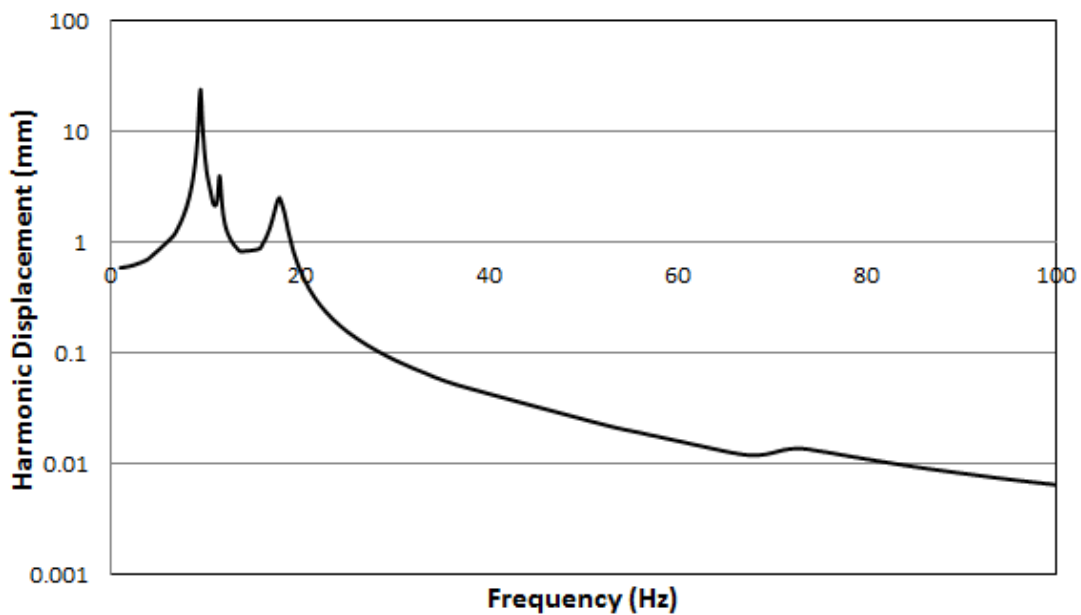


Figure 4-3: Harmonic displacement response at the tip of prototype (0-100 Hz)

From the modal analyses results presented in Section 3.1, the difference between first and second modal frequency (side-off) is calculated as about 1.56 Hz. It means that there is an about %16.7 difference between the first two dominating modal frequencies of the prototype. Therefore, it is concluded that the natural frequencies of

the dominating first two modes of the physical structure are very close to each other. By considering this situation, an SDOF tuned vibration absorber design is approved rather than the MDOF or multiple tuned vibration absorber design. That's why, an SDOF tuned vibration absorber would satisfy the vibration suppression requirement with an appropriate selection of the TVA parameters (mass, stiffness and damping) if the difference between the two modes are sufficiently low.

TVA parameters are identified through the ABAQUS finite element analysis software. For that purpose, the SDOF tuned vibration absorber is modelled as a combination of discrete mass, stiffness and damping elements and attached on the FEA model of the physical structure as shown in Figure 4-4. As seen in the Figure 4-4, two reference points are created and one of these points are connected to the tube with continuum distributing coupling (RBE3) option of the ABAQUS. Concentrated mass is located to the second reference point and the spring/dashpot feature of the ABAQUS is assigned to the line between these reference points in order to reflect the stiffness and damping properties of the TVA. These two reference points are constrained with the kinematic coupling (RBE2) option as shown in Figure 4-5. With this constraint, motion of the concentrated mass is allowed in only axial direction of the spring/dashpot feature while the other degrees of freedoms are restrained.

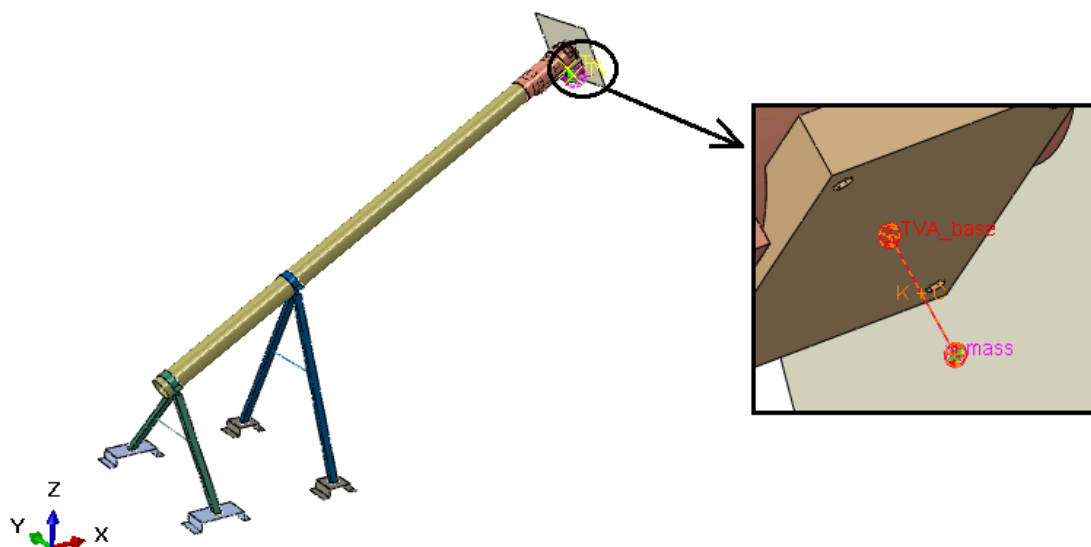


Figure 4-4: TVA modelling on the FEA model

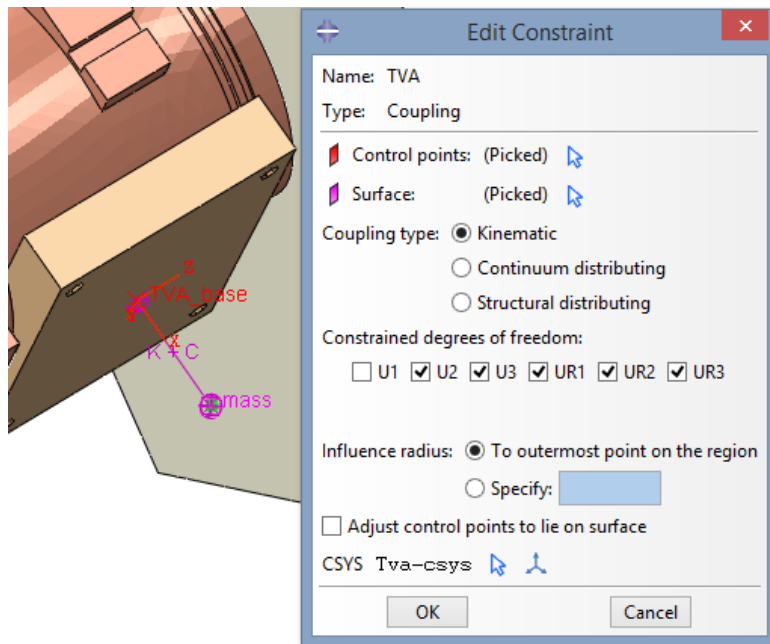


Figure 4-5: Constraint between two points of the spring/dashpot feature

In order to identify the optimum TVA parameters, a set of mass, natural frequency and damping values are established. The mass values are adjusted in a way that the maximum mass is about %10 of the total mass of the physical structure. Measurements revealed that the total mass of the prototype is 5.2 kg. Therefore, it is desired that the mass of TVA should not exceed 0.5 kg in order to reach a meaningful design in mass term. On the other side, the tuning frequency values are arranged around the first and second modal frequencies of the prototype since these modes are the most effective modes over the dynamics of prototype. For the damping ratio parameter, five values are selected and the maximum of them is specified as equal to 1.0 in order to have a feasible damping. All of these TVA parameters are tabulated in Table 4-1:

Table 4-1: Selected TVA Parameters

Mass (grams)	Tuning Frequency (Hz)	Damping Ratio
100	8.5	0.1
200	8.7	0.3
300	8.9	0.5
400	9.1	0.7
500	9.3	1.0
	9.5	
	9.7	
	9.9	
	10.1	
	10.3	

As observed in Table 4-1, 5 values for the mass parameter, 10 values for the tuning frequency parameter and 5 values for the damping ratio parameter are selected. Therefore, totally 250 harmonic analyses ($5 \times 10 \times 5 = 250$) are run in order to sweep the combination of these parameters entirely.

In the analyses, stiffness parameters of the TVA are calculated from the undamped natural frequency values presented in Table 4-1 by using the Eqn. 4.2a. Similarly the damping coefficient parameters are calculated from the damping ratio values in the Table 4-1 by using the Eqn. 4.2b:

$$k = m \cdot \omega_n^2 \quad (\text{Eqn. 4.2a})$$

$$c = (2\sqrt{k \cdot m}) \cdot \zeta \quad (\text{Eqn. 4.2b})$$

The main motivation behind the TVA design is to minimize the response of the prototype. For that purpose, a point is selected from the tip of the prototype as shown in Figure 4-6 and the harmonic displacement of this point is read from the harmonic analysis results. Then the TVA parameter set is searched among the combination of parameters given in Table 4-1 that would minimize this harmonic displacement value.

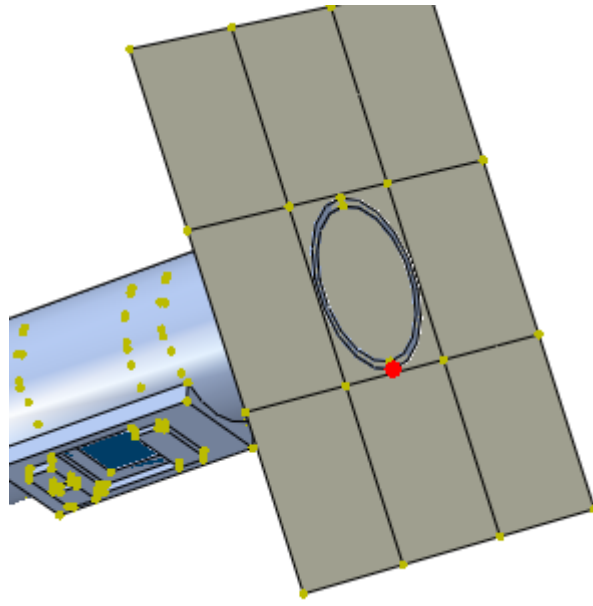


Figure 4-6: Harmonic displacement reading point

As a result of the harmonic analyses those are run with 200 different combinations, the best combination of parameters is found as follows:

Mass: $m=400$ grams

Tuning frequency: $\omega_n=9.3$ Hz

Damping ratio: $\zeta=0.3$

Variation of the harmonic responses with respect to different TVA masses, damping ratios and tuning frequencies are presented in Figure 4-7, Figure 4-8 and Figure 4-9, respectively. In these figures, results are shown for the optimum combination of the parameters except the variable parameter. By observing these figures, it can be said that the mass and damping ratio parameters significantly affect the harmonic response magnitudes whereas the tuning frequency parameter is not so effective. This situation can also be observed from the Figure 4-10, Figure 4-11 and Figure 4-12 which show the variation of maximum harmonic response amplitudes with respect to TVA mass, tuning frequency and damping ratio, respectively.

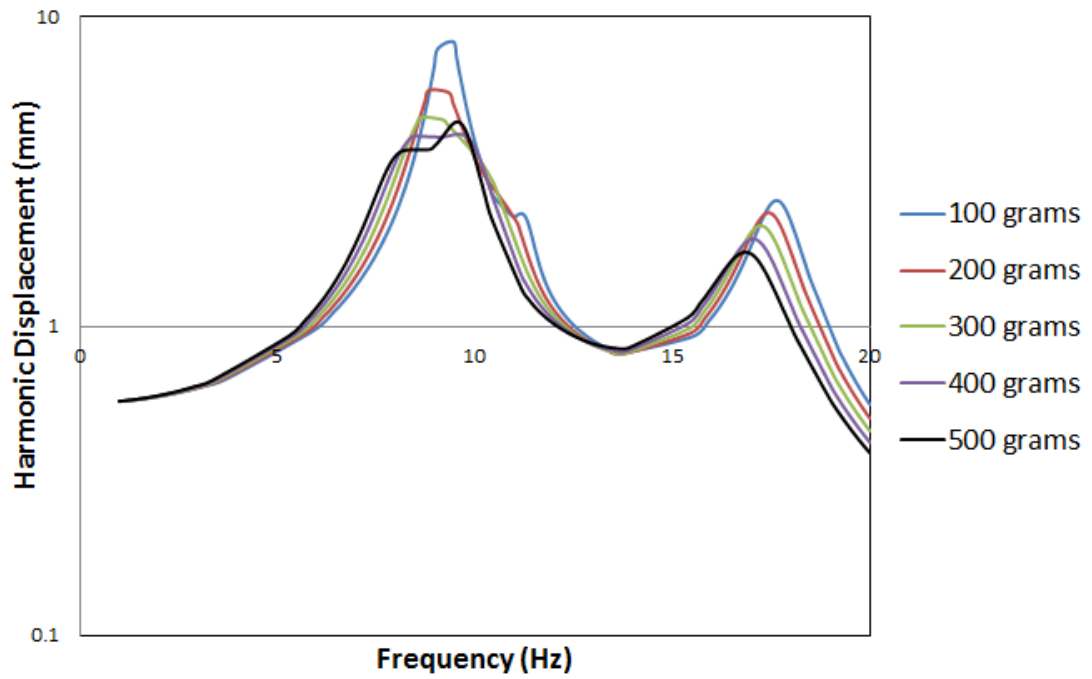


Figure 4-7: Harmonic responses for different TVA masses ($\omega_n=9.3$ Hz; $\zeta=0.3$)

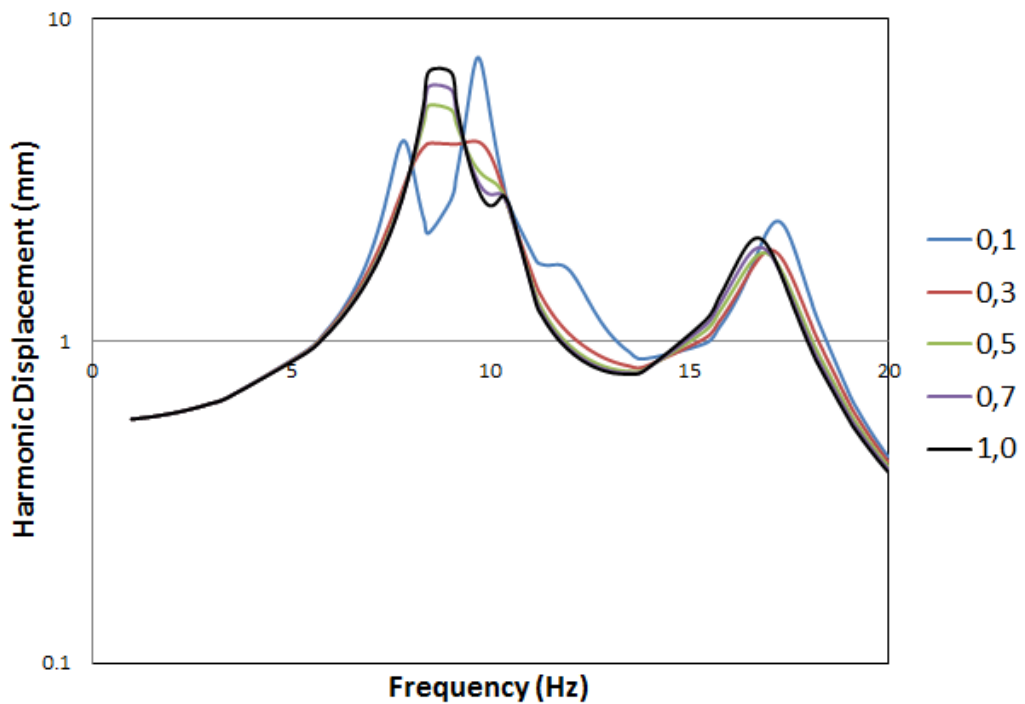


Figure 4-8: Harmonic responses for different damping ratios ($m=400$ grams; $\omega_n=9.3$ Hz)

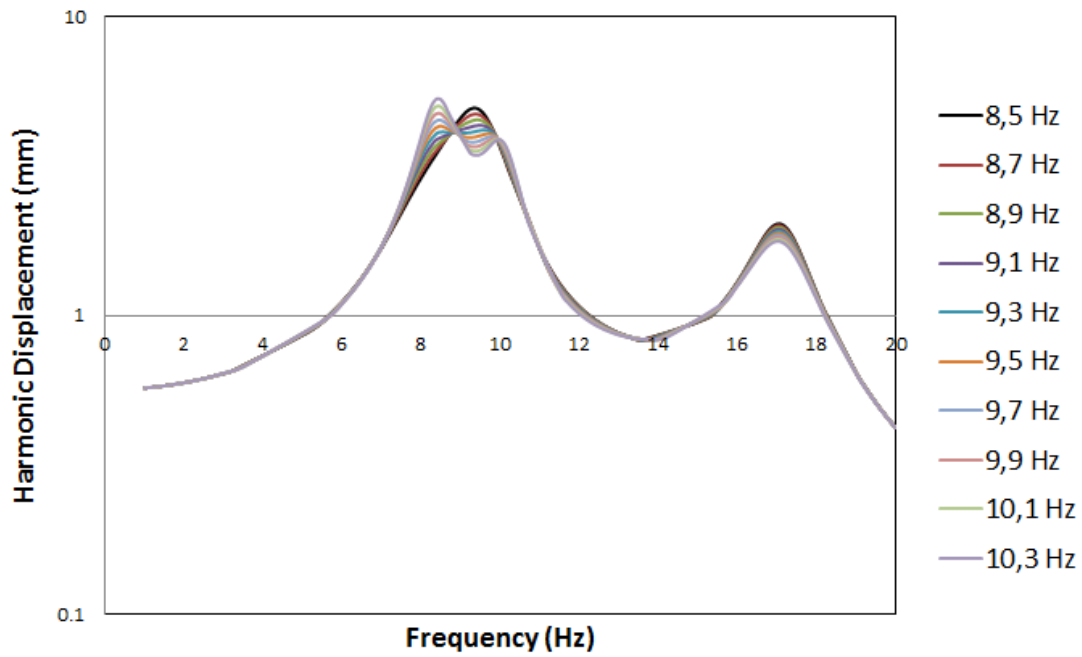


Figure 4-9: Harmonic responses for different tuning frequencies ($m=400$ grams; $\zeta=0.3$)

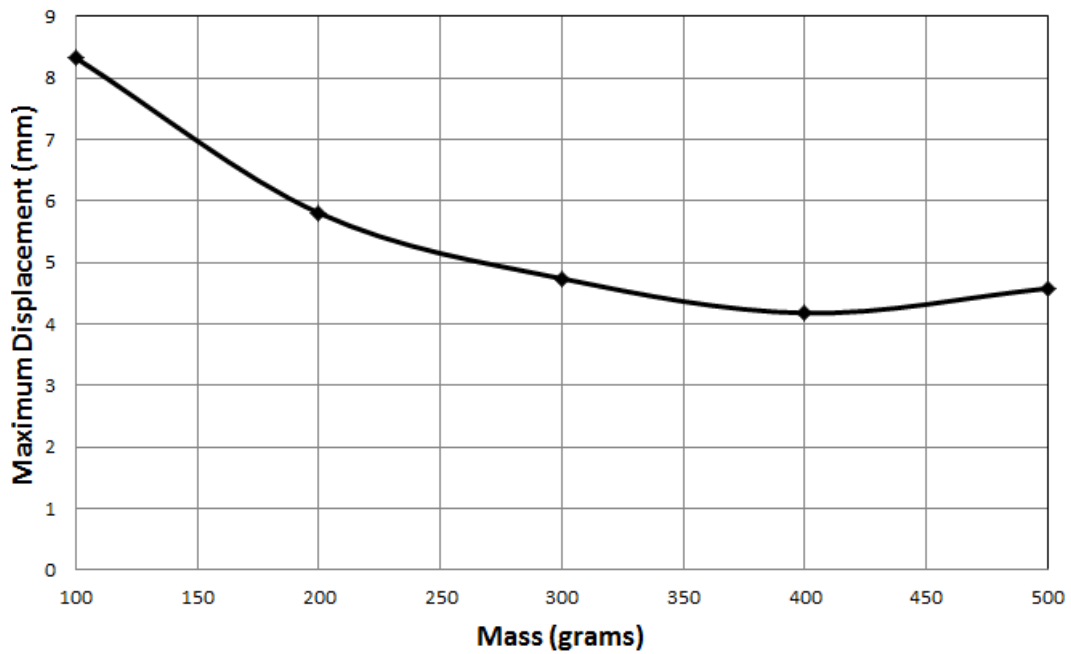


Figure 4-10: Maximum harmonic response amplitudes with respect to different TVA masses

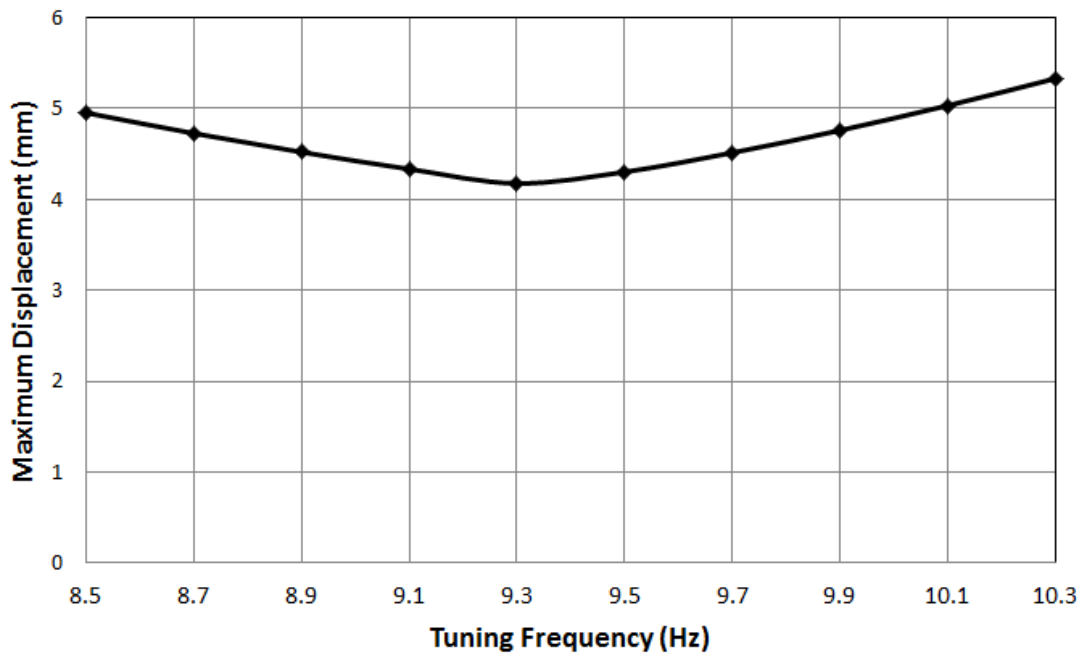


Figure 4-11: Maximum harmonic response amplitudes with respect to different tuning frequencies

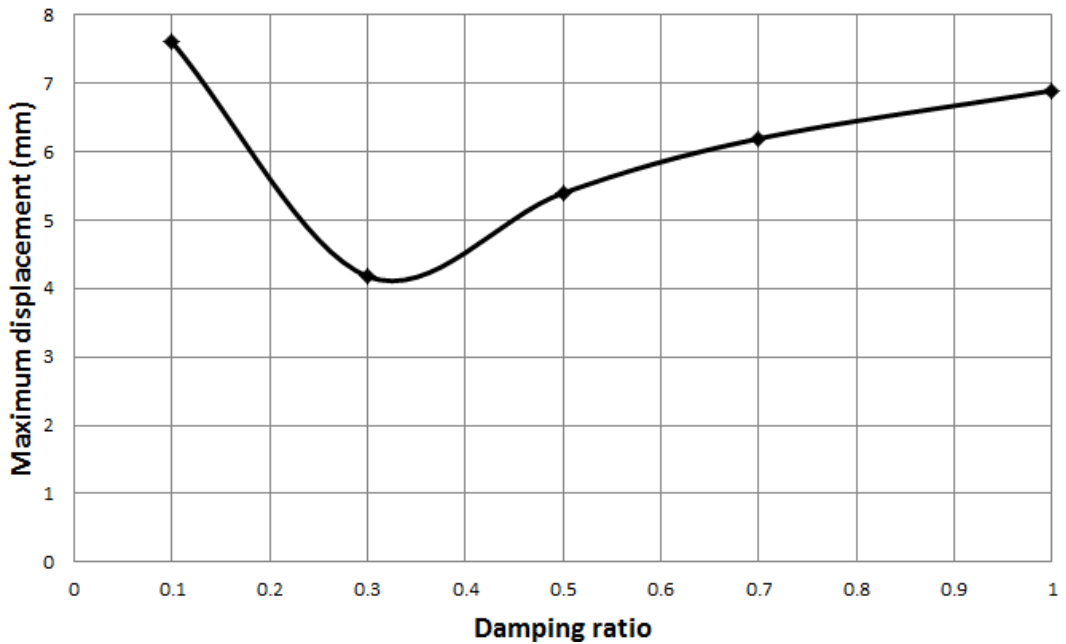


Figure 4-12: Maximum harmonic response amplitudes with respect to different damping ratios

After the optimization of TVA parameters, orientation of the TVA is sought to be determined. In order to determine the angular orientation of the TVA, 5 different values are selected for the angle α shown in the Figure 4-13 and harmonic analyses are run with the optimum parameter combination for these 5 different angular orientations. The maximum harmonic response amplitudes obtained from these 5 analyses are presented in Table 4-2 and Figure 4-14 and the harmonic responses are shown in Figure 4-15. From Table 4-2 and Figure 4-14, it can easily be observed that the minimum response is obtained from 30° angle orientation.

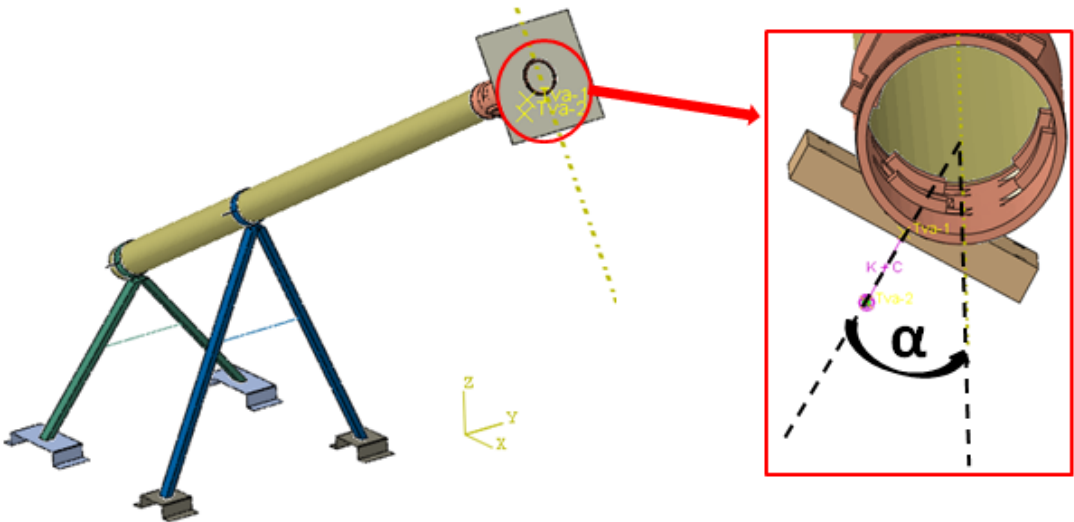


Figure 4-13: Angular orientation of the TVA on the FEA model

Table 4-2: Maximum harmonic response amplitudes for different angular orientations of the TVA

Angle	Displacement (mm)
25°	4.496
30°	3.965
35°	4.179
40°	4.727
45°	5.535

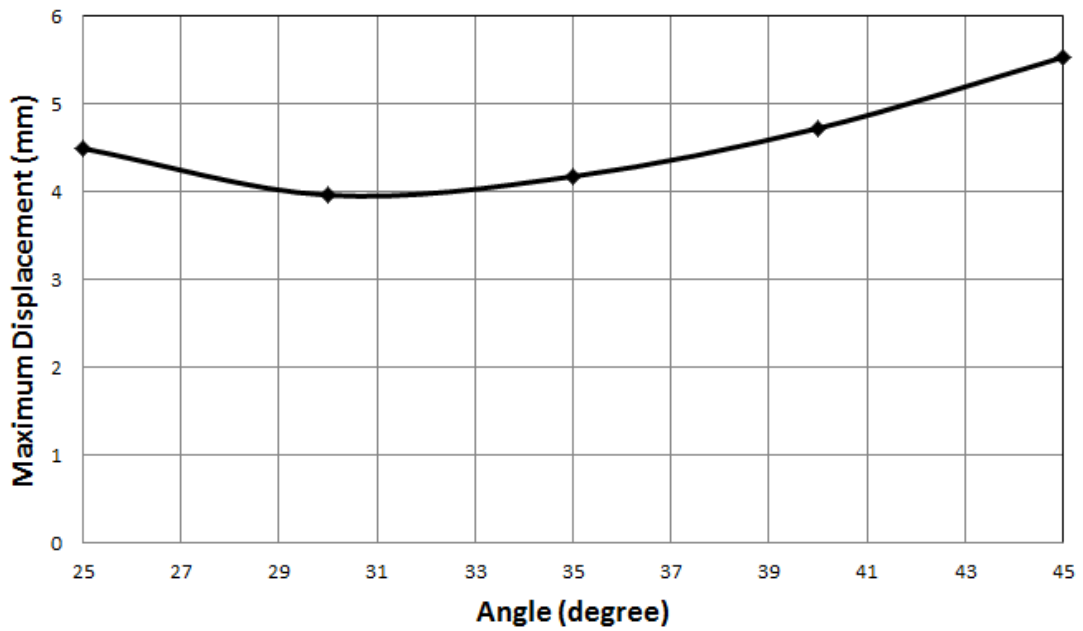


Figure 4-14: Maximum harmonic response amplitudes for different angular orientations of the TVA

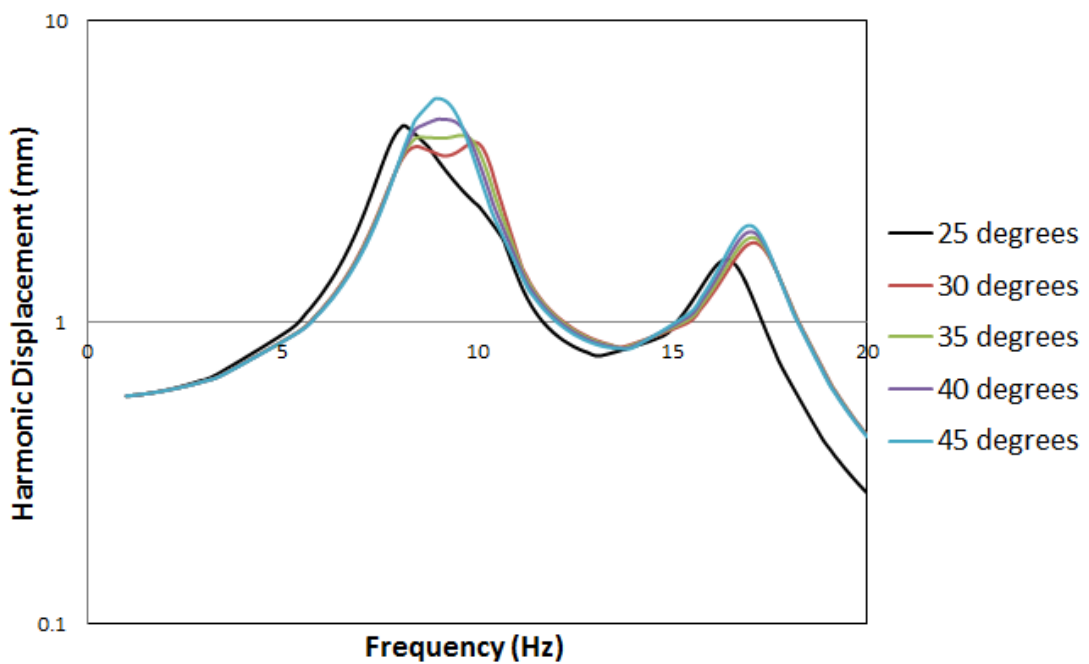


Figure 4-15: Harmonic responses for different angular orientations of the TVA

Another issue that should be considered in the TVA design process is the additional mass effect. This effect causes some amount of deviation in the modal frequencies of the structure. For that purpose, a simple part is designed which has a total mass equal

to 1/5 of the prototype mass. After then, this part is attached to the tube of the prototype model in such a way that the mass center would be on the mass center of the tube (See Figure 4-16). The harmonic analyses are run on this mass added FEA model for the unmodified case and modified with the optimized TVA case. The unmodified harmonic displacement responses are shown in Figure 4-17 and modified harmonic displacement responses are presented in Figure 4-18. In these figures, the results can be compared for the mass added and without mass cases.

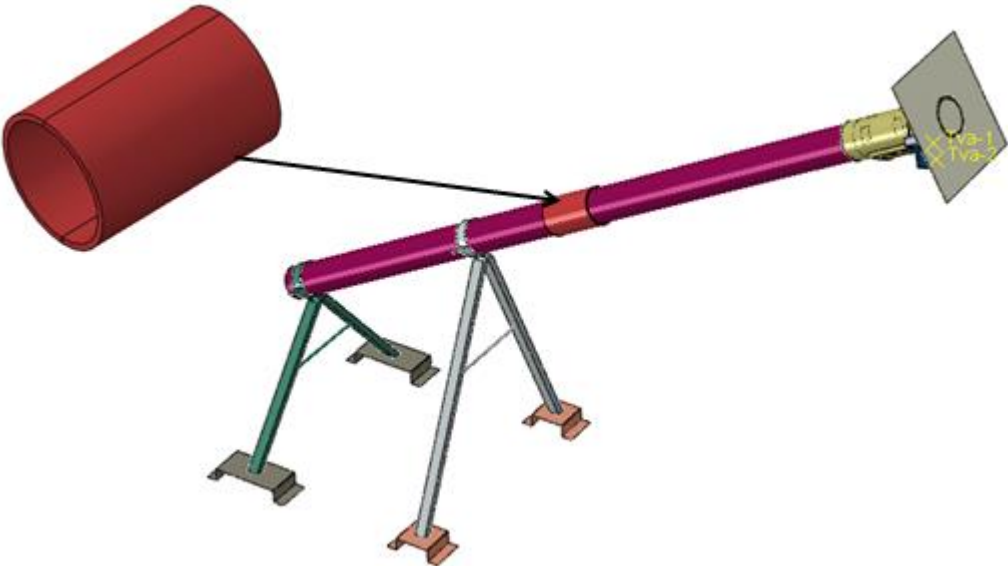


Figure 4-16: Additional mass part and its location on the FEA model

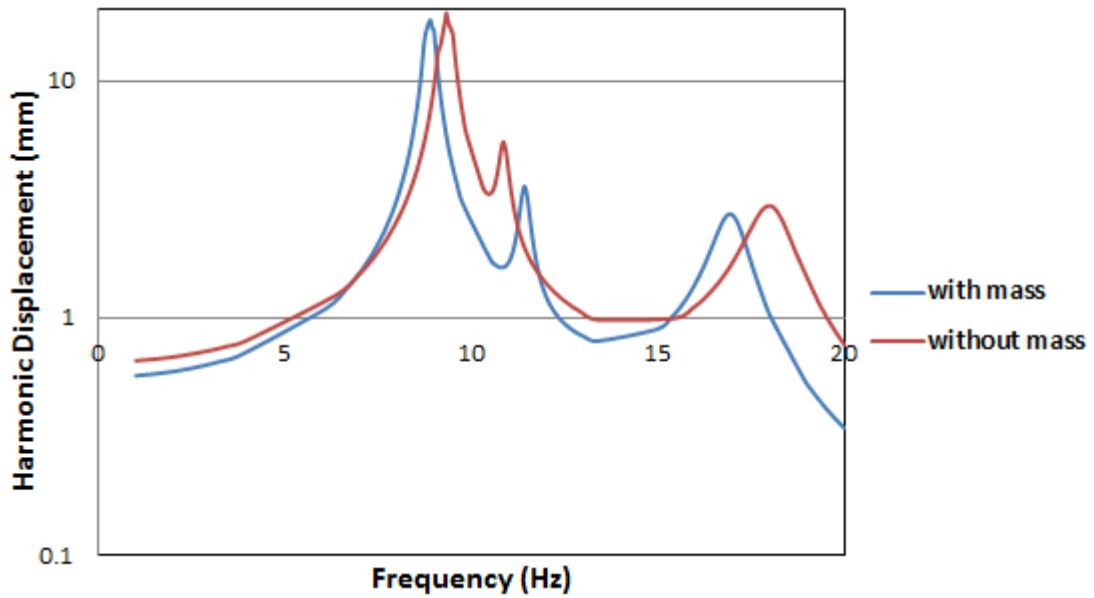


Figure 4-17: Harmonic responses for the unmodified cases

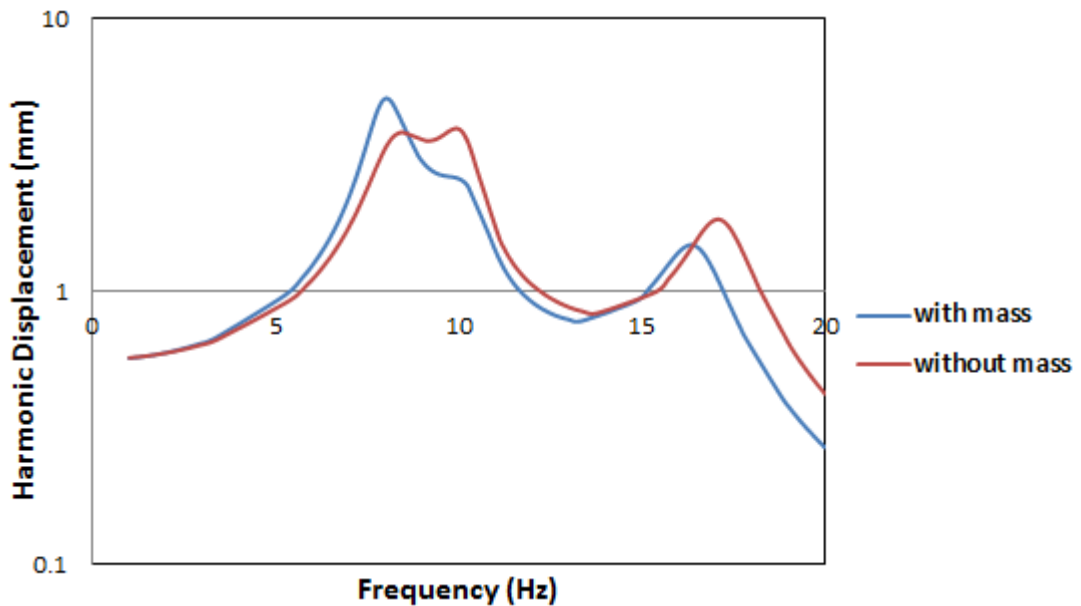


Figure 4-18: Harmonic responses for the modified with optimized TVA cases

From the Figure 4-17 and Figure 4-18, it can be seen that the mass part cause a slight difference in the harmonic responses. In order to obtain a feasible TVA design, peaks of the harmonic responses shown in Figure 4-18 is tried to be equalized. For that purpose, iterations are carried out by playing with the optimized TVA parameter combination. At the end of several iterations the TVA parameter combination given in the Table 4-3 is obtained. The harmonic displacement responses obtained for the

mass added and without mass cases with this TVA parameter combination are presented in Figure 4-19.

Table 4-3: The final TVA parameter combination

m (grams)	380
ω_n (Hz)	8.7
ζ	0.32

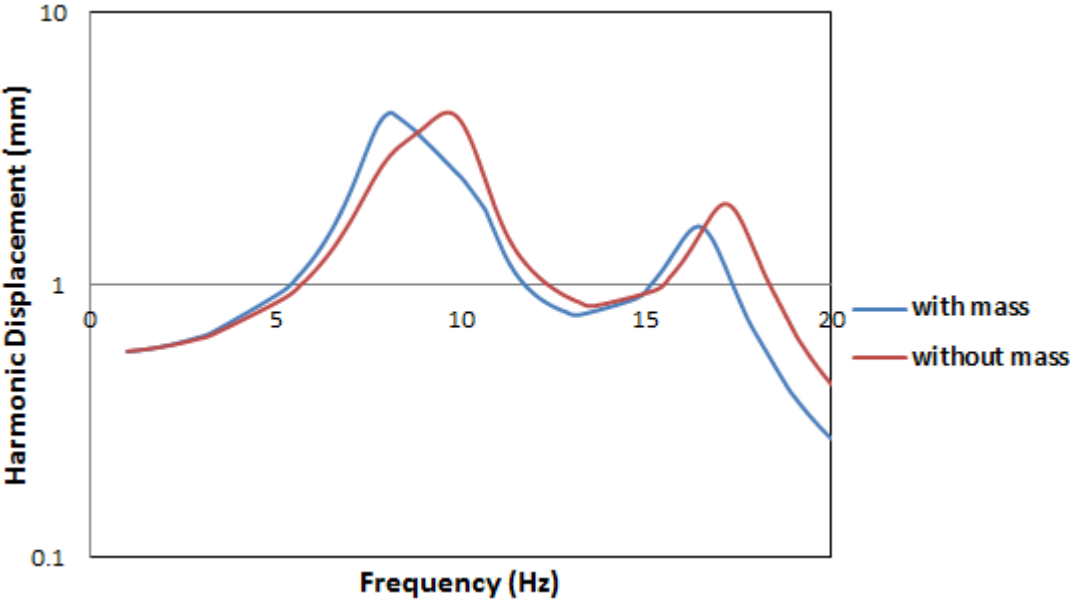


Figure 4-19: Harmonic responses obtained with the final TVA parameter combination

4.2. REALIZATION OF THE TVA DESIGN

After the determination of TVA parameters, the design solutions which realize these TVA parameters are investigated. The most appropriate TVA alternative is selected as a magnetically damped spring-mass system. This system is similar to the TVA proposed for gun barrels in US Patent 6167794 [8]. From the available damping types, magnetic damping is chosen since the damping ratio can be easily adjusted. Moreover, magnetic damping is not affected by temperature effects.

By considering the matters mentioned above, TVA system is designed as demonstrated in Figure 4-20. As observed from this figure, TVA mass consist of an aluminum block (60*40*15 mm) and two copper plates (60*50*5 mm). In TVA assembly, two helical springs are used to operate as the stiffness elements. In order to constrain the motion of TVA to one degree of freedom, two linear bearings are placed into the aluminum block and two shafts are passed through these bearings and helical springs. Rare-earth magnets are placed in parallel to the copper plates. The motivation behind this positioning is to satisfy the damping requirements of the TVA with the eddy-current effect that is induced within the copper plates. Copper material is selected due to its low resistivity so that the damping ratio can be enhanced.

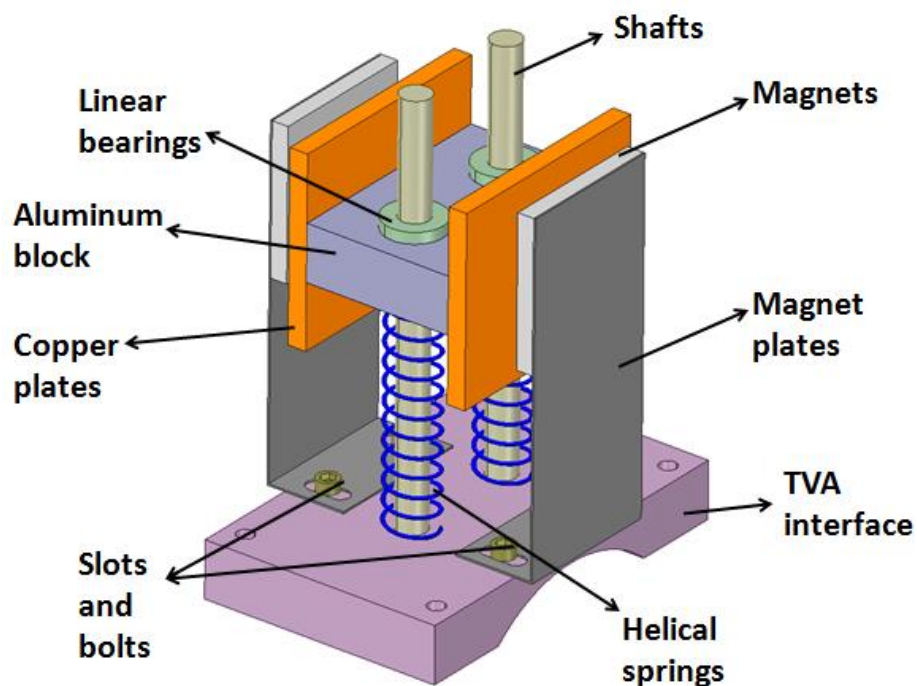


Figure 4-20: CAD model of the TVA assembly

The TVA design is fabricated as shown in Figure 4-21. Linear bearings of LME8 UU type are selected and fastened to the aluminum block from the holes drilled on the block. Two shafts ($\varnothing 8$ mm) were passed through these bearings and welded to the TVA interface. Helical springs are glued to the linear bearings and TVA interface. Copper plates are attached to two sides of the aluminum block symmetrically.

Magnets are attached to the L shaped magnet plates which are made off 1 mm thickness steel plates and these plates are fastened to the TVA interface by means of bolts fixed over the slots under the magnet plates.

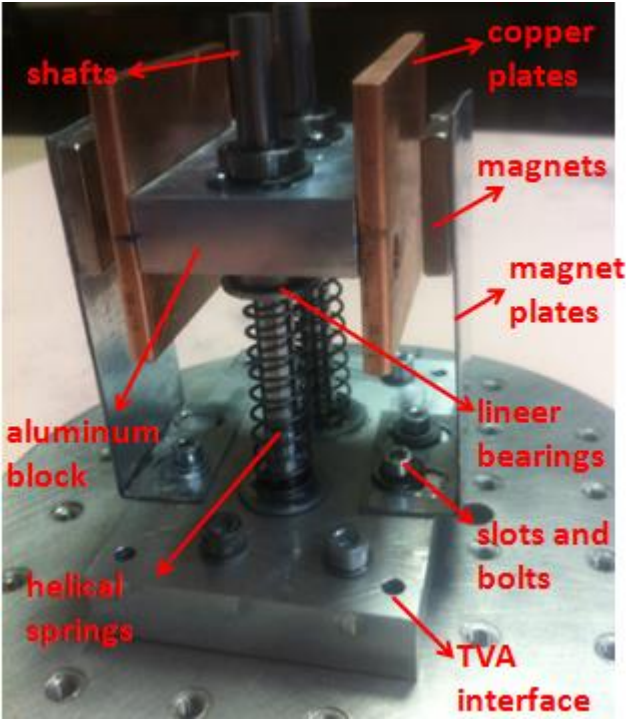


Figure 4-21: Fabricated TVA assembly and components

According to the experiments, eddy-current damping is similar to viscous damping and results in a dissipating force proportional to the velocity. The damping coefficient induced because of the eddy-current damping cannot be calculated by analytical methods easily; however, the following relation is estimated for this type of damping [24]:

$$c = k \frac{B^2 \vartheta}{\rho} \tag{Eqn. 4.3}$$

In this relation, B represents the magnetic flux density, ϑ is the conductor volume inside the magnetic flux, ρ is the resistivity of the conductor and k is a dimensionless constant. Copper is a suitable material for this purpose since its resistivity is too low. According to this relation, it can be stated that the only variable is the magnetic flux

density (B) in order to manipulate the damping coefficient. This can be done by adjusting the distance between the copper plates and magnets or putting additional magnets under the main magnet. For that purpose, the plates which the magnets are attached on are designed with slots as can be seen in Figure 4-22. The distance between the magnets and copper plates can be adjusted by sliding the magnet plates on the slots and these plates are fixed by means of bolts at the desired position.



Figure 4-22: Slotted configuration of the magnet plates

As a result of the optimization study performed with finite element analysis, the optimum TVA parameters are determined as presented in Table 4-3. Firstly the mass requirement of the TVA is verified by weighing on a scale as inspected in Figure 4-23.

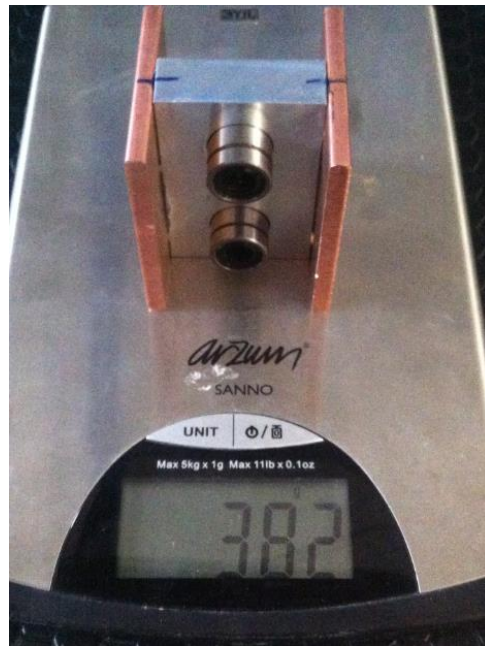


Figure 4-23: Measurement of the TVA mass

Having known the target tuning frequency and the mass of TVA, stiffness of the TVA is calculated and the appropriate helical spring dimensions is determined via following equation [25]:

$$k = \frac{G.d^4}{8.N.D^3} \quad (\text{Eqn. 4.4})$$

where

G : Modulus of rigidity of the spring material

d : Wire diameter of the spring

D : Outer diameter of the spring

N : Number of active coils of the spring

From the available helical spring options of the catalogues, a helical spring made of steel and having the following properties is chosen as appropriate:

$d = 1 \text{ mm}$; $D = 12 \text{ mm}$; $N = 10$; $G = 78000 \text{ MPa}$

By inserting these values into the Eqn. 4.4, stiffness of the springs is found as follows:

$$k = \frac{(78000) \cdot (1^4)}{8 \cdot (10) \cdot (12^3)} = 0,5704 \text{ N/mm}$$

Since two helical springs are used in parallel, this value should be multiplied by two:

$$k = 2 \cdot (0,5704) = 1,1407 \frac{\text{N}}{\text{mm}}$$

Then the tuning frequency of TVA is calculated as follows:

$$\omega_a = \sqrt{\frac{k}{m}} = \sqrt{\frac{(1,1407 \text{ N/mm})}{(0,382 \text{ kg})}} = 54,79 \frac{\text{rad}}{\text{s}} = \mathbf{8,72 \text{ Hz}}$$

After the target mass and target tuning frequency of the TVA is verified, target damping ratio of the TVA should be satisfied. Since there is no available analytical solution to calculate the damping ratio that would be induced due to the eddy-current effect, the damping ratio is verified experimentally.

4.3. EXPERIMENTAL VERIFICATION OF THE TVA PARAMETERS

In order to characterize the TVA design, sine-sweep tests performed by means of a modal shaker on the TVA assembly as demonstrated in Figure 4-24. Technical specifications of the modal shaker are given in Appendix C: Technical Specifications of the Modal Shaker [26]. Sine sweep tests are performed with 0.01 Hz/s sine sweep rate and totally 501 frequency lines are extracted from the frequency range between 5-10 Hz. Experiments are carried out by manipulating the distance between the copper plates and the magnets in order to provide the target damping ratio. Two averages are taken for each case. As a result of the sine-sweep tests, frequency response functions are extracted from the accelerometers shown in Figure 4-24, by selecting the 1st accelerometer as the reference channel.

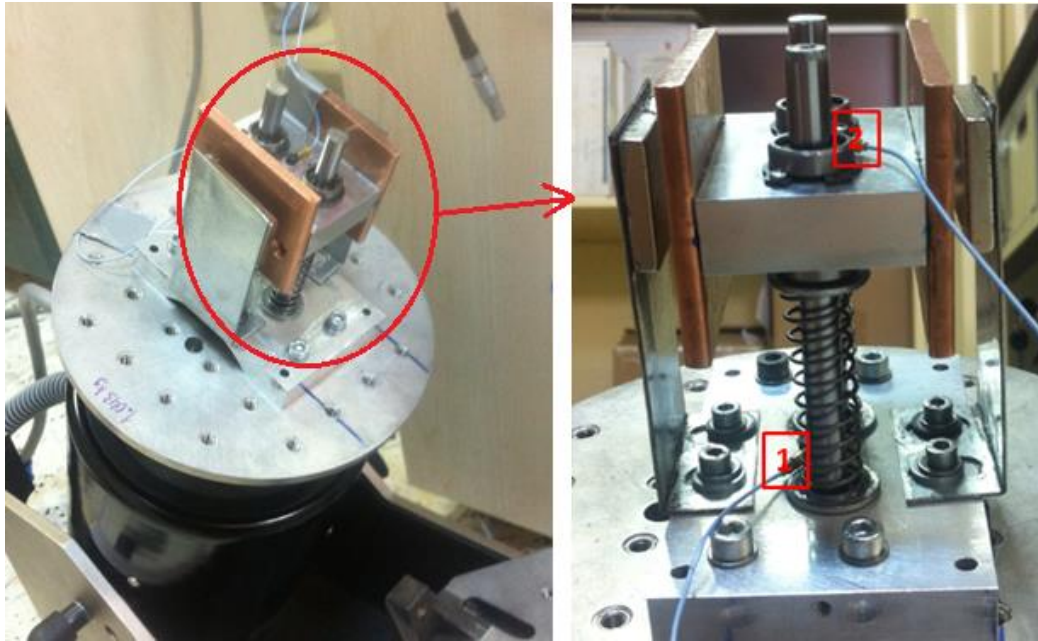


Figure 4-24: Modal shaker and accelerometer locations on the TVA assembly

Sine-sweep tests are carried out on the TVA assembly for 4 different distances and no magnet case. Frequency response functions obtained for these 5 different cases are plotted in logarithmic scale in Figure 4-25. From these FRF results, it can easily be observed that the damping of TVA increases as the distance between the magnets and copper plates decrease. Moreover, resonance of the TVA is found as 8,4 Hz which is 0,3 Hz lower than the target tuning frequency (8,7 Hz). This difference is probably caused by the uncertainty of spring stiffness.

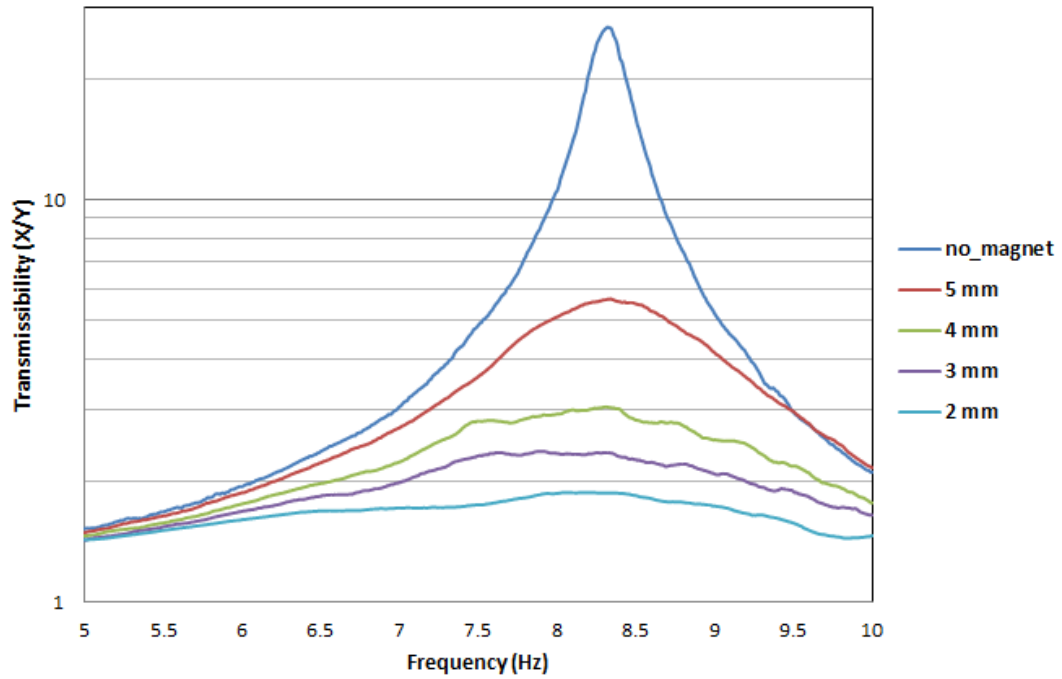


Figure 4-25: FRF results obtained for different magnet-copper plate distances

In order to calculate the damping from the FRF results, the analytical expression given below is used [27]:

$$\frac{X}{Y} = \frac{\sqrt{1+(2\zeta r)^2}}{\sqrt{(1-(r)^2)^2+(2\zeta r)^2}} \quad (\text{Eqn. 4.5})$$

In this expression, r represents the frequency ratio (ω/ω_n) and ζ denotes the damping ratio. This equation is inserted into the MATLAB[®] software and the FRF graphs are obtained. Then, these FRFs are plotted with the FRFs obtained from the test results. Damping ratio in the Equation 5.5 is adjusted so that the theoretical (MATLAB result) and experimental FRF results agree with each other visually. As an example, theoretical and experimental FRF's are plotted in Figure 4-26 for the no magnet case.

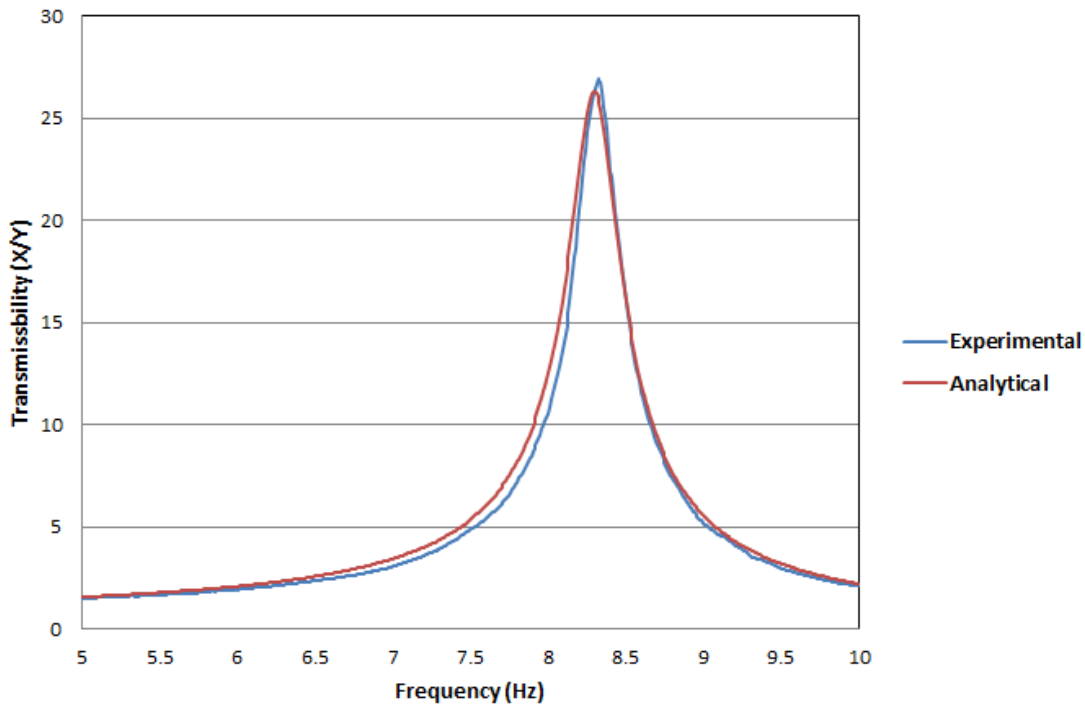


Figure 4-26: Sample FRF comparison for the damping ratio identification

By using the method mentioned above, damping ratios are determined as in Table 4-4. By observing these damping values, 3 mm magnet-copper plate distance is selected as the most appropriate position since the target damping ratio ($\zeta = 0,32$) is almost achieved with this condition.

Table 4-4: Damping ratios with respect to various magnet positions

	Damping ratio (ζ)
No magnet	0,018
5 mm	0,091
4 mm	0,18
3 mm	0,35
2 mm	0,41

CHAPTER 5

CHARACTERIZATION OF THE VIBRATION CONTROL PERFORMANCE OF TVA

In order to verify the performance of TVA system on the physical structure, modal tests are carried out on the prototype for the unmodified (without TVA) and modified (with TVA) cases. During modal tests, prototype is excited from the location demonstrated in Figure 3-13 such that the forcing in the analysis model is replicated. TVA is attached on the prototype at an inclined position as shown in Figure 5-1. TVA assembly is settled to the main structure from the interface part which has a cylindrical groove conforming to the outer face of the tube. This interface part is fastened to the structure by means of two threaded U-shaped rods and tightening them with the aid of four M4 nuts as demonstrated in Figure 5-2.



Figure 5-1: TVA location on the physical structure

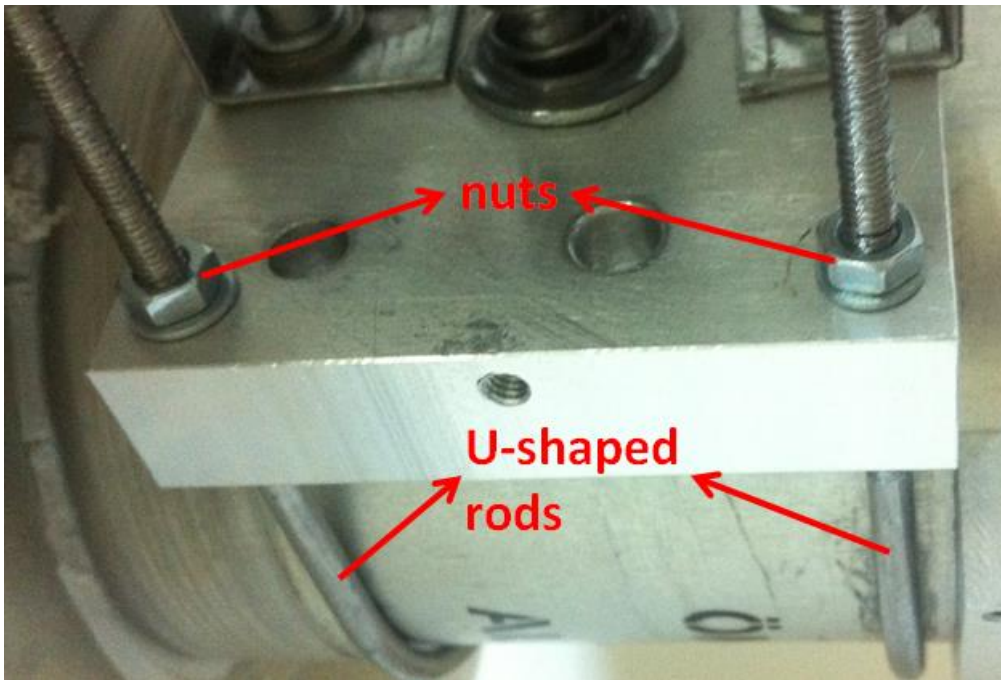


Figure 5-2: Fastening of the TVA assembly

Modal tests are performed for the two cases of prototype:

- 1- Without mass (free) case
- 2- Mass added case

Experimental results are presented and compared for both two cases. Finally, total reductions in the FRFs obtained from the analysis and experimental models are compared.

5.1. COMPARISON FOR THE WITHOUT MASS CASE

In this section, modal test results for the free (without mass) case of the prototype are presented. In addition, the FRFs obtained from the analysis and test studies are compared for the modified (with TVA) case.

Experimental FRF results are plotted together for the unmodified and modified cases which are obtained from the accelerometer demonstrated in Figure 3-28. In Figure 5-3, Figure 5-4 and Figure 5-5, the FRF results obtained in three axes are compared.

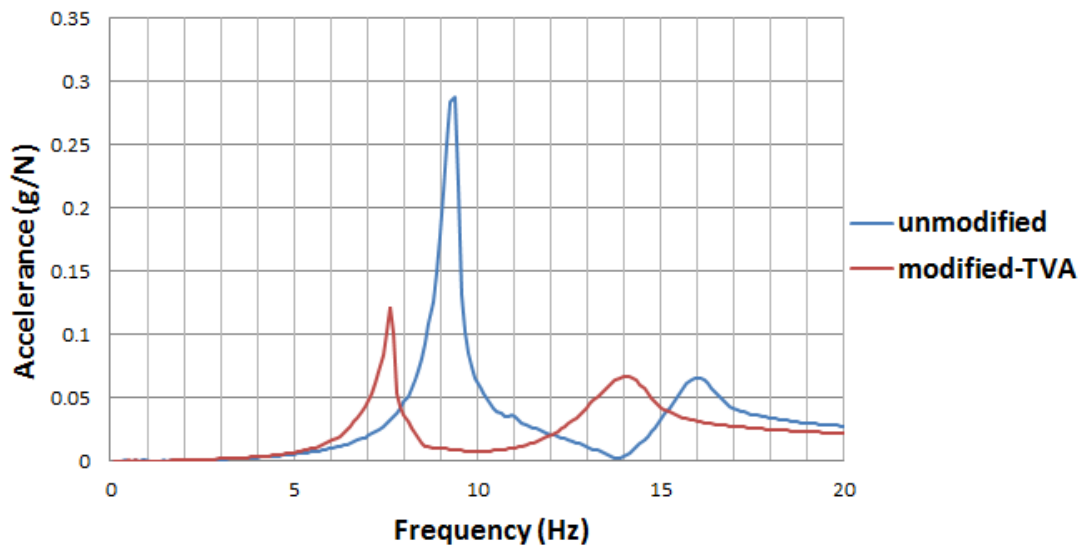


Figure 5-3: Without mass case - Comparison of the test FRF results (x-direction)

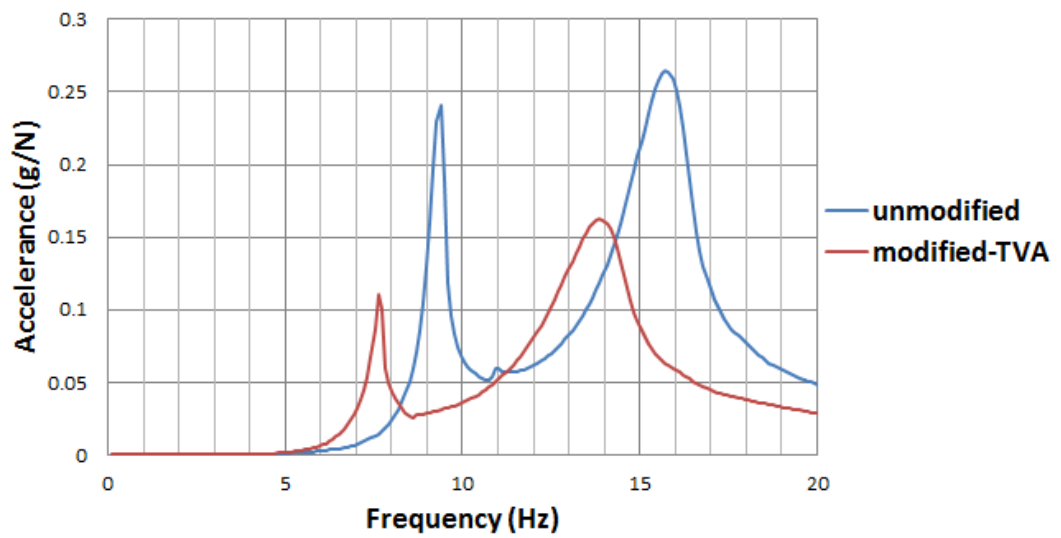


Figure 5-4: Without mass case - Comparison of the test FRF results (y-direction)

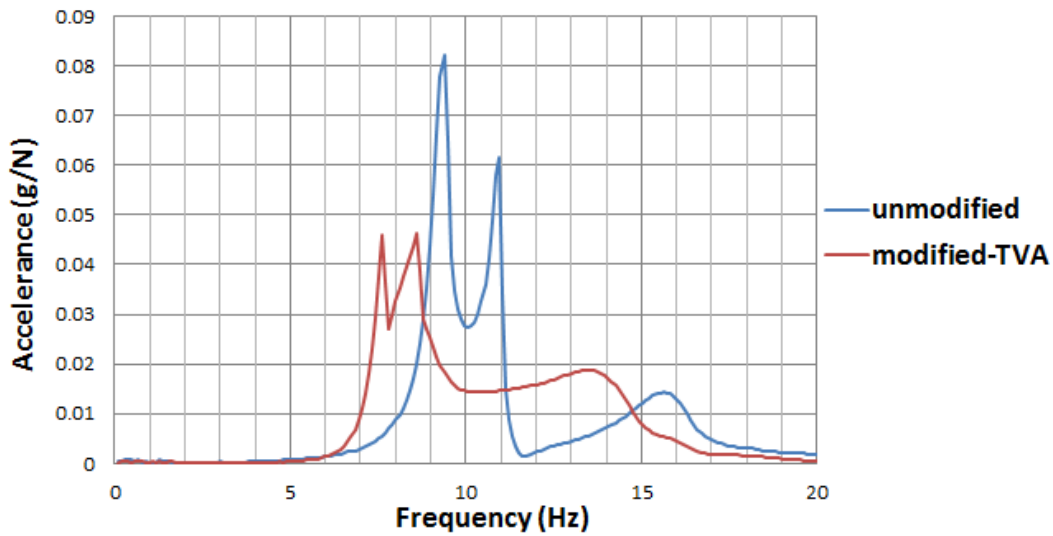


Figure 5-5: Without mass case - Comparison of the test FRF results (z-direction)

Between Figure 5-6 and Figure 5-8, experimental and analysis FRF results are compared which are obtained for the modified case. It can be observed that the peak values are compatible; however, there is a little amount of deviation between the peak frequencies.

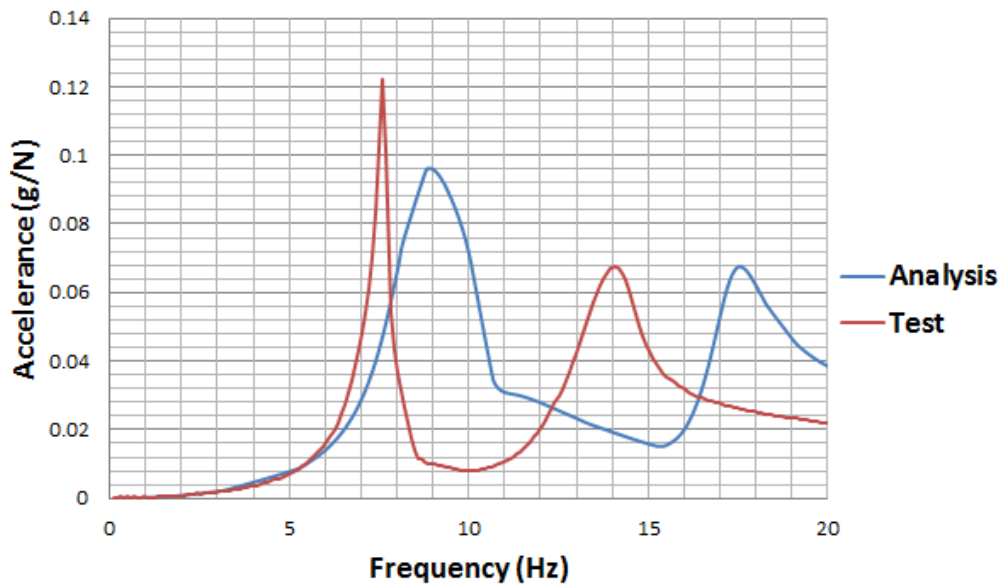


Figure 5-6: Analysis-test FRF comparison for the modified case (x-axes)

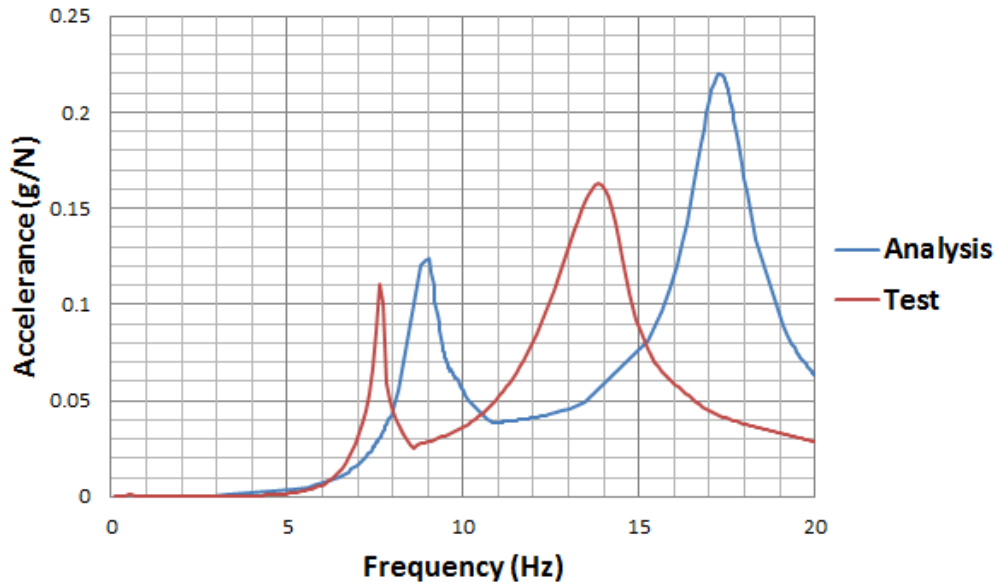


Figure 5-7: Analysis-test FRF comparison for the modified case (y-axis)

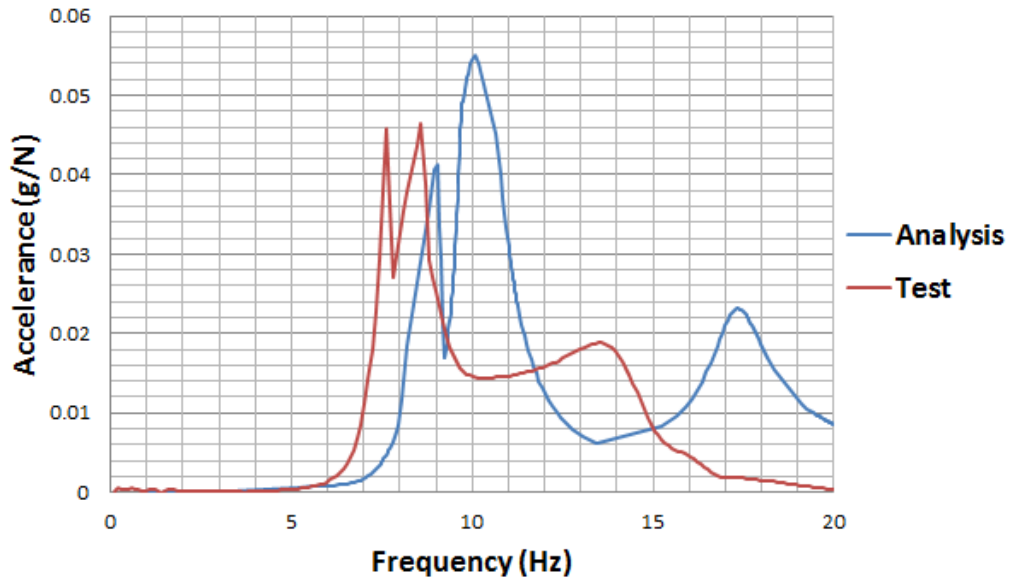


Figure 5-8: Analysis-test FRF comparison for the modified case (z-axis)

5.2. COMPARISON FOR THE MASS ADDED CASE

Experiments are repeated by adopting a mass to the structure which is equal to 1/5 to the total mass of the structure as mentioned in Section 4.1. In this section, experimental results for the mass added case of the prototype are presented. Additional mass is attached to the tube as revealed in Figure 5-9. Verification tests

are repeated with this mass added case and the obtained FRF results for the unmodified and modified cases are compared between Figure 5-10 and Figure 5-12.



Figure 5-9: Attachment of the additional mass on the physical structure

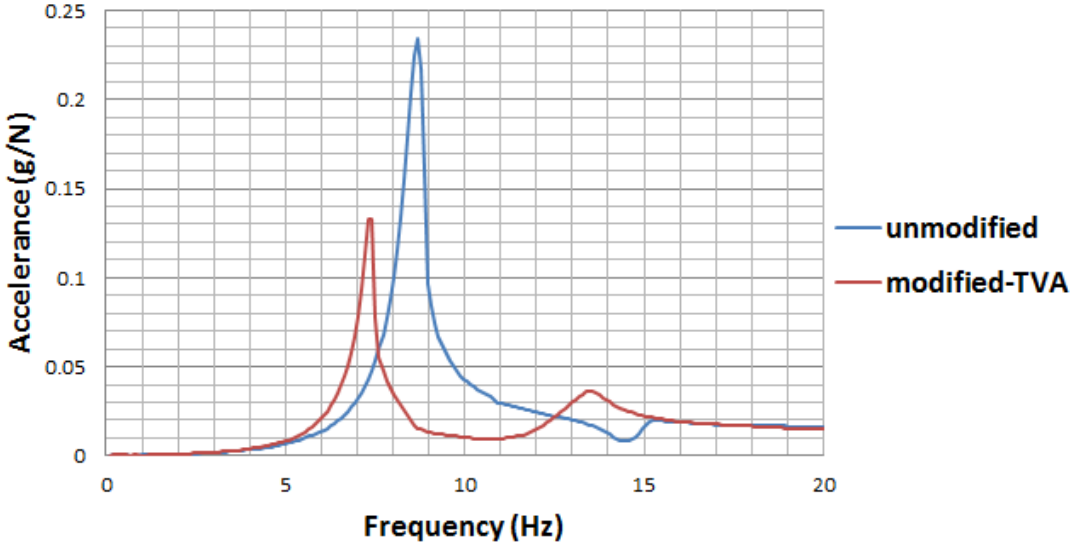


Figure 5-10: Mass added case – Comparison of the test FRF results (x-direction)

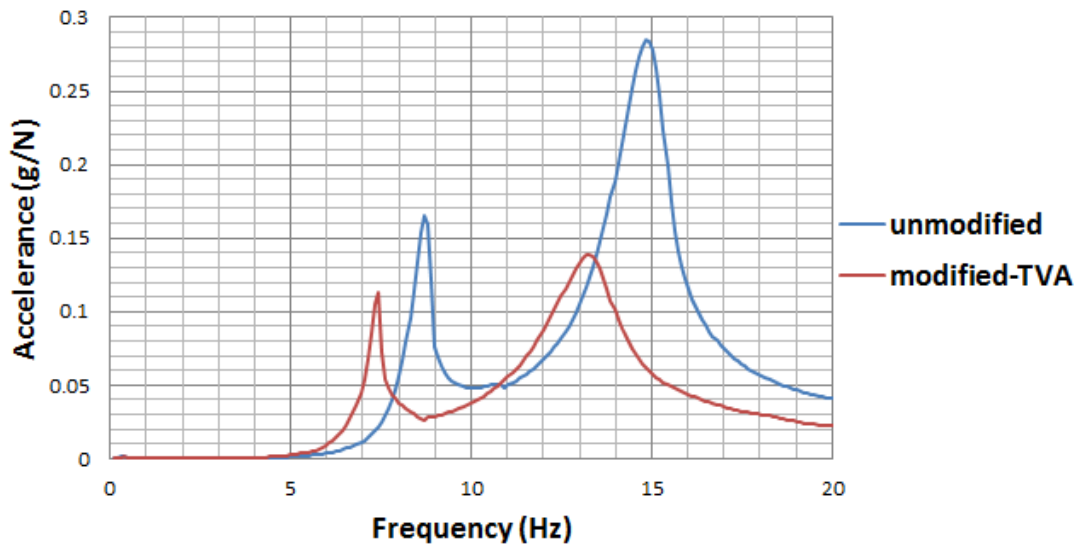


Figure 5-11: Mass added case - Comparison of the test FRF results (y-direction)

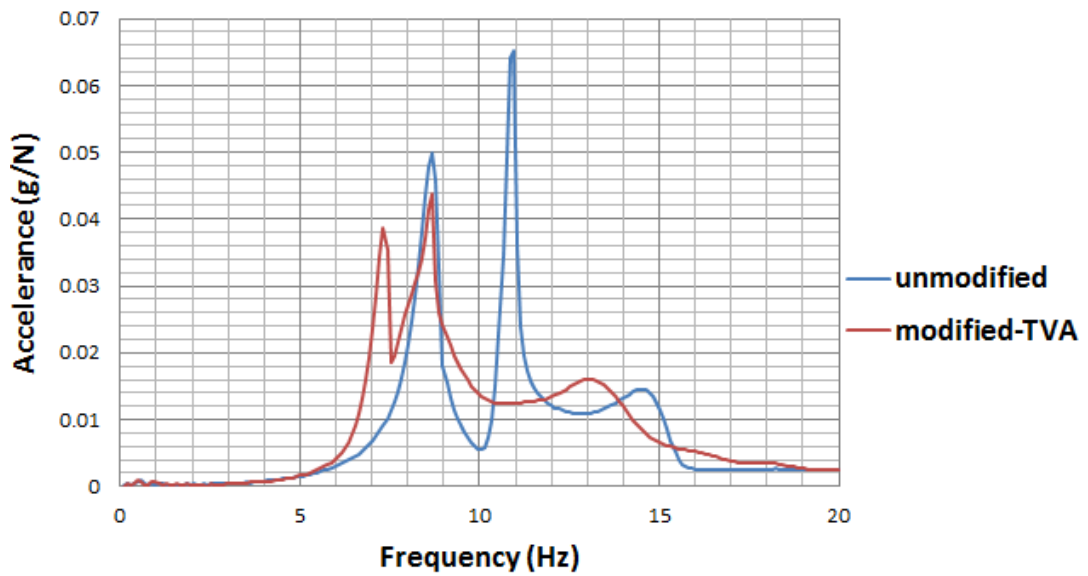


Figure 5-12: Mass added case - Comparison of the test FRF results (z-direction)

As a result of the FRF comparisons, it is observed that the vibration amplitudes again reduced; however, FRFs are slightly different than the without mass case.

5.3. TOTAL ANALYSIS-TEST COMPARISON

In order to evaluate the TVA design study which is performed over the finite element analysis, total vibration reductions obtained from the analysis and experiment are compared. Since the optimized and realized TVA parameters are different, total vibration reductions obtained from the analysis for the realized and optimum TVA parameters are presented separately. In Table 5-1, optimized and realized TVA parameters are compared.

Table 5-1: Comparison of the optimum and realized TVA parameters

	Optimized	Realized	Difference (%)
Mass (g)	380	382	0,5
Tuning frequency (Hz)	8,7	8,4	3,4
Damping ratio	0,32	0,35	8,6

Comparisons of the total harmonic displacement results obtained via finite element analysis for the unit load are presented in Figure 5-13 and Figure 5-14. If the Figure 5-13 and Figure 5-14 are compared, it can be seen that the realized TVA results in some amount of mistuning.

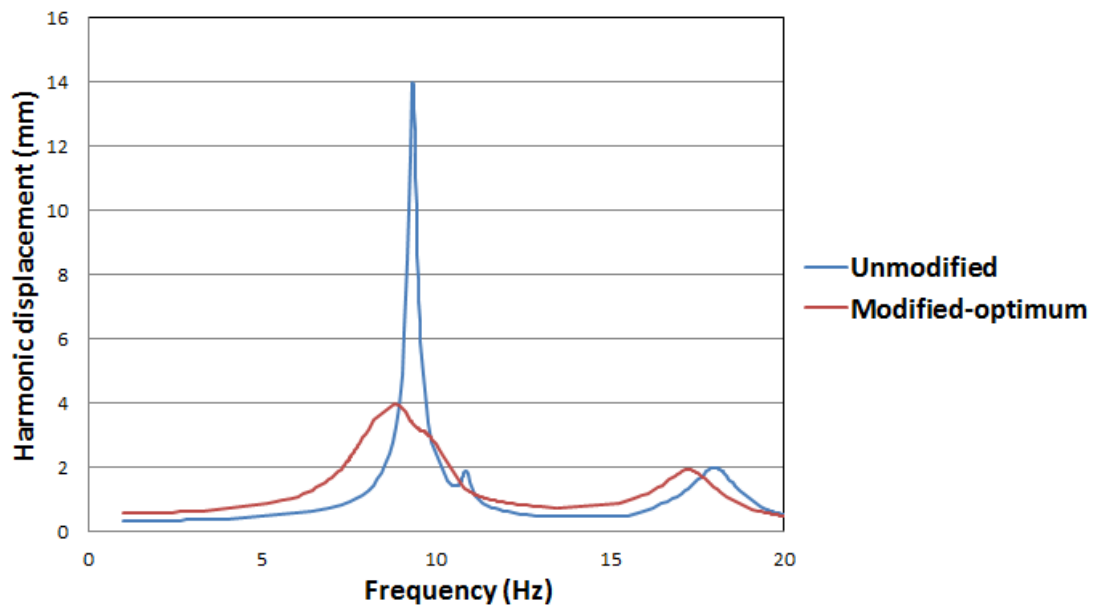


Figure 5-13: Total harmonic displacement comparison for the optimized TVA (Analysis)

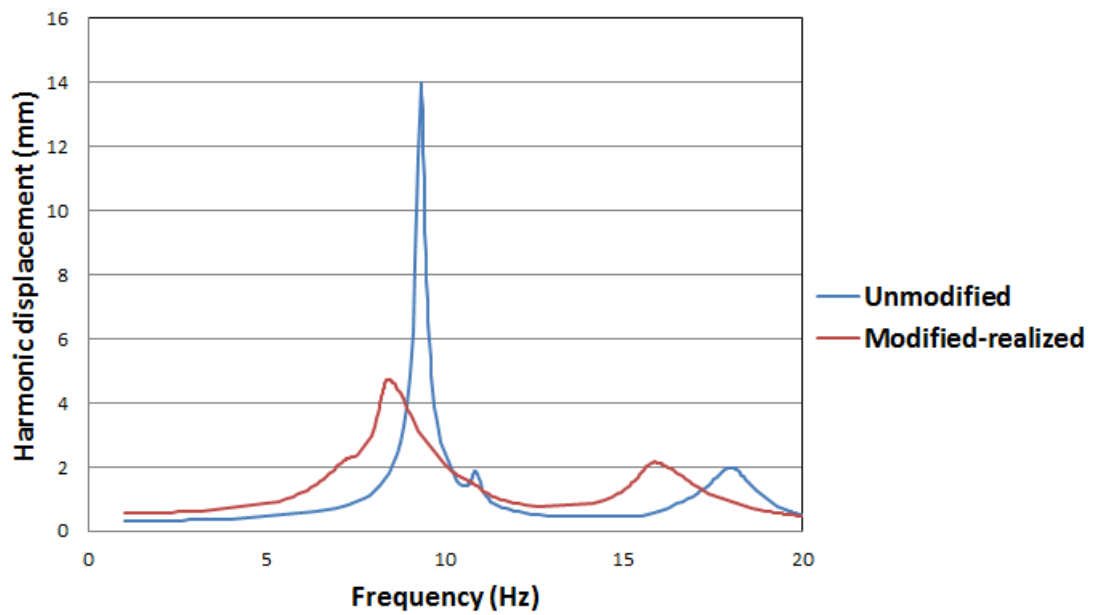


Figure 5-14: Total harmonic displacement comparison for the realized TVA (Analysis)

Since the experimental results are in terms of acceleration, they should be converted to displacement. Therefore, following expression is used to convert the acceleration FRF to the receptance FRF [28]:

$$|\alpha(\omega)| = \left| \frac{A(\omega)}{\omega^2} \right| \quad (\text{Eqn. 5.1})$$

In this expression, $\alpha(\omega)$ denotes the receptance and $A(\omega)$ denotes the accelerance FRFs. By making this conversion, experimental total harmonic displacement results are obtained as in Figure 5-15.

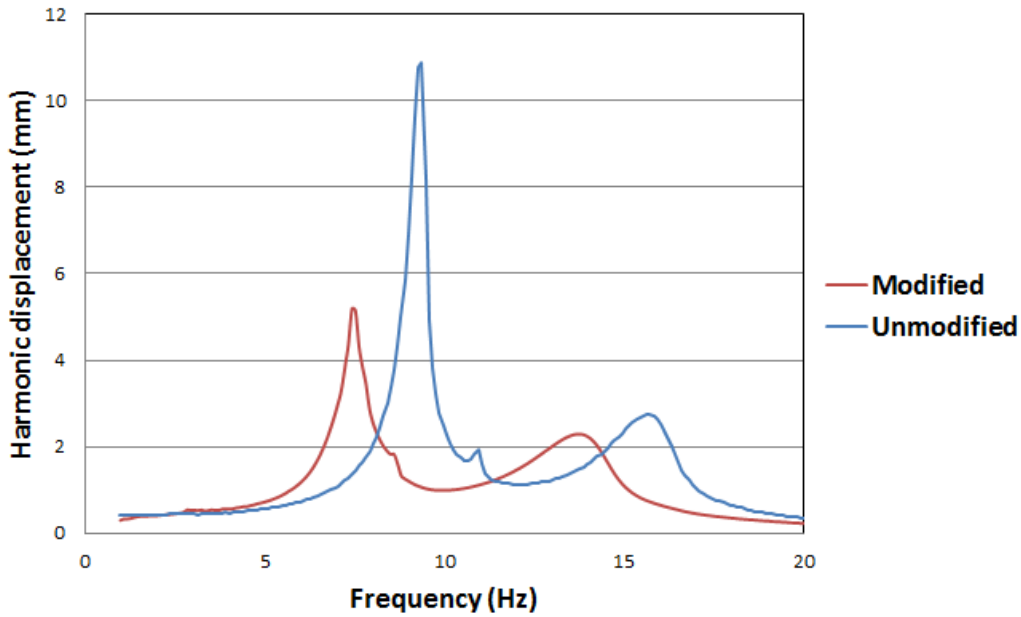


Figure 5-15: Total harmonic displacement comparison (Experimental)

Finally, peak values of the total harmonic displacements and the reductions in the peak values are presented in Table 5-2. From this table, it can be seen that the target reduction for the optimum TVA design is reached with % 85,8 success in realized TVA design. Experimentally, total reduction is achieved by % 68,3 rate with respect to the realized TVA design. As a result, target reduction is satisfied by %58,6 rate with the experiments. This rate can be considered as low. However, there is some amount of difference between the peaks of the FEA and experimental model results for the unmodified case as shown in Figure 5-16 which can account for this low achievement. This difference can be explained with the insufficient estimation of the damping of main structure. Another reason can be considered as the mistuning caused by the difference between the realized and optimum TVA parameters.

Table 5-2: Comparison of the maximum harmonic displacements and total reductions

	Unmodified (mm)	Modified (mm)	Reduction (dB)
FEA-optimized	14,01	3,96	10,96
FEA-realized	14,01	4,74	9,40
Experimental	10,87	5,19	6,42

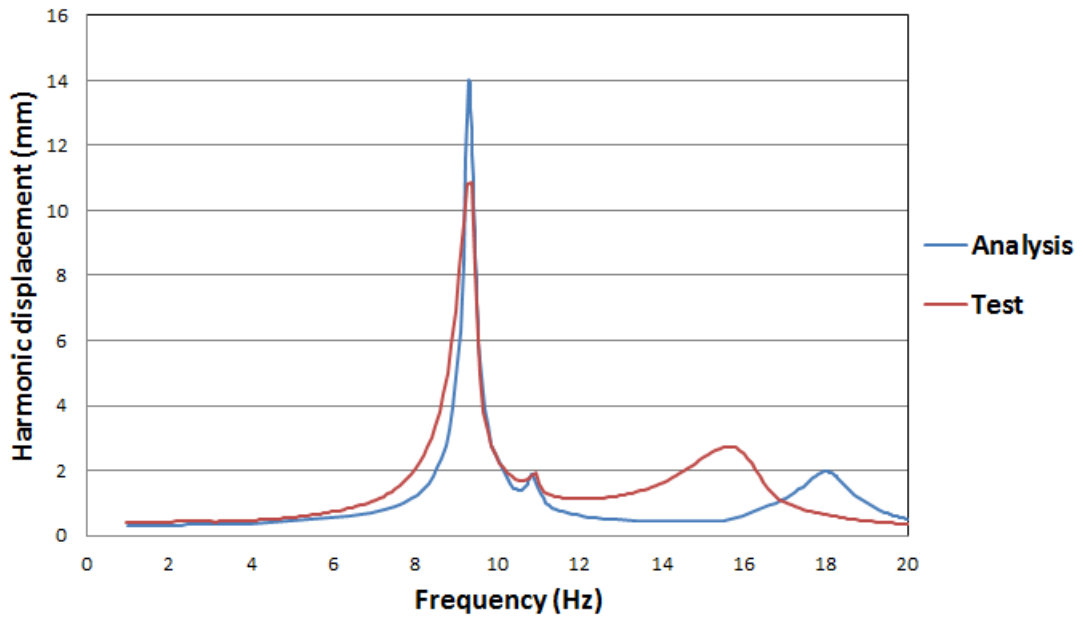


Figure 5-16: Comparison of the harmonic displacements for unmodified case

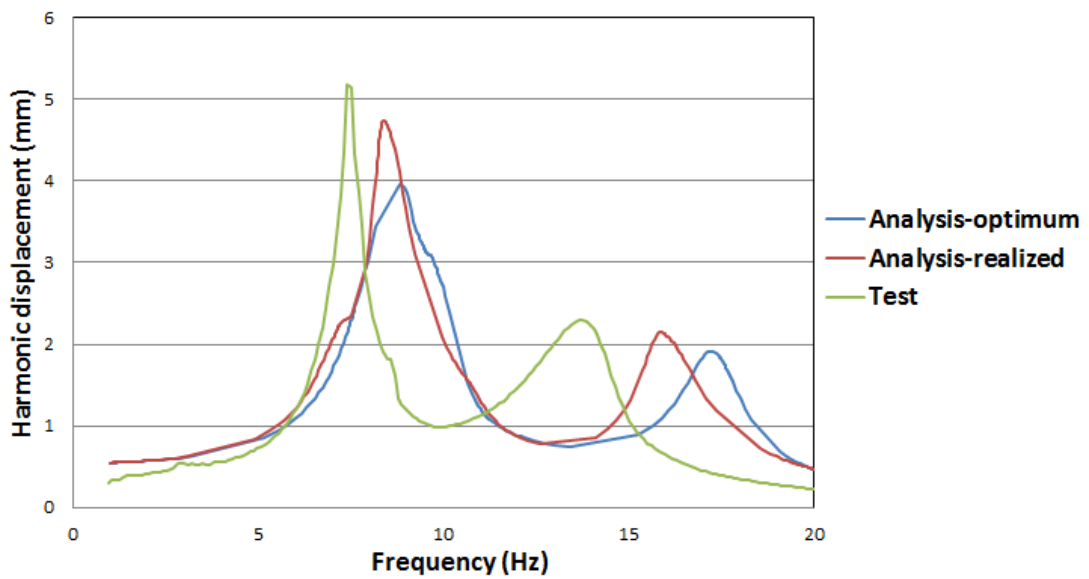


Figure 5-17: Comparison of the harmonic displacements for modified case

CHAPTER 6

CONCLUSION AND FUTURE WORK

Supported hollow cylinder structures exhibit oscillatory behavior due to any excitation. In this thesis work, a representative structure that includes a supported hollow cylinder structure is constructed. Main contribution to this structure's dynamics comes from the two transverse modes of the supported hollow cylinder structure. These modes are mainly caused by the rigid body movement rather than the structural modes. In case of impulsive excitation, dynamics of this structure is shaped by its two dominant vibration modes. In order to reduce the vibration levels of the structure, a TVA design is proposed by targeting the first two dominant transverse modes simultaneously.

A physical structure is fabricated and finite element model of the structure is constructed on ABAQUS software. This finite element model is verified by experiments. TVA design is carried out on this verified finite element model.

Since the excitation on the system is impulsive, vibration control problem is a resonant vibration problem. Therefore, vibration reduction is desired around the resonances of the structure. Experiments show that the first two transverse modes are dominant in the dynamics of system for the excitation under consideration; thus, TVA is designed by targeting these two modes. Since two target modal frequencies are close to each other, an SDOF TVA design is proposed. Basic dynamic parameters (mass, tuning frequency, damping ratio) of the TVA that would minimize the harmonic response of the structure are determined over the verified model of the structure. TVA is designed and fabricated according to these optimum dynamic parameters. Characterization tests are performed on this realized TVA system in order to verify the dynamic parameters of TVA.

TVA system is tested on the physical structure in order to characterize the vibration reduction performance. Experiments are repeated by adding an equivalent mass to the structure in order to investigate the mass effect on the vibration reduction levels

due to the TVA modification. Analysis and test results are compared in terms of accelerance FRFs. It is observed that the first two mode results are compatible; however, there is a little amount of shift between the third mode results. Besides, peak values of the FRFs obtained from the analysis and test models are somewhat different. These differences arise due to the insufficient damping estimation obtained from experiments for the finite element model of the physical structure. They can also be caused by the reason that the connections between parts of the prototype are not elaborately detailed in the finite element model and some simplifications are made. Modified case (with TVA) results have shown that there is a shift between the peaks of the analysis and test results. This can be interpreted with the mistuning effect of the TVA due to the fact that there is a little amount of difference between the designed and measured parameters (target damping ratio and target tuning frequency) of the TVA. For the mass added case test results, it is observed that the FRF's are again reduced. However, the vibration reduction levels are somewhat different than the without mass case.

As a future work, application of the tuned vibration absorber system at different angular orientations is suggested. By this way, the optimum orientation that would minimize the response of the structure can be detected. Furthermore, reductions of the oscillations should be examined in the time domain in order to measure the TVA performance in a more realistic way.

REFERENCES

- [1] Den Hartog J.P. Mechanical Vibrations. McGraw-Hill Book Company, Inc. 1956. Fourth Edition. New York Toronto London.
- [2] Özgüven, H., & Çandır, B. (1986). Suppressing the First and Second Resonances of beams by Dynamic Vibration Absorbers. *Journal of Sound and Vibration*, 111(3), 377-390.
- [3] Zuo, L., & Nayfeh, S. (2004). Minimax optimization of multi-degree-of-freedom tuned-mass dampers. *Journal of Sound and Vibration*, 272, 893-908.
- [4] Snowdon, J., Wolfe, A., & Kerlin, R. (1984). The Cruciform Dynamic Vibration Absorber.
- [5] Vakakis, A., & Paipetis, S. (1986). The Effect of a Viscously Damped Dynamic Absorber on a Linear Multi-Degree-of-Freedom System. *Journal of Sound and Vibration*, 105(1), 49-60.
- [6] Pombo, J., & Laura, P. (1986). Use of Two Dynamic Vibration Absorbers in the Case of Machinery Operating at Two Frequencies which Coincide with Two Natural Frequencies of the System. *Applied Acoustics*, 19, 41-45
- [7] Kathe, E., & Littlefield, A. (2002). Adaptive Gun Barrel Vibration Absorber
- [8] Eric L. Kathe. Gun Barrel Vibration Absorber. U.S. Patent No. 6,167,794 B1, 1998.
- [9] Büyükcivelek, F. (2011). Analysis and Control of Gun Barrel Vibrations (M.s. Thesis).
- [10] Bonsel, J., Fey, R., & Nijmeijer, H. (2004). Application of a Dynamic Vibration Absorber to a Piecewise Linear Beam System. *Nonlinear Dynamics*, (37), 227-243.


- [11] Gu, M., Chang, C., Wu, W., & Xiang, H. (1998). Increase of critical flutter wind speed of long-span bridges using tuned mass dampers. *Journal of Wind Engineering and Industrial Aerodynamic*, 73, 111-123.
- [12] Hill, S., Synder, S., & Cazzolato, B. (2002). An Adaptive Vibration Absorber. *Acoustics 2002 - Innovation in Acoustics and Vibration*.
- [13] Lamb, J. (n.d.). Tuned-Mass Damper Design: A Case Study. Structural Engenuity, Inc. Retrieved from www.structuralengenuity.com
- [14] Mirsanei, R., Hajikhani, A., Peykari, B., & Hamed, J. (2012). Developing a New Design for Adaptive Tuned Dynamic Vibration Absorber (ATDVA) Based on Smart Slider-Crank Mechanism to Control of Undesirable Vibrations. *International Journal of Mechanical Engineering and Mechatronics*, 1(1).
- [15] Maly, J., & Napolitano, K. (1993). A Magnetic Tuned-Mass Damper For Buffet Induced Airfoil Vibration.
- [16] Sayyad, F., & Gadhave, N. (2013). Study of Magnetic Vibration Absorber with Permanent Magnets along Vibrating Beam Structure. *Journal of Structures*, 2013.
- [17] Harris, A. (2003). Multi-Degree of Freedom Passive and Active Vibration Absorbers for the Control of Structural Vibration (M.S. Thesis).
- [18] ABAQUS 6.12 Analysis User's Manual (2012). Providence, USA.
- [19] LMS Test Lab12A Documentation (2012). Leuven, Belgium.
- [20] PCB 086C41 Model ICP Impact Hammer Specification Sheet, 2010.
- [21] PCB 356B21 Model Triaxial ICP Accelerometer Specification Sheet, 2013.
- [22] J. Allemang, R. (n.d.). The Modal Assurance Criterion (MAC): Twenty Years of Use and Abuse. Mechanical, Industrial and Nuclear Engineering University of Cincinnati, USA.

- [23] Lalanne, C. (2009). Fourier transform of simple shocks. In *Mechanical Shock and Vibration Analysis* (2nd ed., Vol. 2, pp. 14-25). London, United Kingdom: Wiley.
- [24] Kienholtz, D., & Pendleton, S. (1994). Demonstration of solar array vibration suppression. *Smart Structures and Materials*, 2193.
- [25] Budynass, R.G., Nisbett, J.K., (2008) *Mechanical Springs*. In *Shigley's Mechanical Engineering Design* (8th ed., pp. 501-550). USA: McGraw-Hill.
- [26] TMS Modal Shop Model 2110E 110 LBF Electrodynamic Exciter Specification Sheet, 2013.
- [27] Kelly, S.G., (2012). Response due to harmonic excitation of support. In *Mechanical Vibrations Theory and Applications* (SI ed., pp. 228-234). Stamford, USA: Cengage Learning.
- [28] Irvine, T. (2000). *An Introduction to Frequency Response Functions*.

APPENDICES

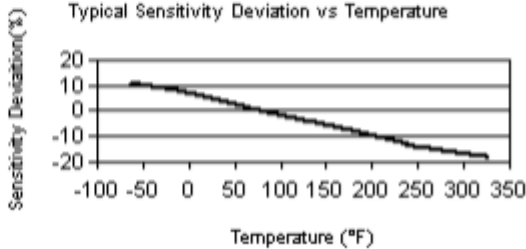
Appendix A: Technical Specifications of the Accelerometers

Model Number 356B21	TRIAxIAL ICP® ACCELEROMETER	
	<u>ENGLISH</u>	<u>SI</u>
Performance		
Sensitivity(± 10 %)	10 mV/g	1.02 mV/(m/s ²)
Measurement Range	± 500 g pk	± 4905 m/s ² pk
Frequency Range(± 5 %)(y or z axis)	2 to 10,000 Hz	2 to 10,000 Hz
Frequency Range(± 5 %)(x axis)	2 to 7000 Hz	2 to 7000 Hz
Resonant Frequency	≥ 55 kHz	≥ 55 kHz
Broadband Resolution(1 to 10,000 Hz)	0.004 g rms	0.04 m/s ² rms
Non-Linearity	≤ 1 %	≤ 1 %
Transverse Sensitivity	≤ 5 %	≤ 5 %
Environmental		
Overload Limit(Shock)	± 10,000 g pk	± 98,100 m/s ² pk
Temperature Range(Operating)	-85 to +250 °F	-54 to +121 °C
Temperature Response	See Graph	See Graph
Electrical		
Excitation Voltage	18 to 30 VDC	18 to 30 VDC
Constant Current Excitation	2 to 20 mA	2 to 20 mA
Output Impedance	≤ 200 Ohm	≤ 200 Ohm
Output Bias Voltage	7 to 12 VDC	7 to 12 VDC
Discharge Time Constant	0.3 to 1.0 sec	0.3 to 1.0 sec
Settling Time(within 10% of bias)	<3 sec	<3 sec
Spectral Noise(1 Hz)	1000 µg/√Hz	9810 (µm/sec ²)/√Hz
Spectral Noise(10 Hz)	300 µg/√Hz	2943 (µm/sec ²)/√Hz
Spectral Noise(100 Hz)	100 µg/√Hz	981 (µm/sec ²)/√Hz
Spectral Noise(1 kHz)	50 µg/√Hz	490 (µm/sec ²)/√Hz
Physical		
Sensing Element	Ceramic	Ceramic
Sensing Geometry	Shear	Shear
Housing Material	Titanium	Titanium
Sealing	Hermetic	Hermetic
Size (Height x Length x Width)	0.4 in x 0.4 in x 0.4 in	10.2 mm x 10.2 mm x 10.2 mm
Weight	0.14 oz	4 gm
Electrical Connector	8-38 4-Pin	8-38 4-Pin
Electrical Connection Position	Side	Side
Mounting Thread	5-40 Female	5-40 Female



[4]

Typical Sensitivity Deviation vs Temperature



All specifications are at room temperature unless otherwise specified.
In the interest of constant product improvement, we reserve the right to change specifications without notice.
ICP® is a registered trademark of PCB Group, Inc.

Figure 0-1

Appendix C: Technical Specifications of the Modal Shaker



SPECIFICATIONS:

PERFORMANCE:

Output Force, sine pk, forced air cooling	110 lbf (489 N) ^[1]
Output Force, random RMS, forced air cooling	45 lbf (334 N) ^[1]
Output Force, shock pk (50 ms)	110 lbf (1000 N)
Stroke Length, continuous pk-pk	1.0 in (25.4 mm)
Stroke Length, between stops	1.03 in (26.2 mm)
Frequency Range, nominal	DC - 6500 Hz ^[2]
Fundamental Resonance	>4000 Hz ^[2]
Maximum Velocity	70 in/s pk (1.8 m/s pk)
Maximum Acceleration, bare table	110 g pk
Maximum Acceleration, 1 lb (0.45 kg) load	55 g pk
Maximum Acceleration, 5 lb (2.38 kg) load	18 g pk
Maximum Acceleration, resonance	150 g pk
Maximum Acceleration, peak shock	200 g pk
Maximum Payload, typical	10 lb (4.5 kg)

PHYSICAL:

Platform Mounting Thread	5x 10-32 ^[3]
Armature Weight	1.0 lb (0.45 kg)
Suspension Stiffness	90 lbf/in (15.8 N/mm)
Rated Drive Current, forced air cooling	22 A RMS
Stray Magnetic Field, 1.5 in (38 mm) above table	<20 Gauss
Stray Magnetic Field, 1.0 in (25 mm) from body	<25 Gauss
Cooling Air	100 cfm/15 in H ₂ O ^[1]
Dimensions (H x W x D), nominal	11.7 x 12.5 x 6.5 in (297 x 318 x 165 mm) ^[4]
Weight, nominal	56 lb (25 kg)
Temperature Operating Range	40-100°F (4-38°C), <85% RH
Field Power Supply	12V, 12A DC, nominal ^[5]

Figure 0-3